



8-2006

Three Population Models Applied to Competition, Disease and Invasion

Erika Asano

University of Tennessee - Knoxville

Recommended Citation

Asano, Erika, "Three Population Models Applied to Competition, Disease and Invasion. " PhD diss., University of Tennessee, 2006.
https://trace.tennessee.edu/utk_graddiss/1634

This Dissertation is brought to you for free and open access by the Graduate School at Trace: Tennessee Research and Creative Exchange. It has been accepted for inclusion in Doctoral Dissertations by an authorized administrator of Trace: Tennessee Research and Creative Exchange. For more information, please contact trace@utk.edu.

To the Graduate Council:

I am submitting herewith a dissertation written by Erika Asano entitled "Three Population Models Applied to Competition, Disease and Invasion." I have examined the final electronic copy of this dissertation for form and content and recommend that it be accepted in partial fulfillment of the requirements for the degree of Doctor of Philosophy, with a major in Mathematics.

Suzanne Lenhart, Major Professor

We have read this dissertation and recommend its acceptance:

Louis Gross, Don Hinton, Vladimir Protopopescu

Accepted for the Council:

Dixie L. Thompson

Vice Provost and Dean of the Graduate School

(Original signatures are on file with official student records.)

To the Graduate Council:

I am submitting herewith a dissertation written by Erika Asano entitled "Three Population Models Applied to Competition, Disease and Invasion." I have examined the final electronic copy of this dissertation for form and content and recommend that it be accepted in partial fulfillment of the requirements for the degree of Doctor of Philosophy, with a major in Mathematics.

Suzanne Lenhart

Major Professor

We have read this dissertation
and recommend its acceptance:

Louis Gross

Don Hinton

Vladimir Protopopescu

Accepted for the Council:

Anne Mayhew

Vice Chancellor and Dean of
Graduate Studies

(Original signatures are on file with official student records.)

Three Population Models Applied to Competition, Disease and Invasion

A Dissertation

Presented for the

Doctor of Philosophy

Degree

The University of Tennessee, Knoxville

Erika Asano

August 2006

Dedication

To Lancelot, Sundance and Chani.

Acknowledgments

I want to thank my advisor Dr. Suzanne Lenhart for her guidance, patience and support during all these years of my stay in Knoxville. I have learnt a lot about PDEs, optimal control and modeling from her, and have grown a lot professionally with her guidance.

I want to thank the other members of my committee, Dr. Louis Gross, Dr. Don Hinton and Dr. Vladimir Protopopescu for their help. I have learnt a lot about mathematical modeling in biology and ecology from Dr. Louis Gross. Dr. Hinton has been a great teacher and mentor starting from when I took his class on differential equations.

My dissertation consists of three projects. The project on competition model was done in collaboration with Dr. Lenhart and Dr. Protopopescu. The project on rabies model was in collaboration with Dr. Leslie Real, Dr. Louis Gross and Dr. Lenhart. The final project on Eurasian collared doves was in collaboration with Dr. Michael Fuller and Dr. Andrew Whittle. I am thankful to all of them for their help.

Fellow graduate students Wandi Ding, Volodymyr Hrynkiv, Atish Mitra, and Mike Saum, have made my stay at UT pleasant.

Abstract

In this work, we present three different types of population models. The first two models are examined in the context of optimal control problems. The third involves the construction of an invasion model using a significant amount of data.

The first model describes the interaction of three populations, motivated by a combat scenario. One of the three populations can switch the mode of alliance with the other two populations between cooperation and competition. The other two populations always compete with each other. In this system of parabolic partial differential equations, the control is the function which measures the strength of alliance.

The second model is a metapopulation SIR model for the spread of rabies among raccoons. This system of ordinary differential equations considers subpopulations connected via movement of individuals between subpopulations. The strength of the connectivity between two subpopulations is inversely proportional to the geographical distance between them. We apply control theory to find the best strategy (timing and location) for vaccination to control the disease.

The third problem involves construction of a model of the spread of Eurasian collared doves in the U.S. using an integrodifference equation. We investigate the effect of spatial variation of the length of the growing season on the growth rate of the collared dove. Since the growing season length affects the breeding season length, we take into account the difference in the number of clutches in estimating the number of offspring produced each breeding season.

Contents

| | | |
|----------|---|-----------|
| 1 | Introduction | 1 |
| 2 | Competition Model | 4 |
| 2.1 | Introduction | 4 |
| 2.2 | Assumptions | 7 |
| 2.3 | Existence of Optimal Control | 24 |
| 2.4 | Derivation of the Optimality System | 29 |
| 2.5 | Uniqueness of the Optimality System | 40 |
| 2.6 | Numerical Results - Control Function $\alpha(t)$ | 47 |
| 2.7 | Numerical Results - Control Function $\alpha(x, t)$ | 59 |
| 2.8 | Conclusions | 64 |
| 3 | Rabies Metapopulation Model | 68 |
| 3.1 | Introduction | 68 |
| 3.2 | Metapopulation Model | 70 |
| 3.3 | Necessary Conditions for the Optimal Control | 74 |
| 3.4 | Numerical Results | 78 |
| 3.5 | Conclusions | 95 |
| 4 | Eurasian Collared Dove Model | 98 |
| 4.1 | Introduction | 98 |
| 4.2 | History of Dove Invasion in the U.S. | 99 |
| 4.3 | Dove Ecology | 100 |

| | | |
|------|--|------------|
| 4.4 | Integrodifference Equations | 100 |
| 4.5 | Model Description | 101 |
| 4.6 | Dispersal Kernel | 111 |
| 4.7 | Breeding Season Length Function | 115 |
| 4.8 | Model Parameters | 120 |
| 4.9 | Bird Data | 122 |
| 4.10 | Numerical Simulation - 1 Spatial Dimension Model | 124 |
| 4.11 | Conclusions | 135 |
| | Bibliography | 137 |
| | Vita | 145 |

List of Tables

| | | |
|-----|--|-----|
| 3.1 | Nomenclature | 72 |
| 4.1 | Number of ring recoveries for the Eurasian collared dove | 112 |
| 4.2 | Kernels used to estimate $k(x)$ | 112 |
| 4.3 | Best fitting curves for dispersal kernels | 113 |
| 4.4 | Zone description for the frost-free days data | 116 |
| 4.5 | Best fit results for $T(x)$ in zone 1 | 120 |
| 4.6 | Parameters of the model | 122 |
| 4.7 | Number of CBC and BBS data points | 125 |

List of Figures

| | | |
|------|--|----|
| 2.1 | Initial population distribution A, B and C | 49 |
| 2.2 | Population distribution and optimal control $\alpha(t)$ with $K = 1, L = 1, M = 0.1, \bar{M} = 5$ | 51 |
| 2.3 | Population distribution and optimal control $\alpha(t)$ with $K = 1, L = 0.1, M = 0.1, \bar{M} = 5$ | 52 |
| 2.4 | Population distribution and optimal control $\alpha(t)$ with $K = 1, L = 0.1, M = 0.01, \bar{M} = 5$ | 53 |
| 2.5 | Population distribution and optimal control $\alpha(t)$ with $K = 1, L = 0.01, M = 0.1, \bar{M} = 5$ | 54 |
| 2.6 | Population distribution and optimal control $\alpha(t)$ with initial population C, $K = 1, L = 0.1, M = 0.01, \bar{M} = 5$ | 56 |
| 2.7 | Population distribution and optimal control $\alpha(t)$ with initial population B, $K = 1, L = 1, M = 0.1, \bar{M} = 5$ | 57 |
| 2.8 | Population distribution and optimal control $\alpha(t)$ with $K = 1, L = 1, M = 0.1, \bar{M} = 5, a^1 = 0.8, a^2 = 0.6, a^3 = 0.4$ | 58 |
| 2.9 | Population distribution and optimal control $\alpha(x, t)$ with $K = 1, L = 1, M = 0.1, \bar{M} = 5$ | 60 |
| 2.10 | Population distribution and optimal control $\alpha(x, t)$ with $K = 1, L = 0.01, M = 0.1, \bar{M} = 5$ | 62 |
| 2.11 | Population distribution and optimal control $\alpha(x, t)$ with initial population C, $K = 1, L = 0.1, M = 0.01, \bar{M} = 5$ | 63 |

| | | |
|------|---|-----|
| 2.12 | Population distribution and optimal control $\alpha(x, t)$ with initial population $C, K = 1, L = 0.1, M = 0.01, \bar{M} = 5, a_1^1 = 0.8, a_1^2 = 0.6, a_1^3 = 0.4$ | 65 |
| 2.13 | Population distribution and optimal control $\alpha(x, t)$ with initial population $C, K = 1, L = 0.1, M = 0.01, \bar{M} = 5, a_1^1 = 0.8, a_1^2 = 0.4, a_1^3 = 0.6$ | 66 |
| 3.1 | Flow diagram | 71 |
| 3.2 | Rate of geographic movement a_{ij} | 72 |
| 3.3 | Spatial arrangement of subpopulations used in numerical simulation | 78 |
| 3.4 | Population distribution and optimal control with $\alpha = 50, I_9(0) = 10$ | 82 |
| 3.5 | Total population with $\alpha = 50, I_9(0) = 10$ | 83 |
| 3.6 | Population distribution and optimal control with $\alpha = 100, I_9(0) = 10$ | 84 |
| 3.7 | Total population with $\alpha = 100, I_9(0) = 10$ | 85 |
| 3.8 | Population distribution and optimal control with $\alpha = 200, I_9(0) = 10$ | 86 |
| 3.9 | Total population with $\alpha = 200, I_9(0) = 10$ | 87 |
| 3.10 | Population distribution without control (examples 1, 2 and 3) | 88 |
| 3.11 | Population distribution and optimal control with $\alpha = 100, I_4(0) = 5$ | 90 |
| 3.12 | Total population with $\alpha = 100, I_4(0) = 5$ | 91 |
| 3.13 | Population distribution without control (example 4) | 92 |
| 3.14 | Population distribution and optimal control with $\alpha = 100, I_7(0) = 25$ | 93 |
| 3.15 | Total population with $\alpha = 100, I_7(0) = 25$ | 94 |
| 3.16 | Population distribution without control (example 5) | 96 |
| 4.1 | Dispersal kernel $k(x)$ with reflective boundary at $x = 0$ | 103 |
| 4.2 | Normalized Beverton-Holt function | 106 |
| 4.3 | Dispersal kernel using a single distribution | 114 |
| 4.4 | Dispersal kernel using two distributions | 114 |
| 4.5 | Zone map for the frost-free days data | 117 |
| 4.6 | Frost-free days and elevation for zone 1 | 117 |
| 4.7 | Frost-free days and elevation for zone 2 | 118 |
| 4.8 | Frost-free days and elevation for zone 3 | 118 |

| | | |
|------|--|-----|
| 4.9 | Frost-free days and elevation for zone 4 | 119 |
| 4.10 | Frost-free days and elevation for zone 5 | 119 |
| 4.11 | Best fit $T(x)$ in zone 1 | 121 |
| 4.12 | Map for CBC data | 123 |
| 4.13 | Bird density for year 1989-1992 (CBC) | 125 |
| 4.14 | Bird density for year 1993-1996 (CBC) | 126 |
| 4.15 | Bird density for year 1997-2000 (CBC) | 126 |
| 4.16 | Bird density for year 2001-2004 (CBC) | 127 |
| 4.17 | Wave front location (CBC) | 129 |
| 4.18 | Graph used to calculate N_0 | 129 |
| 4.19 | Simulation result for population density (zone 1) | 130 |
| 4.20 | Wave front distance (zone 1) | 131 |
| 4.21 | Bird density for year 1989-1992 (BBS) | 132 |
| 4.22 | Bird density for year 1993-1996 (BBS) | 132 |
| 4.23 | Bird density for year 1997-2000 (BBS) | 133 |
| 4.24 | Bird density for year 2001-2004 (BBS) | 133 |
| 4.25 | Wave front location (BBS) | 134 |
| 4.26 | Wave front locations from BBS data and simulation result | 134 |

Chapter 1

Introduction

We present three population models. The first two problems are optimal control problems involving partial differential equations (PDEs) and ordinary differential equations (ODEs). The third problem is modeling of the spread of Eurasian collared dove in the U.S., using an integro-difference equation. We use Pontryagin's Maximum Principle [51] for ODEs and its extended version to PDEs [34]. In Chapter 2, we discuss a competition model using a system of parabolic partial differential equations, which describe the interaction of three populations. One of the three populations can switch its alliances between cooperation and competition with the other two populations. The remaining two populations always compete with each other. The magnitude of the control function measures the strength of alliance and the sign of the control function determines the mode of alliance: cooperation or competition. The three populations are represented as the solutions of a nonlinear system of parabolic partial differential equations with Dirichlet boundary conditions in a bounded, space-time domain. The objective functional is defined from the perspective of the opportunistic population. Our goal is to maximize the size of the opportunistic population while minimizing the difference between the other competing populations and the cost associated with the strength of the alliance.

We obtain a unique optimal control in terms of the solutions to the optimality system, which consists of the state system coupled with an adjoint system. In Section 2 of Chapter 2, we prove the existence of solutions to the state system and corresponding *a priori* estimates.

In Section 3, we prove the existence of an optimal control. The control-to-state map is differentiated to obtain the sensitivity system. Using the sensitivity system, we derive the optimality system by differentiating the objective functional with respect to the control in the fourth section. In Section 5, we prove the uniqueness of the optimal control. Finally, we show numerical results using some simple examples. The first case is with spatially independent control functions and the second case has spatial and temporal dependence in the control. We illustrate how the optimal control function and the final time populations are changed by choosing different values of the weight constants in our objective functional.

In Chapter 3, we briefly discuss a metapopulation SIR (susceptibles, infecteds, removed (immune)) model for the spread of rabies among raccoons. We consider a system of ordinary differential equations, representing subpopulations connected via movement of individuals between subpopulations. The strength of the connectivity between two subpopulations is inversely proportional to the geographical distance between them. Each subpopulation is divided into three classes; the susceptibles, infecteds and the removed who are vaccinated and become immune to rabies. In our model, the control is the rate at which of removal of susceptibles occurs. We apply control theory to find the best strategy (timing and location) to apply vaccination to control the disease. In Section 1, we describe the background on the disease and the current vaccination measures used in the U.S. In Section 2, we present our model to analyze the best strategy to control the spread of rabies for short time period (i.e., no birth occurs in the time interval of our interest). Using Pontryagin's Maximum Principle, we obtain the necessary conditions for the optimal control(vaccination) in Section 3. In Section 4, we numerically solve the problem using an iterative method with the Runge-Kutta 4th order scheme.

In the last chapter, the model for the spread of Eurasian collared dove in the U.S. using an integrodifference equation is addressed. We investigate the effect of spatial variation of the growing season on the growth rate of the collared dove. The length of growing season affects the breeding season length, which affects the number of clutches and thus the number of offspring produced each season.

We used the European banding data [29] to estimate our kernel in the integrodifference

equation which determines how far the individuals disperse. To estimate the breeding season length, we used data on the number of frost free days recorded at numerous weather stations in the U.S. collected by the US National Climatic Data Center in Asheville, NC. We assumed that the breeding season length is proportional to the length of frost free days.

Many parameters, such as the survival rate of offspring and the maximum number of clutches per year, are obtained from the literature, but we estimated the per capita rate of pair formation using the Christmas bird count (CBC) data collected by the National Audubon Society. Our spatial domain was a north-south strip starting with South Florida. Then we simulated the model with one spatial dimension using these parameter values and compared the rate of invasion speed (in terms of the wave front distance) with the North American breeding bird survey (BBS) collected by the United States Geological Survey and the Canadian Wildlife Service.

Chapter 2

Competition Model

2.1 Introduction

We consider optimal control of a nonlinear system of parabolic partial differential equations with Dirichlet boundary conditions in a bounded, space-time domain $Q = \Omega \times (0, T)$, $\Omega \subset \mathbb{R}^n$. Solutions of the system represent populations of three species. One of the populations can switch its alliances between cooperation and competition with the other two populations. The other two populations always compete with each other. The control is the function α , measuring the strength of alliance and the sign of α tells whether the third population is competing or cooperating with the other two populations. The control set is defined as

$$U \equiv \{ \alpha \in L^\infty(Q) : |\alpha(x, t)| \leq \bar{M} \text{ a.e. in } Q \},$$

where $\bar{M} > 0$. Given a control $\alpha \in U$, the corresponding state variables, $u_1(x, t)$, $u_2(x, t)$ and $u_3(x, t)$ satisfy the state system:

$$\begin{aligned} L_1 u_1 &= -u_1 \int_{\Omega} \frac{u_2}{1+u_2} dx + \alpha u_1 \int_{\Omega} \frac{u_3}{1+u_3} dx + f_1 \\ L_2 u_2 &= -u_2 \int_{\Omega} \frac{u_1}{1+u_1} dx - \alpha u_2 \int_{\Omega} \frac{u_3}{1+u_3} dx + f_2 \\ L_3 u_3 &= \alpha u_3 \int_{\Omega} \frac{u_1}{1+u_1} dx - \alpha u_3 \int_{\Omega} \frac{u_2}{1+u_2} dx + f_3 \end{aligned} \tag{2.1}$$

ICs:

$$u_k(x, 0) = u_{k0}(x) \text{ for } x \in \Omega, k = 1, 2, 3 \quad (2.2)$$

BCs:

$$u_k = 0 \text{ on } \partial\Omega \times (0, T), k = 1, 2, 3 \quad (2.3)$$

where

$$L_k u_k \equiv (u_k)_t - \sum_{i,j=1}^n (a_{ij}^k (u_k)_{x_i})_{x_j} + \sum_{i=1}^n (b_i)^k (u_k)_{x_i} + c^k u_k. \quad (2.4)$$

The functions f_i^j s represent either immigration or emigration. The first and second terms on the right hand of each equation represent the non-local interaction between two populations. For example, the terms in the right hand side of the u_1 PDE represent the non-local interaction between populations 1 and 2 and populations 1 and 3 respectively. This model was designed with a combat application in mind [52]. The main reason why the interaction terms have the form, $\int_{\Omega} \frac{u_i}{1+u_i} dx$, is to bound the states. If the interaction term was simply of the form, $\int_{\Omega} u_i dx$, and the source terms are positive then the solutions may blow up at finite time, since quadratic growth terms may cause such behavior. We need to put a bound on the cooperative interaction terms. Such cooperative terms can be seen in related work on combat coalitions [37].

The objective functional is

$$J(\alpha) = \frac{1}{2} \int_Q [K u_3^2 - L(u_2 - u_1)^2 - M \alpha^2] dxdt \quad (2.5)$$

where K , L and M are positive weighting constants, which balance the importance of the three terms. The functional is defined from the perspective of the opportunistic population 3. The second term in the integrand reflects the risk of disparity between 1 and 2. The last term reflects the cost of switching alliances. The goal is to maximize the size of population 3 while keeping the sizes of the other two populations close to equal and to minimize cost. We seek to maximize the functional over the admissible class of control space such that

$$J(\alpha^*) = \max_{\alpha \in U} J(\alpha). \quad (2.6)$$

Cosner, Lenhart and Protopopescu studied problems involving parabolic systems with nonlinear local or nonlocal interactions[10]. They proved global existence and comparison results under suitable assumptions on the interaction terms and a uniqueness result for the stationary state with some restrictions on the interaction terms, domain size and boundary conditions. They also made a comparison with an equivalent ODE system which has been used in modeling combat. Extending this model, Lenhart, Protopopescu and Stojanovic consider a two-sided game for the control of a stationary semi-linear competitive system with autonomous sources, where the controls are the kernels of the nonlocal interaction terms [36]. Lenhart and Protopopescu also studied a parabolic system with general competitive interactions as a two-player game with conflicting objectives and with controls on the source terms [35]. He, Leung and Stojanovic studied the optimal harvesting control problem governed by a time-periodic competing parabolic Volterra-Lotka system [27]. Fister also studied similar harvesting control problem of a parabolic system with Neumann boundary condition [21]. Lenhart, Protopopescu and Szpiro consider optimal control for competing coalitions. They consider the situation in which the players are grouped in two coalitions. The players of each coalition cooperate with each other in their own group, and the two coalitions compete with each other. They studied a semi-linear non-degenerate parabolic system with general nonlocal interactions, general inhomogeneous boundary conditions and distributed sources. The source terms play the role of the controls[37].

We obtain a unique optimal control in terms of the solutions to the optimality system, which consists of the state system coupled with an adjoint system. In Section 2, we prove the existence of solutions to the state system and *a priori* estimates for the state solutions. In Section 3, we prove the existence of an optimal control. The control-to-state map is differentiated to obtain the sensitivity system. Using the sensitivity system, we derive the optimality system by differentiating the objective functional with respect to the control in the fourth section. In Section 5, we prove the uniqueness of the optimal control. Finally, we show numerical results using some simple examples. The first example is the case with spatially independent control function $\alpha(t)$ and the second one is the more general form of control function $\alpha(x, t)$.

2.2 Assumptions

We make the following assumptions:

$$u_{k0}(x) \in L^\infty(\Omega), \quad \text{for } k = 1, 2, 3 \quad (2.7)$$

$$a_{ij}^k \in C^1(\overline{Q}), a_{ij}^k = a_{ji}^k \quad \text{for } k = 1, 2, 3, \quad i, j = 1, 2, 3, \dots, n \quad (2.8)$$

$$b_i^k \in C^1(\overline{Q}), c_i^k \in C(\overline{Q}) \quad \text{for } k = 1, 2, 3, \quad i = 1, 2, 3, \dots, n \quad (2.9)$$

$$\sum_{i,j=1}^n a_{ij}^k(x, t) \xi_i \xi_j \geq \theta \xi_i^2 \quad \text{for } k = 1, 2, 3, \quad \text{where } \theta > 0, \quad \text{for all } (x, t) \in Q, \xi \in R^n \quad (2.10)$$

$$a_{ij} = a_{ji} \quad \text{for all } i \neq j \quad (2.11)$$

$$f_k \in L^\infty(Q), \quad \text{for } k = 1, 2, 3 \quad \text{and} \quad f_k(x, t) \geq 0 \quad \text{for all } (x, t) \in Q. \quad (2.12)$$

The underlying state space for system (2.1)-(2.4) is $V = L^2(0, T; H_0^1(\Omega))$.

Definition 1. We define for each $t \in (0, T)$ the bilinear form in $H^1(\Omega)$:

$$a^k(t, \psi, \phi) = \int_{\Omega} \sum_{i,j=1}^n a_{ij}^k \psi_{x_i} \phi_{x_j} dx + \int_{\Omega} \sum_{i=1}^n (b_i)^k \psi_{x_i} \phi dx + \int_{\Omega} c^k \psi \phi dx$$

for $k = 1, 2, 3$.

Definition 2. (u_1, u_2, u_3) in V^3 is a solution of system (2.1) - (2.4) provided

$$\begin{aligned}
& (i) (u_1)_t, (u_2)_t, (u_3)_t \in L^2(0, T; H^{-1}(\Omega)) \\
& (ii) \int_0^T (\langle (u_1)_t, \phi_1 \rangle + a^1(t, u_1, \phi_1)) dt \\
& \quad = \int_Q (-u_1 \int_{\Omega} \frac{u_2}{1+u_2} dy + \alpha u_1 \int_{\Omega} \frac{u_3}{1+u_3} dy + f_1) \phi_1 dx dt \\
& \quad \int_0^T (\langle (u_2)_t, \phi_2 \rangle + a^2(t, u_2, \phi_2)) dt \\
& \quad = \int_Q (-u_2 \int_{\Omega} \frac{u_1}{1+u_1} dy - \alpha u_2 \int_{\Omega} \frac{u_3}{1+u_3} dy + f_2) \phi_2 dx dt \\
& \quad \int_0^T (\langle (u_3)_t, \phi_3 \rangle + a^3(t, u_3, \phi_3)) dt \\
& \quad = \int_Q (\alpha u_3 \int_{\Omega} \frac{u_1}{1+u_1} dy - \alpha u_3 \int_{\Omega} \frac{u_2}{1+u_2} dy + f_3) \phi_3 dx dt \\
& \text{for all } \phi_1, \phi_2, \phi_3 \in L^2(0, T; H_0^1(\Omega)) \text{ and,} \\
& (iii) u_1(x, 0) = u_{10}(x), u_2(x, 0) = u_{20}(x), u_3(x, 0) = u_{30}(x) \text{ for } x \in \Omega.
\end{aligned}$$

where $\langle (u_k)_t, \phi_k \rangle$ denotes duality action between $H^{-1}(\Omega)$ and $H_0^1(\Omega)$.

Remark: Since u_i for $i = 1, 2, 3$ are continuous in time, i.e., $u_i \in C([0, T]; L^2(\Omega))$ by Evans [18], the initial conditions (iii) in Definition 2 make sense in $L^2(\Omega)$.

Next, we prove the existence of solutions to the state system (2.1) - (2.4) using a fixed point method.

Theorem 1. For T sufficiently small, given control $\alpha \in U$, there exists a unique solution $u = (u_1, u_2, u_3)$ in V^3 , solving system (2.1)-(2.4) and there exists $C > 0$ such that $0 \leq u_i \leq C$ a.e..

Proof. By using a change of variables, we can rewrite the state system (2.1)-(2.4) as follows.

Let $u_1 = e^{\lambda t} w_1$, $u_2 = e^{\lambda t} w_2$, $u_3 = e^{\lambda t} w_3$, where $\lambda > 0$ is to be chosen later.

$$\begin{aligned}
\hat{L}_1 w_1 &= -w_1 \int_{\Omega} \frac{w_2}{e^{-\lambda t} + w_2} dx + \alpha w_1 \int_{\Omega} \frac{w_3}{e^{-\lambda t} + w_3} dx + e^{-\lambda t} f_1 \\
\hat{L}_2 w_2 &= -w_2 \int_{\Omega} \frac{w_1}{e^{-\lambda t} + w_1} dx - \alpha w_2 \int_{\Omega} \frac{w_3}{e^{-\lambda t} + w_3} dx + e^{-\lambda t} f_2 \\
\hat{L}_3 w_3 &= \alpha w_3 \int_{\Omega} \frac{w_1}{e^{-\lambda t} + w_1} dx - \alpha w_3 \int_{\Omega} \frac{w_2}{e^{-\lambda t} + w_2} dx + e^{-\lambda t} f_3
\end{aligned} \tag{2.13}$$

ICs:

$$w_k(x, 0) = u_{k0}(x) \text{ for } x \in \Omega, k = 1, 2, 3 \quad (2.14)$$

BCs:

$$w_k = 0 \text{ on } \partial\Omega \times (0, T), k = 1, 2, 3 \quad (2.15)$$

where

$$\hat{L}_k w_k \equiv (w_k)_t - \sum_{i,j=1}^n (a_{ij}^k (w_k)_{x_i})_{x_j} + \sum_{i=1}^n (b_i)^k (w_k)_{x_i} + (c^k + \lambda)w_k. \quad (2.16)$$

We will show the existence of solutions to the state system (2.13)-(2.16) by applying Banach's Fixed Point Theorem in the space, X^3 , where

$$X = C([0, T]; L^2(\Omega)) \cap \{W \in L^\infty(Q) | 0 \leq W \leq K_1 \text{ a.e. in } Q\},$$

with the norm

$$\|v\| = \sup_{0 \leq t \leq T} \|v(t)\|_{L^2(\Omega)} \quad \text{and} \quad K_1 \geq 2u_{i0} \quad \text{for } i = 1, 2, 3.$$

From the assumption (2.12), $f_i(t) \in L^\infty(Q)$. Let $v_i \in X$, $i = 1, 2, 3$. Then, by replacing w_i in the integrands on the right-hand side of equations (2.13) -(2.16), we obtain the following linear system of parabolic PDEs:

$$\begin{aligned} \hat{L}_1 w_1 &= -w_1 \int_{\Omega} \frac{v_2}{e^{-\lambda t} + v_2} dx + \alpha w_1 \int_{\Omega} \frac{v_3}{e^{-\lambda t} + v_3} dx + e^{-\lambda t} f_1(x, t) \\ \hat{L}_2 w_2 &= -w_2 \int_{\Omega} \frac{v_1}{e^{-\lambda t} + v_1} dx - \alpha w_2 \int_{\Omega} \frac{v_3}{e^{-\lambda t} + v_3} dx + e^{-\lambda t} f_2(x, t) \\ \hat{L}_3 w_3 &= \alpha w_3 \int_{\Omega} \frac{v_1}{e^{-\lambda t} + v_1} dx - \alpha w_3 \int_{\Omega} \frac{v_2}{e^{-\lambda t} + v_2} dx + e^{-\lambda t} f_3(x, t) \end{aligned} \quad (2.17)$$

ICs:

$$w_k(x, 0) = u_{k0}(x) \text{ for } x \in \Omega, k = 1, 2, 3 \quad (2.18)$$

BCs:

$$w_k = 0 \text{ on } \partial\Omega \times (0, T), k = 1, 2, 3 \quad (2.19)$$

Problem (2.17)-(2.19) has a unique weak solution in V^3 . Define $A : X^3 \rightarrow X^3$ by setting $A[v] = w$ where w is the solution of system (2.17)-(2.19). By Evans [18], solution $w_i \in V$ is

also in $C([0, T]; L^2(\Omega))$.

First, we show that $0 \leq w_i \leq K_1$ if $0 \leq v_i \leq K_1$ for $w = A(v)$.

From the assumption (2.12) and the PDEs (2.1), we have

$$\hat{L}_1 w_1 + g_1 w_1 = e^{-\lambda t} f_1 \geq 0$$

$$\hat{L}_2 w_2 + g_2 w_2 = e^{-\lambda t} f_2 \geq 0$$

$$\hat{L}_3 w_3 + g_3 w_3 = e^{-\lambda t} f_3 \geq 0$$

where

$$\begin{aligned} g_1 &\equiv g_1(t) = \int_{\Omega} \frac{v_2}{e^{-\lambda t} + v_2} dx - \alpha \int_{\Omega} \frac{v_3}{e^{-\lambda t} + v_3} dx \\ g_2 &\equiv g_2(t) = \int_{\Omega} \frac{v_1}{e^{-\lambda t} + v_1} dx + \alpha \int_{\Omega} \frac{v_3}{e^{-\lambda t} + v_3} dx \\ g_3 &\equiv g_3(t) = \alpha \left(\int_{\Omega} \frac{v_2}{e^{-\lambda t} + v_2} dx - \int_{\Omega} \frac{v_1}{e^{-\lambda t} + v_1} dx \right). \end{aligned}$$

Since 0 is the lower bound for the state variable v_i ,

$$\frac{v_i}{e^{-\lambda t} + v_i} < 1,$$

therefore, we have

$$\int_{\Omega} \frac{v_i}{e^{-\lambda t} + v_i} dx \leq C \quad \text{for } i = 1, 2, 3.$$

Since the control function α is also bounded, the functions g_i for $i = 1, 2, 3$ are also bounded,

i.e.,

$$\begin{aligned} |g_1| &= \left| \int_{\Omega} \frac{v_2}{e^{-\lambda t} + v_2} dx - \alpha \int_{\Omega} \frac{v_3}{e^{-\lambda t} + v_3} dx \right| \leq C_1 \\ |g_2| &= \left| \int_{\Omega} \frac{v_1}{e^{-\lambda t} + v_1} dx + \alpha \int_{\Omega} \frac{v_3}{e^{-\lambda t} + v_3} dx \right| \leq C_2 \\ |g_3| &= \left| \alpha \left(\int_{\Omega} \frac{v_2}{e^{-\lambda t} + v_2} dx - \int_{\Omega} \frac{v_1}{e^{-\lambda t} + v_1} dx \right) \right| \leq C_3 \end{aligned}$$

If we choose $\lambda > 0$ sufficiently large such that $\lambda \geq -(c^i + g_i)$ for all $i = 1, 2, 3$, we have

$$\begin{aligned}
\lambda + c^1 + \int_{\Omega} \frac{v_2}{e^{-\lambda t} + v_2} dx + \alpha \int_{\Omega} \frac{v_3}{e^{-\lambda t} + v_3} dx &\geq 0 \\
\lambda + c^2 + \int_{\Omega} \frac{v_1}{e^{-\lambda t} + v_1} dx - \alpha \int_{\Omega} \frac{v_3}{e^{-\lambda t} + v_3} dx &\geq 0 \\
\lambda + c^3 + \alpha \left(\int_{\Omega} \frac{v_1}{e^{-\lambda t} + v_1} dx - \int_{\Omega} \frac{v_2}{e^{-\lambda t} + v_2} dx \right) &\geq 0.
\end{aligned} \tag{2.20}$$

From the weak version of the Maximum Principle for parabolic operators [34], we have $w_i \geq 0$.

Next, we show $w_i \leq K_1$. Consider the following system:

$$\begin{aligned}
\tilde{L}_1 w_1 &\leq C_1 \\
\tilde{L}_2 w_2 &\leq C_2 \\
\tilde{L}_3 w_3 &\leq C_3
\end{aligned} \tag{2.21}$$

where $C_i > |e^{-\lambda t} f_i|$ for $i = 1, 2, 3$, and

$$\begin{aligned}
\tilde{L}_1 w_1 &= \hat{L}_1 w_1 + w_1 \left(\int_{\Omega} \frac{v_2}{e^{-\lambda t} + v_2} dx + \alpha \int_{\Omega} \frac{v_3}{e^{-\lambda t} + v_3} dx \right) \\
\tilde{L}_2 w_2 &= \hat{L}_2 w_2 + w_2 \left(\int_{\Omega} \frac{v_1}{e^{-\lambda t} + v_1} dx - \alpha \int_{\Omega} \frac{v_3}{e^{-\lambda t} + v_3} dx \right) \\
\tilde{L}_3 w_3 &= \hat{L}_3 w_3 + \alpha w_3 \left(\int_{\Omega} \frac{v_1}{e^{-\lambda t} + v_1} dx - \int_{\Omega} \frac{v_2}{e^{-\lambda t} + v_2} dx \right).
\end{aligned}$$

Let $W_i = w_i - C_i t$, for $i = 1, 2, 3$, then the system (2.17)-(2.19) implies

$$\begin{aligned}
\tilde{L}_1 W_1 &\leq -(\lambda + c^1 + \int_{\Omega} \frac{v_2}{e^{-\lambda t} + v_2} dx + \alpha \int_{\Omega} \frac{v_3}{e^{-\lambda t} + v_3} dx) C_1 t \\
\tilde{L}_2 W_2 &\leq -(\lambda + c^2 + \int_{\Omega} \frac{v_1}{e^{-\lambda t} + v_1} dx - \alpha \int_{\Omega} \frac{v_3}{e^{-\lambda t} + v_3} dx) C_2 t \\
\tilde{L}_3 W_3 &\leq -(\lambda + c^3 + \int_{\Omega} \frac{v_1}{e^{-\lambda t} + v_1} dx - \int_{\Omega} \frac{v_2}{e^{-\lambda t} + v_2} dx) C_3 t
\end{aligned} \tag{2.22}$$

ICs:

$$W_i = w_i = u_{i0} \tag{2.23}$$

BCs:

$$W_i = -C_1 t \leq 0 \quad \text{on } \partial\Omega \times (0, T), \quad i = 1, 2, 3 \quad (2.24)$$

By the extension of the Maximum Principle to weak solutions [34],

$w_i - C_i t = W_i \leq \max |u_{i0}|$, and therefore $w_i \leq \max |u_{i0}| + C_i t$.

For $t \leq \frac{K_1}{2C_i}$, $w_i \leq \frac{K_1}{2} + \frac{K_1}{2} = K_1$.

By choosing $T < \min_i \frac{K_1}{2C_i}$, we have $w_i \leq K_1$ for $i = 1, 2, 3$.

Next, we prove that if $T > 0$ is small enough, then, the mapping A is a strict contraction.

Choose $v, \tilde{v} \in X^3$, and define $w = A[v]$, $\tilde{w} = A[\tilde{v}]$.

We subtract the bilinear forms of w_i and \tilde{w}_i . The equation for $w_1 - \tilde{w}_1$ is illustrated below.

$$\begin{aligned} & \int_Q ((w_1 - \tilde{w}_1)_t \phi + \sum_{i,j=1}^n a_{ij}^1 (w_1 - \tilde{w}_1)_{x_i} \phi_{x_j} + \sum_{i=1}^n b_i^1 (w_1 - \tilde{w}_1)_{x_i} \phi + (c^1 + \lambda)(w_1 - \tilde{w}_1) \phi) dx dt \\ &= - \int_Q (w_1 \int_{\Omega} \frac{v_2}{e^{-\lambda t} + v_2} dy - \tilde{w}_1 \int_{\Omega} \frac{\tilde{v}_2}{e^{-\lambda t} + \tilde{v}_2} dy) \phi dx dt \\ & \quad + \int_Q (\alpha w_1 \int_{\Omega} \frac{v_3}{e^{-\lambda t} + v_3} dy - \alpha \tilde{w}_1 \int_{\Omega} \frac{\tilde{v}_3}{e^{-\lambda t} + \tilde{v}_3} dy) \phi dx dt \\ &= - \int_Q [(w_1 - \tilde{w}_1) (\int_{\Omega} \frac{v_2}{e^{-\lambda t} + v_2} dy + \tilde{w}_1 \int_{\Omega} \frac{e^{-\lambda t} (v_2 - \tilde{v}_2)}{(e^{-\lambda t} + v_2)(e^{-\lambda t} + \tilde{v}_2)} dy) \\ & \quad - (\alpha w_1 - \alpha \tilde{w}_1) \int_{\Omega} \frac{v_3}{e^{-\lambda t} + v_3} dy - \alpha \tilde{w}_1 \int_{\Omega} \frac{e^{-\lambda t} (v_3 - \tilde{v}_3)}{(e^{-\lambda t} + v_3)(e^{-\lambda t} + \tilde{v}_3)} dy)] \phi dx dt \end{aligned}$$

where $\phi \in L^2(0, T; H_0^1(\Omega))$. We can get similar expressions for $w_2 - \tilde{w}_2$ and $w_3 - \tilde{w}_3$.

By using test functions $w_i - \tilde{w}_i$ in the corresponding equations and using $\frac{d}{dt} \frac{(w_k - \tilde{w}_k)^2}{2} =$

$(w_k - \tilde{w}_k)((w_k - \tilde{w}_k)_t$ in weak sense, we obtain for $0 \leq s \leq T$, $Q_s = \Omega \times (0, s)$,

$$\begin{aligned}
& \frac{1}{2} \int_{\Omega \times \{t=s\}} ((w_1 - \tilde{w}_1)^2 + (w_2 - \tilde{w}_2)^2 + (w_3 - \tilde{w}_3)^2) dx + \int_{Q_s} \left(\sum_{i,j=1}^n a_{ij}^1 (w_1 - \tilde{w}_1)_{x_i} (w_1 - \tilde{w}_1)_{x_j} \right. \\
& \quad + \sum_{i,j=1}^n a_{ij}^2 (w_2 - \tilde{w}_2)_{x_i} (w_2 - \tilde{w}_2)_{x_j} + \sum_{i,j=1}^n a_{ij}^3 (w_3 - \tilde{w}_3)_{x_i} (w_3 - \tilde{w}_3)_{x_j} \Big) dx dt \\
& + \int_{Q_s} \left(\sum_{i=1}^n b_i^1 (w_1 - \tilde{w}_1)_{x_i} (w_1 - \tilde{w}_1) + \sum_{i=1}^n b_i^2 (w_2 - \tilde{w}_2)_{x_i} (w_2 - \tilde{w}_2) \right. \\
& \quad \left. + \sum_{i=1}^n b_i^3 (w_3 - \tilde{w}_3)_{x_i} (w_3 - \tilde{w}_3) \right) dx dt \\
& + \int_{Q_s} ((c^1 + \lambda)(w_1 - \tilde{w}_1)^2 + (c^2 + \lambda)(w_2 - \tilde{w}_2)^2 + (c^3 + \lambda)(w_3 - \tilde{w}_3)^2) dx dt \\
& = - \int_{Q_s} ((w_1 - \tilde{w}_1)^2 \int_{\Omega} \frac{v_2}{e^{-\lambda t} + v_2} dy + \tilde{w}_1 (w_1 - \tilde{w}_1) \int_{\Omega} \left(\frac{v_2}{e^{-\lambda t} + v_2} - \frac{\tilde{v}_2}{e^{-\lambda t} + \tilde{v}_2} \right) dy) dx dt \\
& + \int_{Q_s} \alpha ((w_1 - \tilde{w}_1)^2 \int_{\Omega} \frac{v_3}{e^{-\lambda t} + v_3} dy + \tilde{w}_1 (w_1 - \tilde{w}_1) \int_{\Omega} \left(\frac{v_3}{e^{-\lambda t} + v_3} - \frac{\tilde{v}_3}{e^{-\lambda t} + \tilde{v}_3} \right) dy) dx dt \\
& - \int_{Q_s} ((w_2 - \tilde{w}_2)^2 \int_{\Omega} \frac{v_1}{e^{-\lambda t} + v_1} dy + \tilde{w}_2 (w_2 - \tilde{w}_2) \int_{\Omega} \left(\frac{v_1}{e^{-\lambda t} + v_1} - \frac{\tilde{v}_1}{e^{-\lambda t} + \tilde{v}_1} \right) dy) dx dt \\
& - \int_{Q_s} \alpha ((w_2 - \tilde{w}_2)^2 \int_{\Omega} \frac{v_3}{e^{-\lambda t} + v_3} dy + \tilde{w}_2 (w_2 - \tilde{w}_2) \int_{\Omega} \left(\frac{v_3}{e^{-\lambda t} + v_3} - \frac{\tilde{v}_3}{e^{-\lambda t} + \tilde{v}_3} \right) dy) dx dt \\
& + \int_{Q_s} \alpha ((w_3 - \tilde{w}_3)^2 \int_{\Omega} \frac{v_1}{e^{-\lambda t} + v_1} dy + \tilde{w}_3 (w_3 - \tilde{w}_3) \int_{\Omega} \left(\frac{v_1}{e^{-\lambda t} + v_1} - \frac{\tilde{v}_1}{e^{-\lambda t} + \tilde{v}_1} \right) dy) dx dt \\
& - \int_{Q_s} \alpha ((w_3 - \tilde{w}_3)^2 \int_{\Omega} \frac{v_2}{e^{-\lambda t} + v_2} dy + \tilde{w}_3 (w_3 - \tilde{w}_3) \int_{\Omega} \left(\frac{v_2}{e^{-\lambda t} + v_2} - \frac{\tilde{v}_2}{e^{-\lambda t} + \tilde{v}_2} \right) dy) dx dt \\
& = - \int_{Q_s} ((w_1 - \tilde{w}_1)^2 \int_{\Omega} \frac{v_2}{e^{-\lambda t} + v_2} dy + \tilde{w}_1 (w_1 - \tilde{w}_1) \int_{\Omega} \frac{e^{-\lambda t} (v_2 - \tilde{v}_2)}{(e^{-\lambda t} + v_2)(e^{-\lambda t} + \tilde{v}_2)} dy) dx dt \\
& + \int_{Q_s} \alpha ((w_1 - \tilde{w}_1)^2 \int_{\Omega} \frac{v_3}{e^{-\lambda t} + v_3} dy + \tilde{w}_1 (w_1 - \tilde{w}_1) \int_{\Omega} \frac{e^{-\lambda t} (v_3 - \tilde{v}_3)}{(e^{-\lambda t} + v_3)(e^{-\lambda t} + \tilde{v}_3)} dy) dx dt \\
& - \int_{Q_s} ((w_2 - \tilde{w}_2)^2 \int_{\Omega} \frac{v_1}{e^{-\lambda t} + v_1} dy + \tilde{w}_2 (w_2 - \tilde{w}_2) \int_{\Omega} \frac{e^{-\lambda t} (v_1 - \tilde{v}_1)}{(e^{-\lambda t} + v_1)(e^{-\lambda t} + \tilde{v}_1)} dy) dx dt \\
& - \int_{Q_s} \alpha ((w_2 - \tilde{w}_2)^2 \int_{\Omega} \frac{v_3}{e^{-\lambda t} + v_3} dy + \tilde{w}_2 (w_2 - \tilde{w}_2) \int_{\Omega} \frac{e^{-\lambda t} (v_3 - \tilde{v}_3)}{(e^{-\lambda t} + v_3)(e^{-\lambda t} + \tilde{v}_3)} dy) dx dt \\
& + \int_{Q_s} \alpha ((w_3 - \tilde{w}_3)^2 \int_{\Omega} \frac{v_1}{e^{-\lambda t} + v_1} dy + \tilde{w}_3 (w_3 - \tilde{w}_3) \int_{\Omega} \frac{e^{-\lambda t} (v_1 - \tilde{v}_1)}{(e^{-\lambda t} + v_1)(e^{-\lambda t} + \tilde{v}_1)} dy) dx dt \\
& - \int_{Q_s} \alpha ((w_3 - \tilde{w}_3)^2 \int_{\Omega} \frac{v_2}{e^{-\lambda t} + v_2} dy + \tilde{w}_3 (w_3 - \tilde{w}_3) \int_{\Omega} \frac{e^{-\lambda t} (v_2 - \tilde{v}_2)}{(e^{-\lambda t} + v_2)(e^{-\lambda t} + \tilde{v}_2)} dy) dx dt
\end{aligned}$$

Using uniform ellipticity, we have

$$\begin{aligned}
& \frac{1}{2} \int_{\Omega \times \{t=s\}} (|w_1 - \tilde{w}_1|^2 + |w_2 - \tilde{w}_2|^2 + |w_3 - \tilde{w}_3|^2) dx \\
& + \theta \int_{Q_s} (|\nabla (w_1 - \tilde{w}_1)|^2 + |\nabla (w_2 - \tilde{w}_2)|^2 + |\nabla (w_3 - \tilde{w}_3)|^2) dx dt \\
& + \int_{Q_s} ((c^1 + \lambda)|w_1 - \tilde{w}_1|^2 + (c^2 + \lambda)|w_2 - \tilde{w}_2|^2 + (c^3 + \lambda)|w_3 - \tilde{w}_3|^2) dx dt \\
\leq & \int_{Q_s} (|w_1 - \tilde{w}_1|^2 \int_{\Omega} \left| \frac{v_2}{e^{-\lambda t} + v_2} \right| dy + |\tilde{w}_1| |w_1 - \tilde{w}_1| \int_{\Omega} \frac{e^{-\lambda t} |v_2 - \tilde{v}_2|}{|e^{-\lambda t} + v_2| |e^{-\lambda t} + \tilde{v}_2|} dy) dx dt \\
& + \int_{Q_s} |\alpha| (|w_1 - \tilde{w}_1|^2 \int_{\Omega} \left| \frac{v_3}{e^{-\lambda t} + v_3} \right| dy + |\tilde{w}_1| |w_1 - \tilde{w}_1| \int_{\Omega} \frac{e^{-\lambda t} |v_3 - \tilde{v}_3|}{|e^{-\lambda t} + v_3| |e^{-\lambda t} + \tilde{v}_3|} dy) dx dt \\
& + \int_{Q_s} (|w_2 - \tilde{w}_2|^2 \int_{\Omega} \left| \frac{v_1}{e^{-\lambda t} + v_1} \right| dy + |\tilde{w}_2| |w_2 - \tilde{w}_2| \int_{\Omega} \frac{e^{-\lambda t} |v_1 - \tilde{v}_1|}{|e^{-\lambda t} + v_1| |e^{-\lambda t} + \tilde{v}_1|} dy) dx dt \\
& + \int_{Q_s} |\alpha| (|w_2 - \tilde{w}_2|^2 \int_{\Omega} \left| \frac{v_3}{e^{-\lambda t} + v_3} \right| dy + |\tilde{w}_2| |w_2 - \tilde{w}_2| \int_{\Omega} \frac{e^{-\lambda t} |v_3 - \tilde{v}_3|}{|e^{-\lambda t} + v_3| |e^{-\lambda t} + \tilde{v}_3|} dy) dx dt \\
& + \int_{Q_s} |\alpha| (|w_3 - \tilde{w}_3|^2 \int_{\Omega} \left| \frac{v_1}{e^{-\lambda t} + v_1} \right| dy + |\tilde{w}_3| |w_3 - \tilde{w}_3| \int_{\Omega} \frac{e^{-\lambda t} |v_1 - \tilde{v}_1|}{|e^{-\lambda t} + v_1| |e^{-\lambda t} + \tilde{v}_1|} dy) dx dt \\
& + \int_{Q_s} |\alpha| (|w_3 - \tilde{w}_3|^2 \int_{\Omega} \left| \frac{v_2}{e^{-\lambda t} + v_2} \right| dy + |\tilde{w}_3| |w_3 - \tilde{w}_3| \int_{\Omega} \frac{e^{-\lambda t} |v_2 - \tilde{v}_2|}{|e^{-\lambda t} + v_2| |e^{-\lambda t} + \tilde{v}_2|} dy) dx dt \\
& + \int_{Q_s} \sum_{i=1}^n (|b_i^1| |(w_1 - \tilde{w}_1)_{x_i}| |w_1 - \tilde{w}_1| + |b_i^2| |(w_2 - \tilde{w}_2)_{x_i}| |w_2 - \tilde{w}_2| \\
& \quad + |b_i^3| |(w_3 - \tilde{w}_3)_{x_i}| |w_3 - \tilde{w}_3|) dx dt \\
\leq & \int_{Q_s} (|w_1 - \tilde{w}_1|^2 \int_{\Omega} \left| \frac{v_2}{e^{-\lambda t} + v_2} \right| dy + |\tilde{w}_1| |w_1 - \tilde{w}_1| \int_{\Omega} \frac{e^{-\lambda t} |v_2 - \tilde{v}_2|}{|e^{-\lambda t} + v_2| |e^{-\lambda t} + \tilde{v}_2|} dy) dx dt \\
& + \int_{Q_s} |\alpha| (|w_1 - \tilde{w}_1|^2 \int_{\Omega} \left| \frac{v_3}{e^{-\lambda t} + v_3} \right| dy + |\tilde{w}_1| |w_1 - \tilde{w}_1| \int_{\Omega} \frac{e^{-\lambda t} |v_3 - \tilde{v}_3|}{|e^{-\lambda t} + v_3| |e^{-\lambda t} + \tilde{v}_3|} dy) dx dt \\
& + \int_{Q_s} (|w_2 - \tilde{w}_2|^2 \int_{\Omega} \left| \frac{v_1}{e^{-\lambda t} + v_1} \right| dy + |\tilde{w}_2| |w_2 - \tilde{w}_2| \int_{\Omega} \frac{e^{-\lambda t} |v_1 - \tilde{v}_1|}{|e^{-\lambda t} + v_1| |e^{-\lambda t} + \tilde{v}_1|} dy) dx dt \\
& + \int_{Q_s} |\alpha| (|w_2 - \tilde{w}_2|^2 \int_{\Omega} \left| \frac{v_3}{e^{-\lambda t} + v_3} \right| dy + |\tilde{w}_2| |w_2 - \tilde{w}_2| \int_{\Omega} \frac{e^{-\lambda t} |v_3 - \tilde{v}_3|}{|e^{-\lambda t} + v_3| |e^{-\lambda t} + \tilde{v}_3|} dy) dx dt \\
& + \int_{Q_s} |\alpha| (|w_3 - \tilde{w}_3|^2 \int_{\Omega} \left| \frac{v_1}{e^{-\lambda t} + v_1} \right| dy + |\tilde{w}_3| |w_3 - \tilde{w}_3| \int_{\Omega} \frac{e^{-\lambda t} |v_1 - \tilde{v}_1|}{|e^{-\lambda t} + v_1| |e^{-\lambda t} + \tilde{v}_1|} dy) dx dt \\
& + \int_{Q_s} |\alpha| (|w_3 - \tilde{w}_3|^2 \int_{\Omega} \left| \frac{v_2}{e^{-\lambda t} + v_2} \right| dy + |\tilde{w}_3| |w_3 - \tilde{w}_3| \int_{\Omega} \frac{e^{-\lambda t} |v_2 - \tilde{v}_2|}{|e^{-\lambda t} + v_2| |e^{-\lambda t} + \tilde{v}_2|} dy) dx dt \\
& + C_1 \int_{Q_s} (|\nabla (w_1 - \tilde{w}_1)| |w_1 - \tilde{w}_1| + |\nabla (w_2 - \tilde{w}_2)| |w_2 - \tilde{w}_2| \\
& \quad + |\nabla (w_3 - \tilde{w}_3)| |w_3 - \tilde{w}_3|) dx dt.
\end{aligned}$$

Applying Cauchy's inequality with ε on the last integral of the right-hand side of above expression, we have

$$\begin{aligned}
& \frac{1}{2} \int_{\Omega \times \{t=s\}} (|w_1 - \tilde{w}_1|^2 + |w_2 - \tilde{w}_2|^2 + |w_3 - \tilde{w}_3|^2) dx \\
& + \theta \int_{Q_s} (|\nabla (w_1 - \tilde{w}_1)|^2 + |\nabla (w_2 - \tilde{w}_2)|^2 + |\nabla (w_3 - \tilde{w}_3)|^2) dx dt \\
& + \int_{Q_s} ((c^1 + \lambda)|w_1 - \tilde{w}_1|^2 + (c^2 + \lambda)|w_2 - \tilde{w}_2|^2 + (c^3 + \lambda)|w_3 - \tilde{w}_3|^2) dx dt \\
\leq & \int_{Q_s} (|w_1 - \tilde{w}_1|^2 \int_{\Omega} \left| \frac{v_2}{e^{-\lambda t} + v_2} \right| dy + |\tilde{w}_1| |w_1 - \tilde{w}_1| \int_{\Omega} \frac{e^{-\lambda t} |v_2 - \tilde{v}_2|}{|e^{-\lambda t} + v_2| |e^{-\lambda t} + \tilde{v}_2|} dy) dx dt \\
& + \int_{Q_s} |\alpha| (|w_1 - \tilde{w}_1|^2 \int_{\Omega} \left| \frac{v_3}{e^{-\lambda t} + v_3} \right| dy + |\tilde{w}_1| |w_1 - \tilde{w}_1| \int_{\Omega} \frac{e^{-\lambda t} |v_3 - \tilde{v}_3|}{|e^{-\lambda t} + v_3| |e^{-\lambda t} + \tilde{v}_3|} dy) dx dt \\
& + \int_{Q_s} (|w_2 - \tilde{w}_2|^2 \int_{\Omega} \left| \frac{v_1}{e^{-\lambda t} + v_1} \right| dy + |\tilde{w}_2| |w_2 - \tilde{w}_2| \int_{\Omega} \frac{e^{-\lambda t} |v_1 - \tilde{v}_1|}{|e^{-\lambda t} + v_1| |e^{-\lambda t} + \tilde{v}_1|} dy) dx dt \\
& + \int_{Q_s} |\alpha| (|w_2 - \tilde{w}_2|^2 \int_{\Omega} \left| \frac{v_3}{e^{-\lambda t} + v_3} \right| dy + |\tilde{w}_2| |w_2 - \tilde{w}_2| \int_{\Omega} \frac{e^{-\lambda t} |v_3 - \tilde{v}_3|}{|e^{-\lambda t} + v_3| |e^{-\lambda t} + \tilde{v}_3|} dy) dx dt \\
& + \int_{Q_s} |\alpha| (|w_3 - \tilde{w}_3|^2 \int_{\Omega} \left| \frac{v_1}{e^{-\lambda t} + v_1} \right| dy + |\tilde{w}_3| |w_3 - \tilde{w}_3| \int_{\Omega} \frac{e^{-\lambda t} |v_1 - \tilde{v}_1|}{|e^{-\lambda t} + v_1| |e^{-\lambda t} + \tilde{v}_1|} dy) dx dt \\
& + \int_{Q_s} |\alpha| (|w_3 - \tilde{w}_3|^2 \int_{\Omega} \left| \frac{v_2}{e^{-\lambda t} + v_2} \right| dy + |\tilde{w}_3| |w_3 - \tilde{w}_3| \int_{\Omega} \frac{e^{-\lambda t} |v_2 - \tilde{v}_2|}{|e^{-\lambda t} + v_2| |e^{-\lambda t} + \tilde{v}_2|} dy) dx dt \\
& + C_1 \varepsilon \int_{Q_s} (|\nabla (w_1 - \tilde{w}_1)|^2 + |\nabla (w_2 - \tilde{w}_2)|^2 + |\nabla (w_3 - \tilde{w}_3)|^2) dx dt \\
& + \frac{C_1}{4\varepsilon} \int_{Q_s} (|w_1 - \tilde{w}_1|^2 + |w_2 - \tilde{w}_2|^2 + |w_3 - \tilde{w}_3|^2) dx dt.
\end{aligned}$$

By choosing $\varepsilon = \frac{\theta}{2C_1}$ and combining like terms, we obtain

$$\begin{aligned}
& \frac{1}{2} \int_{\Omega \times \{t=s\}} (|w_1 - \tilde{w}_1|^2 + |w_2 - \tilde{w}_2|^2 + |w_3 - \tilde{w}_3|^2) dx \\
& + \frac{\theta}{2} \int_{Q_s} (|\nabla (w_1 - \tilde{w}_1)|^2 + |\nabla (w_2 - \tilde{w}_2)|^2 + |\nabla (w_3 - \tilde{w}_3)|^2) dx dt \\
& + \int_{Q_s} (-C_2 + \lambda)(|w_1 - \tilde{w}_1|^2 + |w_2 - \tilde{w}_2|^2 + |w_3 - \tilde{w}_3|^2) dx dt \\
\leq & \int_{Q_s} (|w_1 - \tilde{w}_1|^2 \int_{\Omega} \left| \frac{v_2}{e^{-\lambda t} + v_2} \right| dy + |\tilde{w}_1| |w_1 - \tilde{w}_1| \int_{\Omega} \frac{e^{-\lambda t} |v_2 - \tilde{v}_2|}{|e^{-\lambda t} + v_2| |e^{-\lambda t} + \tilde{v}_2|} dy) dx dt \\
& + \int_{Q_s} |\alpha| (|w_1 - \tilde{w}_1|^2 \int_{\Omega} \left| \frac{v_3}{e^{-\lambda t} + v_3} \right| dy + |\tilde{w}_1| |w_1 - \tilde{w}_1| \int_{\Omega} \frac{e^{-\lambda t} |v_3 - \tilde{v}_3|}{|e^{-\lambda t} + v_3| |e^{-\lambda t} + \tilde{v}_3|} dy) dx dt \\
& + \int_{Q_s} (|w_2 - \tilde{w}_2|^2 \int_{\Omega} \left| \frac{v_1}{e^{-\lambda t} + v_1} \right| dy + |\tilde{w}_2| |w_2 - \tilde{w}_2| \int_{\Omega} \frac{e^{-\lambda t} |v_1 - \tilde{v}_1|}{|e^{-\lambda t} + v_1| |e^{-\lambda t} + \tilde{v}_1|} dy) dx dt \\
& + \int_{Q_s} |\alpha| (|w_2 - \tilde{w}_2|^2 \int_{\Omega} \left| \frac{v_3}{e^{-\lambda t} + v_3} \right| dy + |\tilde{w}_2| |w_2 - \tilde{w}_2| \int_{\Omega} \frac{e^{-\lambda t} |v_3 - \tilde{v}_3|}{|e^{-\lambda t} + v_3| |e^{-\lambda t} + \tilde{v}_3|} dy) dx dt \\
& + \int_{Q_s} |\alpha| (|w_3 - \tilde{w}_3|^2 \int_{\Omega} \left| \frac{v_1}{e^{-\lambda t} + v_1} \right| dy + |\tilde{w}_3| |w_3 - \tilde{w}_3| \int_{\Omega} \frac{e^{-\lambda t} |v_1 - \tilde{v}_1|}{|e^{-\lambda t} + v_1| |e^{-\lambda t} + \tilde{v}_1|} dy) dx dt \\
& + \int_{Q_s} |\alpha| (|w_3 - \tilde{w}_3|^2 \int_{\Omega} \left| \frac{v_2}{e^{-\lambda t} + v_2} \right| dy + |\tilde{w}_3| |w_3 - \tilde{w}_3| \int_{\Omega} \frac{e^{-\lambda t} |v_2 - \tilde{v}_2|}{|e^{-\lambda t} + v_2| |e^{-\lambda t} + \tilde{v}_2|} dy) dx dt \\
& + C_3 \int_{Q_s} (|w_1 - \tilde{w}_1|^2 + |w_2 - \tilde{w}_2|^2 + |w_3 - \tilde{w}_3|^2) dx dt
\end{aligned}$$

where $-C_2$ is a lower bound on c^i for $i = 1, 2, 3$.

Since $|\alpha| \leq \overline{M}$, and $|\tilde{w}_i| \leq K_1$,

$$\begin{aligned}
& \frac{1}{2} \int_{\Omega \times \{t=s\}} (|w_1 - \tilde{w}_1|^2 + |w_2 - \tilde{w}_2|^2 + |w_3 - \tilde{w}_3|^2) dx \\
& + \int_{Q_s} (-C_2 + \lambda)(|w_1 - \tilde{w}_1|^2 + |w_2 - \tilde{w}_2|^2 + |w_3 - \tilde{w}_3|^2) dx dt \\
& \leq \int_{Q_s} (|w_1 - \tilde{w}_1|^2 \int_{\Omega} \left| \frac{v_2}{e^{-\lambda t} + v_2} \right| dy + K_1 |w_1 - \tilde{w}_1| \int_{\Omega} \frac{e^{-\lambda t} |v_2 - \tilde{v}_2|}{|e^{-\lambda t} + v_2| |e^{-\lambda t} + \tilde{v}_2|} dy) dx dt \\
& + \int_{Q_s} \overline{M} (|w_1 - \tilde{w}_1|^2 \int_{\Omega} \left| \frac{v_3}{e^{-\lambda t} + v_3} \right| dy + K_1 |w_1 - \tilde{w}_1| \int_{\Omega} \frac{e^{-\lambda t} |v_3 - \tilde{v}_3|}{|e^{-\lambda t} + v_3| |e^{-\lambda t} + \tilde{v}_3|} dy) dx dt \\
& + \int_{Q_s} (|w_2 - \tilde{w}_2|^2 \int_{\Omega} \left| \frac{v_1}{e^{-\lambda t} + v_1} \right| dy + K_1 |w_2 - \tilde{w}_2| \int_{\Omega} \frac{e^{-\lambda t} |v_1 - \tilde{v}_1|}{|e^{-\lambda t} + v_1| |e^{-\lambda t} + \tilde{v}_1|} dy) dx dt \\
& + \int_{Q_s} \overline{M} (|w_2 - \tilde{w}_2|^2 \int_{\Omega} \left| \frac{v_3}{e^{-\lambda t} + v_3} \right| dy + K_1 |w_2 - \tilde{w}_2| \int_{\Omega} \frac{e^{-\lambda t} |v_3 - \tilde{v}_3|}{|e^{-\lambda t} + v_3| |e^{-\lambda t} + \tilde{v}_3|} dy) dx dt \\
& + \int_{Q_s} \overline{M} (|w_3 - \tilde{w}_3|^2 \int_{\Omega} \left| \frac{v_1}{e^{-\lambda t} + v_1} \right| dy + K_1 |w_3 - \tilde{w}_3| \int_{\Omega} \frac{e^{-\lambda t} |v_1 - \tilde{v}_1|}{|e^{-\lambda t} + v_1| |e^{-\lambda t} + \tilde{v}_1|} dy) dx dt \\
& + \int_{Q_s} \overline{M} (|w_3 - \tilde{w}_3|^2 \int_{\Omega} \left| \frac{v_2}{e^{-\lambda t} + v_2} \right| dy + K_1 |w_3 - \tilde{w}_3| \int_{\Omega} \frac{e^{-\lambda t} |v_2 - \tilde{v}_2|}{|e^{-\lambda t} + v_2| |e^{-\lambda t} + \tilde{v}_2|} dy) dx dt \\
& + C_3 \int_{Q_s} (|w_1 - \tilde{w}_1|^2 + |w_2 - \tilde{w}_2|^2 + |w_3 - \tilde{w}_3|^2) dx dt.
\end{aligned}$$

Since $v_i \geq 0$, the terms of the form $\left| \frac{v_i}{e^{-\lambda t} + v_i} \right|$, for $i = 1, 2, 3$ are bounded by 1. Similarly, using the positivity of v_i 's, we have $\frac{e^{-\lambda t}}{|e^{-\lambda t} + v_i| |e^{-\lambda t} + \tilde{v}_i|} \leq \frac{1}{e^{-\lambda t}} \leq e^{\lambda T}$ for $i = 1, 2, 3$. By

using these estimates, we have

$$\begin{aligned}
& \frac{1}{2} \int_{\Omega \times \{t=s\}} (|w_1 - \tilde{w}_1|^2 + |w_2 - \tilde{w}_2|^2 + |w_3 - \tilde{w}_3|^2) dx \\
& + \int_{Q_s} (-C_2 + \lambda)(|w_1 - \tilde{w}_1|^2 + |w_2 - \tilde{w}_2|^2 + |w_3 - \tilde{w}_3|^2) dx dt \\
& \leq K_1 \int_{Q_s} |w_1 - \tilde{w}_1| \left(\int_{\Omega} \frac{|v_2 - \tilde{v}_2|}{|e^{-\lambda t} + v_2||e^{-\lambda t} + \tilde{v}_2|} dy + \bar{M} \int_{\Omega} \frac{|v_3 - \tilde{v}_3|}{|e^{-\lambda t} + v_3||e^{-\lambda t} + \tilde{v}_3|} dy \right) dx dt \\
& + K_1 \int_{Q_s} |w_2 - \tilde{w}_2| \left(\int_{\Omega} \frac{|v_1 - \tilde{v}_1|}{|e^{-\lambda t} + v_1||e^{-\lambda t} + \tilde{v}_1|} dy + \bar{M} \int_{\Omega} \frac{|v_3 - \tilde{v}_3|}{|e^{-\lambda t} + v_3||e^{-\lambda t} + \tilde{v}_3|} dy \right) dx dt \\
& + K_1 \bar{M} \int_{Q_s} |w_3 - \tilde{w}_3| \left(\int_{\Omega} \frac{|v_1 - \tilde{v}_1|}{|e^{-\lambda t} + v_1||e^{-\lambda t} + \tilde{v}_1|} dy + \int_{\Omega} \frac{|v_2 - \tilde{v}_2|}{|e^{-\lambda t} + v_2||e^{-\lambda t} + \tilde{v}_2|} dy \right) dx dt \\
& + C_3 \int_{Q_s} (|w_1 - \tilde{w}_1|^2 + |w_2 - \tilde{w}_2|^2 + |w_3 - \tilde{w}_3|^2) dx dt \\
& \leq K_1 e^{\lambda T} \int_{Q_s} |w_1 - \tilde{w}_1| \left(\int_{\Omega} |v_2 - \tilde{v}_2| dy + \bar{M} e \int_{\Omega} |v_3 - \tilde{v}_3| dy \right) dx dt \\
& + K_1 e^{\lambda T} \int_{Q_s} |w_2 - \tilde{w}_2| \left(\int_{\Omega} |v_1 - \tilde{v}_1| dy + \bar{M} \int_{\Omega} |v_3 - \tilde{v}_3| dy \right) dx dt \\
& + K_1 \bar{M} e^{\lambda T} \int_{Q_s} |w_3 - \tilde{w}_3| \left(\int_{\Omega} |v_1 - \tilde{v}_1| dy + \int_{\Omega} |v_2 - \tilde{v}_2| dy \right) dx dt \\
& + C_3 \int_{Q_s} (|w_1 - \tilde{w}_1|^2 + |w_2 - \tilde{w}_2|^2 + |w_3 - \tilde{w}_3|^2) dx dt \\
& \leq K_1 e^{\lambda T} \int_{Q_s} |w_1 - \tilde{w}_1| \left(\sup_{0 \leq t \leq T} \int_{\Omega} |v_2 - \tilde{v}_2| dy + \bar{M} \sup_{0 \leq t \leq T} \int_{\Omega} |v_3 - \tilde{v}_3| dy \right) dx dt \\
& + K_1 e^{\lambda T} \int_{Q_s} |w_2 - \tilde{w}_2| \left(\sup_{0 \leq t \leq T} \int_{\Omega} |v_1 - \tilde{v}_1| dy + K_1 \bar{M} \sup_{0 \leq t \leq T} \int_{\Omega} |v_3 - \tilde{v}_3| dy \right) dx dt \\
& + K_1 \bar{M} e^{\lambda T} \int_{Q_s} |w_3 - \tilde{w}_3| \left(\sup_{0 \leq t \leq T} \int_{\Omega} |v_1 - \tilde{v}_1| dy + K_1 \bar{M} \sup_{0 \leq t \leq T} \int_{\Omega} |v_2 - \tilde{v}_2| dy \right) dx dt \\
& + C_3 \int_{Q_s} (|w_1 - \tilde{w}_1|^2 + |w_2 - \tilde{w}_2|^2 + |w_3 - \tilde{w}_3|^2) dx dt
\end{aligned}$$

Applying Cauchy's inequality on the K_1 terms of the right-hand side, we have

$$\begin{aligned}
& \frac{1}{2} \int_{\Omega \times \{t=s\}} (|w_1 - \tilde{w}_1|^2 + |w_2 - \tilde{w}_2|^2 + |w_3 - \tilde{w}_3|^2) dx \\
& + \int_{Q_s} ((c^1 + \lambda)|w_1 - \tilde{w}_1|^2 + (c^2 + \lambda)|w_2 - \tilde{w}_2|^2 + (c^3 + \lambda)|w_3 - \tilde{w}_3|^2) dx dt \\
& \leq K_1(1 + \bar{M})e^{\lambda T} \int_{Q_s} (|w_1 - \tilde{w}_1|^2 + |w_2 - \tilde{w}_2|^2) dx dt \\
& + K_1(1 + \bar{M})e^{\lambda T} \int_{Q_s} ((\sup_{0 \leq t \leq T} \int_{\Omega} |v_1 - \tilde{v}_1| dy)^2 + (\sup_{0 \leq t \leq T} \int_{\Omega} |v_2 - \tilde{v}_2| dy)^2) dx dt \\
& + 2K_1\bar{M}e^{\lambda T} \int_{Q_s} (|w_3 - \tilde{w}_3|^2 + (\sup_{0 \leq t \leq T} \int_{\Omega} |v_3 - \tilde{v}_3| dy)^2) dx dt \\
& + C_3 \int_{Q_s} (|w_1 - \tilde{w}_1|^2 + |w_2 - \tilde{w}_2|^2 + |w_3 - \tilde{w}_3|^2) dx
\end{aligned}$$

By rearranging the terms in the above estimates, we have,

$$\begin{aligned}
& \frac{1}{2} \int_{\Omega \times \{t=s\}} (|w_1 - \tilde{w}_1|^2 + |w_2 - \tilde{w}_2|^2 + |w_3 - \tilde{w}_3|^2) dx \\
& + \int_{Q_s} (-C_2 + \lambda - K_1(1 + \bar{M})e^{\lambda T} - C_3)|w_1 - \tilde{w}_1|^2 \\
& + (-C_2 + \lambda - K_1(1 + \bar{M})e^{\lambda T} - C_3)|w_2 - \tilde{w}_2|^2 \\
& + (-C_2 + \lambda - 2K_1\bar{M}e^{\lambda T} - C_3)|w_3 - \tilde{w}_3|^2) dx dt \\
& \leq C_4K_1e^{\lambda T} \int_{Q_s} [(\sup_{0 \leq t \leq T} \int_{\Omega} |v_1 - \tilde{v}_1| dy)^2 + (\sup_{0 \leq t \leq T} \int_{\Omega} |v_2 - \tilde{v}_2| dy)^2 \\
& + (\sup_{0 \leq t \leq T} \int_{\Omega} |v_3 - \tilde{v}_3| dy)^2] dx dt
\end{aligned}$$

Since $K_1(1 + \bar{M})e^{\lambda T} + C_2 + C_3 \leq C_5K_1e^{\lambda T}$ and $2K_1\bar{M}e^{\lambda T} + C_2 + C_3 \leq C_5K_1e^{\lambda T}$ for

some C_5 ,

$$\begin{aligned}
& \frac{1}{2} \int_{\Omega \times \{t=s\}} (|w_1 - \tilde{w}_1|^2 + |w_2 - \tilde{w}_2|^2 + |w_3 - \tilde{w}_3|^2) dx \\
& + \int_{Q_s} (\lambda - C_5 K_1 e^{\lambda T}) (|w_1 - \tilde{w}_1|^2 + |w_2 - \tilde{w}_2|^2 + |w_3 - \tilde{w}_3|^2) dx dt \\
& \leq K_1 e^{\lambda T} C_4 \int_{Q_s} \left(\left(\sup_{0 \leq t \leq T} \int_{\Omega} |v_1 - \tilde{v}_1| dy \right)^2 + \left(\sup_{0 \leq t \leq T} \int_{\Omega} |v_2 - \tilde{v}_2| dy \right)^2 \right. \\
& \quad \left. + \left(\sup_{0 \leq t \leq T} \int_{\Omega} |v_3 - \tilde{v}_3| dy \right)^2 \right) dx dt.
\end{aligned}$$

The terms of the form $\left(\sup_{0 \leq t \leq T} \int_{\Omega} |v_i - \tilde{v}_i| dy \right)^2$ can be estimated as follows.

$$\int_{\Omega} |v_i - \tilde{v}_i| dy \leq C_{\Omega} \left(\int_{\Omega} |v_i - \tilde{v}_i|^2 dy \right)^{1/2}.$$

By taking the sup of both sides over $0 \leq t \leq T$,

$$\sup_{0 \leq t \leq T} \int_{\Omega} |v_i - \tilde{v}_i| dy \leq C_{\Omega} \sup_{0 \leq t \leq T} \left(\int_{\Omega} |v_i - \tilde{v}_i|^2 dy \right)^{1/2}.$$

By squaring both sides, we have

$$\begin{aligned}
\left(\sup_{0 \leq t \leq T} \int_{\Omega} |v_i - \tilde{v}_i| dy \right)^2 & \leq C^2 \left(\sup_{0 \leq t \leq T} \left(\int_{\Omega} |v_i - \tilde{v}_i|^2 dy \right)^{1/2} \right)^2 \\
& = C^2 \left(\sup_{0 \leq t \leq T} \int_{\Omega} |v_i - \tilde{v}_i|^2 dy \right)^{1/2} \\
& = C^2 \sup_{0 \leq t \leq T} \int_{\Omega} |v_i - \tilde{v}_i|^2 dy.
\end{aligned}$$

By using the estimates above, we have

$$\begin{aligned}
& \frac{1}{2} \int_{\Omega \times \{t=s\}} (|w_1 - \tilde{w}_1|^2 + |w_2 - \tilde{w}_2|^2 + |w_3 - \tilde{w}_3|^2) dx \\
& + \int_{Q_s} (\lambda - C_5 K_1 e^{\lambda T}) [|w_1 - \tilde{w}_1|^2 + |w_2 - \tilde{w}_2|^2 + |w_3 - \tilde{w}_3|^2] dx dt \\
& \leq C_7 K_1 e^{\lambda T} T \left(\sup_{0 \leq t \leq T} \int_{\Omega} |v_1 - \tilde{v}_1|^2 dy + \sup_{0 \leq t \leq T} \int_{\Omega} |v_2 - \tilde{v}_2|^2 dy + \sup_{0 \leq t \leq T} \int_{\Omega} |v_3 - \tilde{v}_3|^2 dy \right)
\end{aligned}$$

First, choose $\lambda > 0$ such that

$$\lambda > C_5 K_1.$$

Then, if we choose T such that

$$T < \min\left(\frac{1}{\lambda} \ln\left(\frac{\lambda}{C_5 K_1}\right), \frac{e^{-\frac{\lambda}{2C_7 K_1}}}{2C_7 K_1}\right),$$

we have

$$\lambda - C_5 K_1 e^{\lambda T} > 0 \quad \text{and} \quad 2C_7 K_1 e^{\lambda T} T < 1,$$

therefore, we obtain

$$\begin{aligned} & \frac{1}{2} \int_{\Omega \times \{t=s\}} (|w_1 - \tilde{w}_1|^2 + |w_2 - \tilde{w}_2|^2 + |w_3 - \tilde{w}_3|^2) dx \\ & \leq C_7 K_1 e^{\lambda T} T \left(\sup_{0 \leq t \leq T} \|v_1 - \tilde{v}_1\|_{L^2(\Omega)} + \sup_{0 \leq t \leq T} \|v_2 - \tilde{v}_2\|_{L^2(\Omega)} + \sup_{0 \leq t \leq T} \|v_3 - \tilde{v}_3\|_{L^2(\Omega)} \right) \end{aligned}$$

By taking the supremum of the left-side over the interval $[0, T]$, we have

$$\begin{aligned} & \sup_{0 \leq t \leq T} \|w_1 - \tilde{w}_1\|_{L^2(\Omega)} + \sup_{0 \leq t \leq T} \|w_2 - \tilde{w}_2\|_{L^2(\Omega)} + \sup_{0 \leq t \leq T} \|w_3 - \tilde{w}_3\|_{L^2(\Omega)} \\ & \leq 2C_7 K_1 e^{\lambda T} T \left(\sup_{0 \leq t \leq T} \|v_1 - \tilde{v}_1\|_{L^2(\Omega)} + \sup_{0 \leq t \leq T} \|v_2 - \tilde{v}_2\|_{L^2(\Omega)} + \sup_{0 \leq t \leq T} \|v_3 - \tilde{v}_3\|_{L^2(\Omega)} \right) \end{aligned}$$

Therefore,

$$\|w - \tilde{w}\| = \|A[v] - A[\tilde{v}]\| \leq C \|v - \tilde{v}\|$$

where $C < 1$. Using similar estimates, one can prove the uniqueness of solutions to the state system. \square

Next, we derive an *a priori* estimate for the state solution in V^3 .

Theorem 2. *For all $\alpha \in U$, the corresponding solution to the state system (2.1)-(2.4) in V^3 , is bounded in V^3 , i.e.,*

$$\|u_i\|_{L^2(0,T;H_0^1(\Omega))} \leq C, \quad i = 1, 2, 3,$$

where C depends on the coefficients, initial conditions and the source terms.

Proof. To obtain the necessary *a priori* estimates on the solution of the state system(2.1)-(2.4), we need a change of variable. Let $u_1 = e^{\lambda t}w_1$, $u_2 = e^{\lambda t}w_2$, $u_3 = e^{\lambda t}w_3$, where $\lambda > 0$ is to be chosen later. Using the weak definition of solution, we obtain

$$\begin{aligned}
& \int_0^T (\langle (w_1)_t, w_1 \rangle + a^1(t, w_1, w_1)) dt + \int_Q \lambda w_1^2 dx dt \\
&= - \int_Q w_1^2 \int_{\Omega} \frac{w_2}{e^{-\lambda t} + w_2} dy dx dt + \int_Q \alpha w_1^2 \int_{\Omega} \frac{w_3}{e^{-\lambda t} + w_3} dy dx dt + \int_Q e^{-\lambda t} f_1 w_1 dx dt \\
& \int_0^T (\langle (w_2)_t, w_2 \rangle + a^2(t, w_2, w_2)) dt + \int_Q \lambda w_2^2 dx dt \\
&= - \int_Q w_2^2 \int_{\Omega} \frac{w_1}{e^{-\lambda t} + w_1} dy dx dt - \int_Q \alpha w_1^2 \int_{\Omega} \frac{w_3}{e^{-\lambda t} + w_3} dy dx dt + \int_Q e^{-\lambda t} f_2 w_2 dx dt \\
& \int_0^T (\langle (w_3)_t, w_3 \rangle + a^3(t, w_3, w_3)) dt + \int_Q \lambda w_3^2 dx dt \\
&= \int_Q \alpha w_3^2 \int_{\Omega} \frac{w_1}{e^{-\lambda t} + w_1} dy dx dt - \int_Q \alpha w_3^2 \int_{\Omega} \frac{w_2}{e^{-\lambda t} + w_2} dx dt + \int_Q e^{-\lambda t} f_3 w_3 dx dt.
\end{aligned}$$

By adding these three equations and using $\frac{d}{dt}(\frac{(w_k)^2}{2}) = w_k(w_k)_t$ in weak sense, we obtain

$$\begin{aligned}
& \frac{1}{2} \int_{\Omega \times \{t=T\}} (w_1^2 + w_2^2 + w_3^2) dx + \int_Q \left(\sum_{i,j=1}^n a_{ij}^1(w_1)_{x_i}(w_1)_{x_j} + \sum_{i,j=1}^n a_{ij}^2(w_2)_{x_i}(w_2)_{x_j} \right. \\
& \quad \left. + \sum_{i,j=1}^n a_{ij}^3(w_3)_{x_i}(w_3)_{x_j} \right) dx dt \\
& \quad + \int_Q \left(\sum_{i=1}^n b_i^1(w_1)_{x_i} w_1 + \sum_{i=1}^n b_i^2(w_2)_{x_i} w_2 + \sum_{i=1}^n b_i^3(w_3)_{x_i} w_3 \right) dx dt \\
& \quad + \int_Q ((c^1 + \lambda)w_1^2 + (c^2 + \lambda)w_2^2 + (c^3 + \lambda)w_3^2) dx dt \\
&= - \int_Q (w_1^2 \int_{\Omega} \frac{w_2}{e^{-\lambda t} + w_2} dy + w_2^2 \int_{\Omega} \frac{w_1}{e^{-\lambda t} + w_1} dy - \alpha w_3^2 \int_{\Omega} \frac{w_1}{e^{-\lambda t} + w_1} dy) dx dt \\
& \quad + \int_Q \alpha w_1^2 \int_{\Omega} \frac{w_3}{e^{-\lambda t} + w_3} dy - \alpha w_2^2 \int_{\Omega} \frac{w_3}{e^{-\lambda t} + w_3} dy - \alpha w_3^2 \int_{\Omega} \frac{w_2}{e^{-\lambda t} + w_2} dy dx dt \\
& \quad + \int_Q e^{-\lambda t} (f_1 w_1 + f_2 w_2 + f_3 w_3) dy dx dt + \frac{1}{2} \int_{\Omega \times \{t=0\}} (w_1^2 + w_2^2 + w_3^2) dx.
\end{aligned}$$

Using the uniform ellipticity property, we have the following estimate:

$$\begin{aligned}
& \frac{1}{2} \int_{\Omega \times \{t=T\}} (w_1^2 + w_2^2 + w_3^2) dx + \frac{\theta}{2} \int_Q (|\nabla w_1|^2 + |\nabla w_2|^2 + |\nabla w_3|^2) dx dt \\
& \quad + \int_Q ((c^1 + \lambda)w_1^2 + (c^2 + \lambda)w_2^2 + (c^3 + \lambda)w_3^2) dx dt \\
& \leq \int_Q |\alpha| (w_3^2 \int_{\Omega} \frac{w_1}{e^{-\lambda t} + w_1} dy dx + w_1^2 \int_{\Omega} \frac{w_3}{e^{-\lambda t} + w_3} dy dx + w_2^2 \int_{\Omega} \frac{w_3}{e^{-\lambda t} + w_3} dy dx \\
& \quad + w_3^2 \int_{\Omega} \frac{w_2}{e^{-\lambda t} + w_2} dy dx) dt + \int_Q e^{-\lambda t} (|f_1 w_1| + |f_2 w_2| + |f_3 w_3|) dx dt \\
& \quad + C_1 \int_Q (|w_1|^2 + |w_2|^2 + |w_3|^2) dx dt + \frac{1}{2} \int_{\Omega \times \{t=0\}} (w_1^2 + w_2^2 + w_3^2) dx.
\end{aligned}$$

Note the terms with first derivatives were estimated as

$$\begin{aligned}
\int_Q \sum_{i=1}^n b_i^k (w_k)_{x_i} (w_k) dx dt & \leq \frac{\theta}{2} \int_Q (|\nabla w_1|^2 + |\nabla w_2|^2 + |\nabla w_3|^2) dx dt \\
& \quad + C_1 \int_Q (|w_1|^2 + |w_2|^2 + |w_3|^2) dx dt.
\end{aligned} \tag{2.25}$$

Using that $|w_i| \leq |e^{-\lambda t} + w_i|$ for $0 \leq t \leq T$, $|\frac{w_i}{e^{-\lambda t} + w_i}| \leq 1$, we have

$$\begin{aligned}
& \frac{1}{2} \int_{\Omega \times \{t=T\}} (|w_1|^2 + |w_2|^2 + |w_3|^2) dx + \frac{\theta}{2} \int_Q (|\nabla w_1|^2 + |\nabla w_2|^2 + |\nabla w_3|^2) dx dt \\
& \quad + \int_Q (-C_3 + \lambda)(|w_1|^2 + |w_2|^2 + |w_3|^2) dx dt \\
& \leq C_2 \int_Q (|w_1|^2 + |w_2|^2 + |w_3|^2) dx dt + \frac{1}{2} \int_Q (|f_1|^2 + |f_2|^2 + |f_3|^2) dx dt \\
& \quad + \frac{1}{2} \int_{\Omega \times \{t=0\}} (|w_1|^2 + |w_2|^2 + |w_3|^2) dx
\end{aligned}$$

where $-C_3$ is a lower bound on c^i , $i = 1, 2, 3$.

Combining like terms, we obtain

$$\begin{aligned}
& \frac{1}{2} \int_{\Omega \times \{t=T\}} (|w_1|^2 + |w_2|^2 + |w_3|^2) dx + \frac{\theta}{2} \int_Q (|\nabla w_1|^2 + |\nabla w_2|^2 + |\nabla w_3|^2) dx dt \\
& \quad + \int_Q (-C_3 + \lambda - C_2)(|w_1|^2 + |w_2|^2 + |w_3|^2) dx dt \\
& \leq \frac{1}{2} \int_Q (|f_1|^2 + |f_2|^2 + |f_3|^2) dx dt + \frac{1}{2} \int_{\Omega \times \{t=0\}} (|w_1|^2 + |w_2|^2 + |w_3|^2) dx.
\end{aligned}$$

We choose λ large enough so that $\lambda > C_2 + C_3$, and we conclude

$$\begin{aligned}
& \int_Q (|w_1|^2 + |w_2|^2 + |w_3|^2) dx dt + \int_Q (|\nabla w_1|^2 + |\nabla w_2|^2 + |\nabla w_3|^2) dx dt \\
& \leq C_4 \left(\int_Q (|f_1|^2 + |f_2|^2 + |f_3|^2) dx dt + \frac{1}{2} \int_{\Omega \times \{t=0\}} (|w_1|^2 + |w_2|^2 + |w_3|^2) dx \right).
\end{aligned}$$

Therefore, $\|w_i\|_{L^2(0,T;H_0^1(\Omega))} \leq C_6$ for $i = 1, 2, 3$ and since $u_i = e^{\lambda t} w_i$,

$$\|u_i\|_{L^2(0,T;H_0^1(\Omega))} \leq C_7 \|w_i\|_{L^2(0,T;H_0^1(\Omega))} \leq C_6 \text{ for all } 0 < t < T. \quad \square$$

2.3 Existence of Optimal Control

Next we prove the existence of an optimal control.

Theorem 3. *There exists an optimal control $\alpha^* \in U$ that maximizes the objective functional $J(\alpha)$.*

Proof. Since both the state variables and control are bounded in $L^\infty(Q)$,

$$\sup\{J(\alpha) \mid \alpha \in U\} < \infty,$$

there exists a maximizing sequence $\{\alpha_n\}$ in U such that

$$\lim_{n \rightarrow \infty} J(\alpha_n) = \sup\{J(\alpha) \mid \alpha \in U\}.$$

By the existence and uniqueness of solutions to the state system with control α^n , we define

$u_1^n = u_1(\alpha_n), u_2^n = u_2(\alpha_n), u_3^n = u_3(\alpha_n)$. From the result of *a priori* estimates from Theorem 2 and from PDEs (2.1) - (2.4),

$$\|u_i^n\|_{L^2(0,T;H_0^1(\Omega))} \leq C$$

$$\|(u_i)_t^n\|_{L^2(0,T;H^{-1}(\Omega))} \leq C$$

with C , independent of n . Since the control functions are uniformly bounded in $L^\infty(Q)$ and the domain Q is bounded, on the subsequence $\{\alpha_n\}, \{u_i^n\}$ and $\{(u_i)_t^n\}$ are weakly convergent, i.e., there exists $\alpha^* \in U$ and $u = (u_1^*, u_2^*, u_3^*) \in V^3$ such that

$$u_i^n \rightharpoonup u_i^* \text{ in } L^2(0, T; H_0^1(\Omega)),$$

$$(u_i)_t^n \rightharpoonup u_t^* \text{ in } L^2(0, T; H^{-1}(\Omega)),$$

$$\alpha_n \rightharpoonup \alpha^* \text{ in } L^2(Q).$$

Moreover, by the compactness result of Simon [61], $\{u_i^n\}$ is strongly convergent in $L^2(Q)$. We need to show $u^* = (u_1^*, u_2^*, u_3^*)$ is the weak solution associated with α^* .

Consider the weak formulation satisfied by u_i^n ,

$$\begin{aligned} & \int_0^T (\langle (u_1^n)_t, \phi_1 \rangle + a^1(t, u_1^n, \phi_1)) dt \\ &= \int_Q (-u_1^n \int_\Omega \frac{u_2^n}{1+u_2^n} dy + \alpha^n u_1^n \int_\Omega \frac{u_3^n}{1+u_3^n} + f_1) \phi_1 dx dt \\ & \int_0^T (\langle (u_2^n)_t, \phi_2 \rangle + a^2(t, u_2^n, \phi_2)) dt \\ &= \int_Q (-u_2^n \int_\Omega \frac{u_1^n}{1+u_1^n} dy - \alpha^n u_2^n \int_\Omega \frac{u_3^n}{1+u_3^n} dy + f_2) \phi_2 dx dt \\ & \int_0^T (\langle (u_3^n)_t, \phi_3 \rangle + a^3(t, u_3^n, \phi_3)) dt \\ &= \int_Q (\alpha^n u_3^n \int_\Omega \frac{u_1^n}{1+u_1^n} dy - \alpha^n u_3^n \int_\Omega \frac{u_2^n}{1+u_2^n} dy + f_3) \phi_3 dx dt. \end{aligned}$$

We illustrate the convergence estimate from the equation for u_1^n . From the weak convergence

in $L^2(0, T; H_0^1(\Omega))$ and weak* convergence in $L^2(0, T; H^{-1}(\Omega))$,

$$\begin{aligned} & \int_0^T (\langle (u_1^n)_t, \phi_1 \rangle + a^1(t, u_1^n, \phi_1)) dt \\ & \rightarrow \int_0^T (\langle (u_1^*)_t, \phi_1 \rangle + a^1(t, u_1^*, \phi_1)) dt. \end{aligned}$$

Now, we show that

$$\begin{aligned} & \int_Q -u_1^n \phi_1 \int_{\Omega} \frac{u_2^n}{1+u_2^n} dy dx dt + \int_Q \alpha^n u_1^n \phi_1 \int_{\Omega} \frac{u_3^n}{1+u_3^n} dy dx dt \\ & \rightarrow \int_Q -u_1^* \phi_1 \int_{\Omega} \frac{u_2^*}{1+u_2^*} dy dx dt + \int_Q \alpha^* u_1^* \phi_1 \int_{\Omega} \frac{u_3^*}{1+u_3^*} dy dx dt. \end{aligned}$$

We estimate

$$\begin{aligned} & \left| \int_Q -u_1^n \phi_1 \int_{\Omega} \frac{u_2^n}{1+u_2^n} dy dx dt + \int_Q \alpha^n u_1^n \phi_1 \int_{\Omega} \frac{u_3^n}{1+u_3^n} dy dx dt \right. \\ & \quad \left. + \int_Q u_1^* \phi_1 \int_{\Omega} \frac{u_2^*}{1+u_2^*} dy dx dt - \int_Q \alpha^* u_1^* \phi_1 \int_{\Omega} \frac{u_3^*}{1+u_3^*} dy dx dt \right| \\ & \leq \left| \int_Q u_1^n \phi_1 \int_{\Omega} \frac{u_2^n}{1+u_2^n} dy dx dt - \int_Q u_1^* \phi_1 \int_{\Omega} \frac{u_2^*}{1+u_2^*} dy dx dt \right| \\ & \quad + \left| \int_Q \alpha^n u_1^n \phi_1 \int_{\Omega} \frac{u_3^n}{1+u_3^n} dy dx dt - \int_Q \alpha^* u_1^* \phi_1 \int_{\Omega} \frac{u_3^*}{1+u_3^*} dy dx dt \right|, \end{aligned} \tag{2.26}$$

which converges to zero using the strong L^2 convergence of u_i^n . The first term above is

estimated as follows,

$$\begin{aligned}
& \left| \int_Q u_1^n \phi_1 \int_{\Omega} \frac{u_2^n}{1+u_2^n} dy dx dt - \int_Q u_1^* \phi_1 \int_{\Omega} \frac{u_2^*}{1+u_2^*} dy dx dt \right| \\
& \leq \left| \int_Q (u_1^n - u_1^*) \phi_1 \int_{\Omega} \frac{u_2^n}{1+u_2^n} dy dx dt \right| + \left| \int_Q u_1^* \phi_1 \int_{\Omega} \left(\frac{u_2^n}{1+u_2^n} - \frac{u_2^*}{1+u_2^*} \right) dy dx dt \right| \\
& \leq \left| \int_Q |u_1^n - u_1^*|^2 dx dt \right|^{\frac{1}{2}} \left| \int_Q \left(\phi_1 \int_{\Omega} \frac{u_2^*}{1+u_2^*} dy \right)^2 dx dt \right|^{\frac{1}{2}} \\
& \quad + \left| \int_Q u_1^* \phi_1 \int_{\Omega} \frac{(u_2^n - u_2^*)}{(1+u_2^n)(1+u_2^*)} dy dx dt \right| \\
& \leq C_1 \left(\int_Q |u_1^n - u_1^*|^2 dx dt \right)^{\frac{1}{2}} + \left| \int_Q u_1^* \phi_1 \int_{\Omega} (u_2^n - u_2^*) \frac{1}{(1+u_2^n)(1+u_2^*)} dy dx dt \right| \\
& \leq C_1 \left(\int_Q |u_1^n - u_1^*|^2 dx dt \right)^{\frac{1}{2}} + C_2 \left| \int_Q u_1^* \phi_1 \int_{\Omega} (u_2^n - u_2^*) dy dx dt \right| \\
& \leq C_1 \left(\int_Q |u_1^n - u_1^*|^2 dx dt \right)^{\frac{1}{2}} + C_3 \int_Q \left(\int_{\Omega} |u_2^n - u_2^*|^2 dy \right)^{\frac{1}{2}} |u_1^* \phi_1| dx dt,
\end{aligned}$$

which converges to 0 by the strong L^2 convergence of u_i^n sequences. The second term on

the right-hand side of (2.26) is estimated as follows,

$$\begin{aligned}
& \left| \int_Q \alpha^n u_1^n \phi_1 \int_{\Omega} \frac{u_3^n}{1+u_3^n} dy dx dt - \int_Q \alpha^* u_1^* \phi_1 \int_{\Omega} \frac{u_3^*}{1+u_3^*} dy dx dt \right| \\
& \leq \left| \int_Q \alpha^n u_1^n \phi_1 \int_{\Omega} \frac{u_3^n}{1+u_3^n} dy dx dt - \int_Q \alpha^n u_1^* \phi_1 \int_{\Omega} \frac{u_3^n}{1+u_3^n} dy dx dt \right| \\
& \quad + \left| \int_Q \alpha^n u_1^* \phi_1 \int_{\Omega} \frac{u_3^n}{1+u_3^n} dy dx dt - \int_Q \alpha^* u_1^* \phi_1 \int_{\Omega} \frac{u_3^*}{1+u_3^*} dy dx dt \right| \\
& \leq \left| \int_Q (u_1^n - u_1^*) \alpha^n \phi_1 \int_{\Omega} \frac{u_3^n}{1+u_3^n} dy dx dt \right| \\
& \quad + \left| \int_Q \alpha^n u_1^* \phi_1 \int_{\Omega} \frac{u_3^n}{1+u_3^n} dy dx dt - \int_Q \alpha^n u_1^* \phi_1 \int_{\Omega} \frac{u_3^*}{1+u_3^*} dy dx dt \right| \\
& \quad + \left| \int_Q \alpha^n u_1^* \phi_1 \int_{\Omega} \frac{u_3^*}{1+u_3^*} dy dx dt - \int_Q \alpha^* u_1^* \phi_1 \int_{\Omega} \frac{u_3^*}{1+u_3^*} dy dx dt \right| \\
& \leq \left| \int_Q (u_1^n - u_1^*) \alpha^n \phi_1 \int_{\Omega} \frac{u_3^n}{1+u_3^n} dy dx dt \right| \\
& \quad + \left| \int_Q \alpha^n u_1^* \phi_1 \int_{\Omega} \left(\frac{u_3^n}{1+u_3^n} - \frac{u_3^*}{1+u_3^*} \right) dy dx dt \right| \\
& \quad + \left| \int_Q (\alpha^n - \alpha^*) u_1^* \phi_1 \int_{\Omega} \frac{u_3^*}{1+u_3^*} dy dx dt \right| \\
& \leq C_4 \int_Q |u_1^n - u_1^*| |\alpha^n \phi_1| dx dt \\
& \quad + \left| \int_Q \alpha^n u_1^* \phi_1 \int_{\Omega} \frac{(u_3^n - u_3^*)}{(1+u_3^n)(1+u_3^*)} dy dx dt \right| \\
& \quad + \left| \int_Q (\alpha^n - \alpha^*) u_1^* \phi_1 \int_{\Omega} \frac{u_3^*}{1+u_3^*} dy dx dt \right| \\
& \leq C_6 \int_Q |u_1^n - u_1^*| |\phi_1| dx dt + C_7 \int_Q |\alpha^n| |u_1^* \phi_1| \int_{\Omega} |u_3^n - u_3^*| dy dx dt \\
& \quad + \left| \int_Q (\alpha^n - \alpha^*) u_1^* \phi_1 \int_{\Omega} \frac{u_3^*}{1+u_3^*} dy dx dt \right| \\
& \leq C_6 \int_Q |u_1^n - u_1^*| |\phi_1| dx dt + C_9 \int_Q |\alpha^n| |u_1^* \phi_1| \left(\int_{\Omega} |u_3^n - u_3^*|^2 dy \right)^{\frac{1}{2}} dx dt \\
& \quad + \left| \int_Q (\alpha^n - \alpha^*) u_1^* \phi_1 \int_{\Omega} \frac{u_3^*}{1+u_3^*} dy dx dt \right|,
\end{aligned}$$

which converges due to strong L^2 convergence of u_i^n and weak L^2 convergence of α^n .

We get similar results for u_2^n and u_3^n . Passing to the limit and using the convergence of sequences, we showed that $u^* = (u_1^*, u_2^*, u_3^*)$ is the weak solution associated with α^* .

Next, we show that α^* is an optimal control. Since $\alpha^* \in U$, we have

$$J(\alpha^*) \leq \sup\{J(\alpha^n) \mid \alpha^n \in U\}.$$

For the weakly convergent sequence, we have

$$\int_Q (\alpha^*)^2 dx dt \leq \liminf_{n \rightarrow \infty} \int_Q (\alpha_n)^2 dx dt.$$

By using the upper semi-continuity of the objective functional with respect to weak L^2 convergence to handle the control terms and the strong L^2 convergence of the states,

$$J(\alpha^*) \geq \lim_{n \rightarrow \infty} J(\alpha_n),$$

and then

$$\max_{\alpha \in U} J(\alpha) = J(\alpha^*).$$

We conclude that α^* is an optimal control that maximizes the objective functional. \square

In next section, we derive the optimality system which consists of the state system coupled with the adjoint system with appropriate initial conditions.

2.4 Derivation of the Optimality System

To differentiate the map $\alpha \rightarrow J(\alpha)$, we must first differentiate the map $\alpha \rightarrow (u_1, u_2, u_3)$.

Theorem 4. *(Sensitivities) The mapping $\alpha \in U \rightarrow u(\alpha) = (u_1(\alpha), u_2(\alpha), u_3(\alpha))$ is differentiable in the following sense :*

For $\alpha \in U$ and $h \in L^\infty(Q)$ such that $\alpha + \varepsilon h \in U$, as $\varepsilon \rightarrow 0$, there exist ψ_k , $k = 1, 2, 3$ in

V such that $\frac{u_k(\alpha+\varepsilon h)-u_k(\alpha)}{\varepsilon} \rightharpoonup \psi_k$, as $\varepsilon \rightarrow 0$ for $k = 1, 2, 3$ where the sensitivities, ψ_k in V satisfy the following system:

$$\begin{aligned}
L_1\psi_1 &= -\psi_1\left(\int_{\Omega} \frac{u_2}{1+u_2} dx - \alpha \int_{\Omega} \frac{u_3}{1+u_3} dx\right) - u_1\left(\int_{\Omega} \psi_2 \frac{1}{(1+u_2)^2} dx - \alpha \int_{\Omega} \psi_3 \frac{1}{(1+u_3)^2} dx\right) \\
&\quad + hu_1 \int_{\Omega} \frac{u_3}{1+u_3} dx \\
L_2\psi_2 &= -\psi_2\left(\int_{\Omega} \frac{u_1}{1+u_1} dx + \alpha \int_{\Omega} \frac{u_3}{1+u_3} dx\right) - u_2\left(\int_{\Omega} \psi_1 \frac{1}{(1+u_1)^2} dx + \alpha \int_{\Omega} \psi_3 \frac{1}{(1+u_3)^2} dx\right) \\
&\quad - hu_2 \int_{\Omega} \frac{u_3}{1+u_3} dx \\
L_3\psi_3 &= \alpha\psi_3\left(\int_{\Omega} \frac{u_1}{1+u_1} dx - \int_{\Omega} \frac{u_2}{1+u_2} dx\right) + \alpha u_3\left(\int_{\Omega} \psi_1 \frac{1}{(1+u_1)^2} dx - \int_{\Omega} \psi_2 \frac{1}{(1+u_2)^2} dx\right) \\
&\quad + hu_3\left(\int_{\Omega} \frac{u_1}{1+u_1} dx - \int_{\Omega} \frac{u_2}{1+u_2} dx\right)
\end{aligned} \tag{2.27}$$

in $Q = \Omega \times (0, T)$

$$\psi_k(x, 0) = 0 \text{ for } x \in \Omega, k = 1, 2, 3. \tag{2.28}$$

$$\psi_k = 0 \text{ on } \partial\Omega \times (0, T), k = 1, 2, 3. \tag{2.29}$$

Proof. Define $u_1^\varepsilon = u_1(\alpha + \varepsilon h)$, $u_2^\varepsilon = u_2(\alpha + \varepsilon h)$, $u_3^\varepsilon = u_3(\alpha + \varepsilon h)$. Let $u_1^\varepsilon = e^{\lambda t} w_1^\varepsilon$, $u_2^\varepsilon = e^{\lambda t} w_2^\varepsilon$, $u_3^\varepsilon = e^{\lambda t} w_3^\varepsilon$, and $u_1(\alpha) = e^{\lambda t} w_1$, $u_2(\alpha) = e^{\lambda t} w_2$, $u_3(\alpha) = e^{\lambda t} w_3$, where $\lambda > 0$ is to be

chosen later. We estimate the quotients on $Q_1 = \Omega \times (0, T_1)$:

$$\begin{aligned}
& \frac{1}{2} \int_{\Omega \times \{t=T_1\}} (|\frac{w_1^\varepsilon - w_1}{\varepsilon}|^2 + |\frac{w_2^\varepsilon - w_2}{\varepsilon}|^2 + |\frac{w_3^\varepsilon - w_3}{\varepsilon}|^2) dx \\
& + \theta \int_{Q_1} (|\nabla(\frac{w_1^\varepsilon - w_1}{\varepsilon})|^2 + |\nabla(\frac{w_2^\varepsilon - w_2}{\varepsilon})|^2 + |\nabla(\frac{w_3^\varepsilon - w_3}{\varepsilon})|^2) dx dt \\
& + \int_{Q_1} ((c^1 + \lambda) |\frac{w_1^\varepsilon - w_1}{\varepsilon}|^2 + (c^2 + \lambda) |\frac{w_2^\varepsilon - w_2}{\varepsilon}|^2 + (c^3 + \lambda) |\frac{w_3^\varepsilon - w_3}{\varepsilon}|^2) dx dt \\
& \leq C_1 \int_{Q_1} (|\frac{w_1^\varepsilon - w_1}{\varepsilon}|^2 + |\frac{w_2^\varepsilon - w_2}{\varepsilon}|^2 + |\frac{w_3^\varepsilon - w_3}{\varepsilon}|^2) dx dt \\
& + C_2 \int_{Q_1} |w_1| \left| \frac{w_1^\varepsilon - w_1}{\varepsilon} \right| \int_{\Omega} \frac{1}{\varepsilon} \left| \frac{w_2^\varepsilon}{e^{-\lambda t} + w_2^\varepsilon} - \frac{w_2}{e^{-\lambda t} + w_2} + \frac{w_3^\varepsilon}{e^{-\lambda t} + w_3^\varepsilon} - \frac{w_3}{e^{-\lambda t} + w_3} \right| dy dx dt \\
& + C_3 \int_{Q_1} |w_2| \left| \frac{w_2^\varepsilon - w_2}{\varepsilon} \right| \int_{\Omega} \frac{1}{\varepsilon} \left| \frac{w_1^\varepsilon}{e^{-\lambda t} + w_1^\varepsilon} - \frac{w_1}{e^{-\lambda t} + w_1} + \frac{w_3^\varepsilon}{e^{-\lambda t} + w_3^\varepsilon} - \frac{w_3}{e^{-\lambda t} + w_3} \right| dy dx dt \\
& + C_4 \int_{Q_1} |w_3| \left| \frac{w_3^\varepsilon - w_3}{\varepsilon} \right| \int_{\Omega} \frac{1}{\varepsilon} \left| \frac{w_1^\varepsilon}{e^{-\lambda t} + w_1^\varepsilon} - \frac{w_1}{e^{-\lambda t} + w_1} + \frac{w_2^\varepsilon}{e^{-\lambda t} + w_2^\varepsilon} - \frac{w_2}{e^{-\lambda t} + w_2} \right| dy dx dt \\
& + C_6 \int_{Q_1} h(|w_1^\varepsilon| \left| \frac{w_1^\varepsilon - w_1}{\varepsilon} \right| + |w_2^\varepsilon| \left| \frac{w_2^\varepsilon - w_2}{\varepsilon} \right| + |w_3^\varepsilon| \left| \frac{w_3^\varepsilon - w_3}{\varepsilon} \right|) dx dt \\
& + C_7 \int_{Q_1} (|\nabla(\frac{w_1^\varepsilon - w_1}{\varepsilon})| \left| \frac{w_1^\varepsilon - w_1}{\varepsilon} \right| + |\nabla(\frac{w_2^\varepsilon - w_2}{\varepsilon})| \left| \frac{w_2^\varepsilon - w_2}{\varepsilon} \right| \\
& \quad + |\nabla(\frac{w_3^\varepsilon - w_3}{\varepsilon})| \left| \frac{w_3^\varepsilon - w_3}{\varepsilon} \right|) dx dt.
\end{aligned}$$

The term of the form

$$\int_{\Omega} \left| \frac{w_i^\varepsilon}{e^{-\lambda t} + w_i^\varepsilon} - \frac{w_i}{e^{-\lambda t} + w_i} \right| dy$$

is estimated as follows.

$$\begin{aligned}
& \int_{\Omega} \left| \frac{w_i^\varepsilon}{e^{-\lambda t} + w_i^\varepsilon} - \frac{w_i}{e^{-\lambda t} + w_i} \right| dy = \int_{\Omega} \left| \frac{e^{-\lambda t}(w_i^\varepsilon - w_i)}{(e^{-\lambda t} + w_i^\varepsilon)(e^{-\lambda t} + w_i)} \right| dy \\
& = \int_{\Omega} \left| \frac{e^{\lambda t}(w_i^\varepsilon - w_i)}{(1 + e^{\lambda t}w_i^\varepsilon)(1 + e^{\lambda t}w_i)} \right| dy \\
& \leq e^{\lambda t} \int_{\Omega} |w_i^\varepsilon - w_i| dy.
\end{aligned}$$

The estimates similar to (2.25) in the proof of Theorem 2 were used for the terms of first derivatives in the right-hand side of the above inequality.

$$\begin{aligned}
& \frac{1}{2} \int_{\Omega \times \{t=T_1\}} (|\frac{w_1^\varepsilon - w_1}{\varepsilon}|^2 + |\frac{w_2^\varepsilon - w_2}{\varepsilon}|^2 + |\frac{w_3^\varepsilon - w_3}{\varepsilon}|^2) dx \\
& + \frac{\theta}{2} \int_{Q_1} (|\nabla(\frac{w_1^\varepsilon - w_1}{\varepsilon})|^2 + |\nabla(\frac{w_2^\varepsilon - w_2}{\varepsilon})|^2 + |\nabla(\frac{w_3^\varepsilon - w_3}{\varepsilon})|^2) dx dt \\
& + \int_{Q_1} (-C_8 + \lambda) (|\frac{w_1^\varepsilon - w_1}{\varepsilon}|^2 + |\frac{w_2^\varepsilon - w_2}{\varepsilon}|^2 + |\frac{w_3^\varepsilon - w_3}{\varepsilon}|^2) dx dt \\
& \leq C_7 \int_{Q_1} (|\frac{w_1^\varepsilon - w_1}{\varepsilon}|^2 + |\frac{w_2^\varepsilon - w_2}{\varepsilon}|^2 + |\frac{w_3^\varepsilon - w_3}{\varepsilon}|^2) dx dt \\
& + C_2 e^{\lambda T_1} \int_{Q_1} |w_1| \|\frac{w_1^\varepsilon - w_1}{\varepsilon}\| \int_{\Omega} (|\frac{w_2^\varepsilon - w_2}{\varepsilon}| + |\frac{w_3^\varepsilon - w_3}{\varepsilon}|) dy dx dt \\
& + C_3 e^{\lambda T_1} \int_{Q_1} |w_2| \|\frac{w_2^\varepsilon - w_2}{\varepsilon}\| \int_{\Omega} (|\frac{w_1^\varepsilon - w_1}{\varepsilon}| + |\frac{w_3^\varepsilon - w_3}{\varepsilon}|) dy dx dt \\
& + C_4 e^{\lambda T_1} \int_{Q_1} |w_3| \|\frac{w_3^\varepsilon - w_3}{\varepsilon}\| \int_{\Omega} (|\frac{w_1^\varepsilon - w_1}{\varepsilon}| + |\frac{w_2^\varepsilon - w_2}{\varepsilon}|) dy dx dt \\
& + C_6 \int_{Q_1} h (|w_1^\varepsilon| \|\frac{w_1^\varepsilon - w_1}{\varepsilon}\| + |w_2^\varepsilon| \|\frac{w_2^\varepsilon - w_2}{\varepsilon}\| + |w_3^\varepsilon| \|\frac{w_3^\varepsilon - w_3}{\varepsilon}\|) dx dt
\end{aligned}$$

where $-C_8$ is a lower bound on c^i for $i = 1, 2, 3$. Continuing to estimate gives

$$\begin{aligned}
& \frac{1}{2} \int_{\Omega \times \{t=T_1\}} (|\frac{w_1^\varepsilon - w_1}{\varepsilon}|^2 + |\frac{w_2^\varepsilon - w_2}{\varepsilon}|^2 + |\frac{w_3^\varepsilon - w_3}{\varepsilon}|^2) dx \\
& + \frac{\theta}{2} \int_{Q_1} (|\nabla(\frac{w_1^\varepsilon - w_1}{\varepsilon})|^2 + |\nabla(\frac{w_2^\varepsilon - w_2}{\varepsilon})|^2 + |\nabla(\frac{w_3^\varepsilon - w_3}{\varepsilon})|^2) dx dt \\
& + \int_{Q_1} (-C_8 + \lambda - C_9(1 + e^{\lambda T_1})) (|\frac{w_1^\varepsilon - w_1}{\varepsilon}|^2 + |\frac{w_2^\varepsilon - w_2}{\varepsilon}|^2 + |\frac{w_3^\varepsilon - w_3}{\varepsilon}|^2) dx dt \\
& \leq C \int_{Q_1} |h|^2 dx dt
\end{aligned}$$

First, choose λ to be a positive number satisfying

$$-C_8 + \lambda - C_9 > C_9.$$

Therefore, if we choose T_1 sufficiently small such that

$$\frac{\ln \frac{\lambda - (C_8 + C_9)}{C_9}}{\lambda} > T_1 \quad (2.30)$$

we have

$$-C_8 + \lambda - C_9(1 + e^{\lambda T_1}) > 0$$

The above estimate for λ and T_1 satisfying (2.4), (2.30), we get

$$\left\| \frac{w_i^\varepsilon - w_i}{\varepsilon} \right\|_{L^2(0, T_1; H_0^1(\Omega))} \leq C.$$

By stacking time intervals, we obtain the estimate on $\Omega \times (0, T)$. Then we have the estimate on $\frac{u_i^\varepsilon - u_i}{\varepsilon}$.

Hence, there exists $\psi_i \in V$, $i = 1, 2, 3$, such that on a subsequence $\frac{u_i^\varepsilon - u_i}{\varepsilon} \rightharpoonup \psi_i$ in $L^2(0, T; H_0^1(\Omega))$ for $i = 1, 2, 3$. From PDE's (2.1)-(2.4) and the above estimate, we can show that

$$\left\| \left(\frac{u_i^\varepsilon - u_i}{\varepsilon} \right)_t \right\|_{L^2(0, T; H^{-1}(\Omega))} \leq C$$

and

$$\left(\frac{u_i^\varepsilon - u_i}{\varepsilon} \right)_t \rightharpoonup (\psi_i)_t$$

in $L^2(0, T; H^{-1}(\Omega))$ for $i = 1, 2, 3$. Using the compactness result by Simon [?] ,

$$\frac{u_i^\varepsilon - u_i}{\varepsilon} \rightarrow \psi_i$$

strongly in $L^2(Q)$ for $i = 1, 2, 3$. Considering the PDE satisfied by the quotient:

$$\begin{aligned}
L_1\left(\frac{u_1^\varepsilon - u_1}{\varepsilon}\right) &= -\frac{1}{\varepsilon}\left[u_1^\varepsilon \int_{\Omega} \frac{u_2^\varepsilon}{1+u_2^\varepsilon} dy - u_1 \int_{\Omega} \frac{u_2^\varepsilon}{1+u_2^\varepsilon} dy + u_1 \int_{\Omega} \frac{u_2^\varepsilon}{1+u_2^\varepsilon} dy - u_1 \int_{\Omega} \frac{u_2}{1+u_2} dy\right] \\
&\quad + \frac{1}{\varepsilon}\left[(\alpha + \varepsilon h)u_1^\varepsilon \int_{\Omega} \frac{u_3^\varepsilon}{1+u_3^\varepsilon} dy - \alpha u_1 \int_{\Omega} \frac{u_3^\varepsilon}{1+u_3^\varepsilon} dy + \alpha u_1 \int_{\Omega} \frac{u_3^\varepsilon}{1+u_3^\varepsilon} dy\right. \\
&\quad \left. - \alpha u_1 \int_{\Omega} \frac{u_3}{1+u_3} dy\right] \\
&= -\frac{u_1^\varepsilon - u_1}{\varepsilon} \int_{\Omega} \frac{u_2^\varepsilon}{1+u_2^\varepsilon} dy - u_1 \int_{\Omega} \frac{u_2^\varepsilon - u_2}{\varepsilon} \frac{1}{(1+u_2^\varepsilon)(1+u_2)} dy \\
&\quad + \alpha \left(\frac{u_1^\varepsilon - u_1}{\varepsilon}\right) \int_{\Omega} \frac{u_3^\varepsilon}{1+u_3^\varepsilon} dy + \alpha u_1 \int_{\Omega} \frac{u_3^\varepsilon - u_3}{\varepsilon} \frac{1}{(1+u_3^\varepsilon)(1+u_3)} dy \\
&\quad + hu_1^\varepsilon \int_{\Omega} \frac{u_3^\varepsilon}{1+u_3^\varepsilon} dy.
\end{aligned}$$

Similarly, we get

$$\begin{aligned}
L_2\left(\frac{u_2^\varepsilon - u_2}{\varepsilon}\right) &= -\frac{u_2^\varepsilon - u_2}{\varepsilon} \int_{\Omega} \frac{u_1^\varepsilon}{1+u_1^\varepsilon} dy - u_2 \int_{\Omega} \frac{u_1^\varepsilon - u_1}{\varepsilon} \frac{1}{(1+u_1^\varepsilon)(1+u_1)} dy \\
&\quad - \alpha \left(\frac{u_2^\varepsilon - u_2}{\varepsilon}\right) \int_{\Omega} \frac{u_3^\varepsilon}{1+u_3^\varepsilon} dy - \alpha u_2 \int_{\Omega} \frac{u_3^\varepsilon - u_3}{\varepsilon} \frac{1}{(1+u_3^\varepsilon)(1+u_3)} dy \\
&\quad - hu_2^\varepsilon \int_{\Omega} \frac{u_3^\varepsilon}{1+u_3^\varepsilon} dy \\
L_3\left(\frac{u_3^\varepsilon - u_3}{\varepsilon}\right) &= \alpha \frac{u_3^\varepsilon - u_3}{\varepsilon} \int_{\Omega} \frac{u_1^\varepsilon}{1+u_1^\varepsilon} dy + \alpha u_3 \int_{\Omega} \frac{u_1^\varepsilon - u_1}{\varepsilon} \frac{1}{(1+u_1^\varepsilon)(1+u_1)} dy \\
&\quad - \alpha \left(\frac{u_3^\varepsilon - u_3}{\varepsilon}\right) \int_{\Omega} \frac{u_3^\varepsilon}{1+u_3^\varepsilon} dy - \alpha u_3 \int_{\Omega} \frac{u_2^\varepsilon - u_2}{\varepsilon} \frac{1}{(1+u_2^\varepsilon)(1+u_2)} dy \\
&\quad + hu_3^\varepsilon \int_{\Omega} \left(\frac{u_1^\varepsilon}{1+u_1^\varepsilon} - \frac{u_2^\varepsilon}{1+u_2^\varepsilon}\right) dy.
\end{aligned}$$

Taking the limit in the weak form of the PDEs satisfied by $\frac{u_i^\varepsilon - u_i}{\varepsilon}$ for $i = 1, 2, 3$, we obtain the PDE system for the sensitivities ψ_i , $i = 1, 2, 3$. \square

To derive the optimality system and to characterize the optimal control, we introduce adjoint variables and the adjoint operator in the sensitivity system for ψ_1, ψ_2, ψ_3 . We denote

the system of PDEs in ψ_1, ψ_2, ψ_3 as

$$\mathcal{L} \begin{pmatrix} \psi_1 \\ \psi_2 \\ \psi_3 \end{pmatrix} = \begin{pmatrix} hu_1 \int_{\Omega} \frac{u_3}{1+u_3} dx \\ -hu_2 \int_{\Omega} \frac{u_3}{1+u_3} dx \\ hu_3 \int_{\Omega} \left(\frac{u_1}{1+u_1} - \frac{u_2}{1+u_2} \right) dx \end{pmatrix}$$

where

$$\mathcal{L} \begin{pmatrix} \psi_1 \\ \psi_2 \\ \psi_3 \end{pmatrix} = \begin{pmatrix} L_1 \psi_1 \\ L_2 \psi_2 \\ L_3 \psi_3 \end{pmatrix} + B \begin{pmatrix} \psi_1 \\ \psi_2 \\ \psi_3 \end{pmatrix}$$

and

$$B \begin{pmatrix} \psi_1 \\ \psi_2 \\ \psi_3 \end{pmatrix} = \begin{pmatrix} \psi_1 \left(\int_{\Omega} \frac{u_2}{1+u_2} dx - \alpha \int_{\Omega} \frac{u_3}{1+u_3} dx \right) + u_1 \left(\int_{\Omega} \psi_2 \frac{1}{(1+u_2)^2} dx - \alpha \int_{\Omega} \psi_3 \frac{1}{(1+u_3)^2} dx \right) \\ \psi_2 \left(\int_{\Omega} \frac{u_1}{1+u_1} dx + \alpha \int_{\Omega} \frac{u_3}{1+u_3} dx \right) + u_2 \left(\int_{\Omega} \psi_1 \frac{1}{(1+u_1)^2} dx + \alpha \int_{\Omega} \psi_3 \frac{1}{(1+u_3)^2} dx \right) \\ -\alpha \psi_3 \int_{\Omega} \left(\frac{u_1}{1+u_1} - \frac{u_2}{1+u_2} \right) dx - \alpha u_3 \int_{\Omega} \left(\psi_1 \frac{1}{(1+u_1)^2} - \psi_2 \frac{1}{(1+u_2)^2} \right) dx \end{pmatrix}$$

Similarly, we denote the adjoint PDE system in p_1, p_2 and p_3 as

$$\mathcal{L}^* \begin{pmatrix} p_1 \\ p_2 \\ p_3 \end{pmatrix} = \begin{pmatrix} L(u_2 - u_1) \\ -L(u_2 - u_1) \\ Ku_3 \end{pmatrix}$$

where

$$\mathcal{L}^* \begin{pmatrix} p_1 \\ p_2 \\ p_3 \end{pmatrix} = \begin{pmatrix} L_1^* p_1 \\ L_2^* p_2 \\ L_3^* p_3 \end{pmatrix} + B^* \begin{pmatrix} p_1 \\ p_2 \\ p_3 \end{pmatrix}$$

and

$$B^* \begin{pmatrix} p_1 \\ p_2 \\ p_3 \end{pmatrix} = \begin{pmatrix} p_1 \left(\int_{\Omega} \frac{u_2}{1+u_2} dx - \alpha \int_{\Omega} \frac{u_3}{1+u_3} dx \right) + \frac{1}{(1+u_1)^2} \left(\int_{\Omega} p_2 u_2 dx - \int_{\Omega} \alpha p_3 u_3 dx \right) \\ p_2 \left(\int_{\Omega} \frac{u_1}{1+u_1} dx + \alpha \int_{\Omega} \frac{u_3}{1+u_3} dx \right) + \frac{1}{(1+u_2)^2} \left(\int_{\Omega} p_1 u_1 dx + \int_{\Omega} \alpha p_3 u_3 dx \right) \\ -\alpha p_3 \int_{\Omega} \left(\frac{u_1}{1+u_1} - \frac{u_2}{1+u_2} \right) dx - \frac{1}{(1+u_3)^2} \left(\int_{\Omega} \alpha p_1 u_1 dx - \int_{\Omega} \alpha p_2 u_2 dx \right) \end{pmatrix}$$

$$L_k \psi_k \equiv (\psi_k)_t - \sum_{i,j=1}^n (a_{ij}^k (\psi_k)_{x_i})_{x_j} + \sum_{i=1}^n b_i^k (\psi_k)_{x_i} + c^k \psi_k$$

$$L_k^* p_k \equiv -(p_k)_t - \sum_{i,j=1}^n (a_{ij}^k (p_k)_{x_i})_{x_j} - \sum_{i=1}^n (b_i^k p_k)_{x_i} + c^k p_k.$$

Finally we obtain the adjoint system and the characterization of the optimal control, which, together with state PDEs, form the optimality system.

Theorem 5. *Given an optimal control $\alpha \in U$ and corresponding solution $u = (u_1, u_2, u_3)$, there exists $p = (p_1, p_2, p_3)$, each component in $L^2(0, T; H_0^1(\Omega))$, satisfying the adjoint system:*

$$\begin{aligned} L_1^* p_1 &= L(u_2 - u_1) - p_1 \left(\int_{\Omega} \frac{u_2}{1+u_2} dx - \alpha \int_{\Omega} \frac{u_3}{1+u_3} dx \right) \\ &\quad - \frac{1}{(1+u_1)^2} \left(\int_{\Omega} p_2 u_2 dx - \int_{\Omega} \alpha p_3 u_3 dx \right) \\ L_2^* p_2 &= -L(u_2 - u_1) - p_2 \left(\int_{\Omega} \frac{u_1}{1+u_1} dx + \alpha \int_{\Omega} \frac{u_3}{1+u_3} dx \right) \\ &\quad - \frac{1}{(1+u_2)^2} \left(\int_{\Omega} p_1 u_1 dx + \int_{\Omega} \alpha p_3 u_3 dx \right) \\ L_3^* p_3 &= K u_3 + \alpha p_3 \left(\int_{\Omega} \frac{u_1}{1+u_1} dx - \int_{\Omega} \frac{u_2}{1+u_2} dx \right) \\ &\quad + \frac{1}{(1+u_3)^2} \left(\int_{\Omega} \alpha p_1 u_1 dx - \int_{\Omega} \alpha p_2 u_2 dx \right) \end{aligned} \tag{2.31}$$

in $Q = \Omega \times (0, T)$

$$\begin{aligned} p_k(x, T) &= 0 \text{ for } x \in \Omega, k = 1, 2, 3 \\ p_k &= 0 \text{ on } \partial\Omega \times (0, T), k = 1, 2, 3 \end{aligned} \tag{2.32}$$

for $k = 1, 2, 3$.

Futhermore we conclude

$$\alpha = \min\{\max\{\frac{1}{M}(p_1 u_1 - p_2 u_2) \int_{\Omega} \frac{u_3}{1+u_3} dx + \frac{p_3 u_3}{M} \int_{\Omega} (\frac{u_1}{1+u_1} - \frac{u_2}{1+u_2}) dx, -\overline{M}\}, \overline{M}\}. \quad (2.33)$$

Proof. Let α be an optimal control and (u_1, u_2, u_3) the corresponding solution. Given u_1, u_2, u_3 , the structure of the adjoint system is simpler than the state system due to the linearity of terms in p_1, p_2, p_3 . A fixed point argument in $C(0, T; L^2(\Omega))$ gives the existence of the solution to the adjoint system in $C(0, T; L^2(\Omega)) \cap L^2(0, T; H_0^1(\Omega))$. Note that we can estimate

$$\sup_t \int_{\Omega} (p_1^2 + p_2^2 + p_3^2)(x, t) dx$$

in terms of bounds on coefficients and the states u_i for $i = 1, 2, 3$. Then the right hand side of the adjoint system is L^∞ bounded, which implies the L^∞ boundedness of the adjoint function by the Maximum Principle.

Let $\alpha + \varepsilon h \in U$ for $\varepsilon > 0$. Let $u_k^\varepsilon = u_k(\alpha + \varepsilon h)$. The directional derivative of the objective functional $J(\alpha)$ with respect to α in the direction of h is calculated below:

$$\begin{aligned} \frac{J(\alpha + \varepsilon h) - J(\alpha)}{\varepsilon} &= \frac{1}{2} \int_Q [-L(u_2^\varepsilon + u_2 - u_1^\varepsilon - u_1) (\frac{u_2^\varepsilon - u_2}{\varepsilon} - \frac{u_1^\varepsilon - u_1}{\varepsilon}) + K \frac{(u_3^\varepsilon - u_3)(u_3^\varepsilon + u_3)}{\varepsilon} \\ &\quad - 2M\alpha h + \varepsilon M h^2] dx dt \end{aligned}$$

$$\lim_{\varepsilon \rightarrow 0^+} \frac{J(\alpha + \varepsilon h) - J(\alpha)}{\varepsilon} = \int_Q [L(u_2 - u_1)\psi_1 - L(u_2 - u_1)\psi_2 + K u_3 \psi_3 - M\alpha h] dx dt.$$

Since $J(\alpha)$ is the maximum value, we have

$$\begin{aligned}
0 &\geq \lim_{\varepsilon \rightarrow 0^+} \frac{J(\alpha + \varepsilon h) - J(\alpha)}{\varepsilon} \\
&= \int_Q [L(u_2 - u_1)\psi_1 - L(u_2 - u_1)\psi_2 + Ku_3\psi_3 - M\alpha h] dx dt \\
&= \int_Q \left[\begin{pmatrix} \psi_1 & \psi_2 & \psi_3 \end{pmatrix} \begin{pmatrix} L(u_2 - u_1) \\ -L(u_2 - u_1) \\ Ku_3 \end{pmatrix} - M\alpha h \right] dx dt \\
&= \int_Q \left[\begin{pmatrix} \psi_1 & \psi_2 & \psi_3 \end{pmatrix} \mathcal{L}^* \begin{pmatrix} p_1 \\ p_2 \\ p_3 \end{pmatrix} - M\alpha h \right] dx dt \text{ in weak sense} \\
&= \int_Q [-(p_1)_t \psi_1 + \sum_{i,j=1}^n a_{ij}^1(p_1)_{x_i}(\psi_1)_{x_j} - \sum_{i=1}^n (b_i^1 p_1)_{x_i} \psi_1 + c^1 p_1 \psi_1 \\
&\quad - (p_2)_t \psi_2 + \sum_{i,j=1}^n a_{ij}^2(p_2)_{x_i}(\psi_2)_{x_j} - \sum_{i=1}^n (b_i^2 p_2)_{x_i} \psi_2 + c^1 p_2 \psi_2 \\
&\quad - (p_3)_t \psi_3 + \sum_{i,j=1}^n a_{ij}^3(p_3)_{x_i}(\psi_3)_{x_j} - \sum_{i=1}^n (b_i^3 p_3)_{x_i} \psi_3 + c^3 p_3 \psi_3 \\
&\quad + \begin{pmatrix} \psi_1 & \psi_2 & \psi_3 \end{pmatrix} B^* \begin{pmatrix} p_1 \\ p_2 \\ p_3 \end{pmatrix}] dx dt - \int_Q M\alpha h dx dt \\
&= \int_Q [p_1(\psi_1)_t + \sum_{i,j=1}^n a_{ij}^1(p_1)_{x_i}(\psi_1)_{x_j} + \sum_{i=1}^n b_i^1 p_1(\psi_1)_{x_i} + c^1 p_1 \psi_1 \\
&\quad + p_2(\psi_2)_t + \sum_{i,j=1}^n a_{ij}^2(p_2)_{x_i}(\psi_2)_{x_j} + \sum_{i=1}^n b_i^2 p_2(\psi_2)_{x_i} + c^2 p_2 \psi_2
\end{aligned}$$

$$\begin{aligned}
& + p_3(\psi_3)_t + \sum_{i,j=1}^n a_{ij}^3(p_3)_{x_i}(\psi_3)_{x_j} + \sum_{i=1}^n b_i^3 p_3(\psi_3)_{x_i} + c^3 p_3 \psi_3 \\
& + \begin{pmatrix} p_1 & p_2 & p_3 \end{pmatrix} B \begin{pmatrix} \psi_1 \\ \psi_2 \\ \psi_3 \end{pmatrix} dx dt - \int_Q M \alpha h dx dt \\
& = \int_Q \left[\begin{pmatrix} p_1 & p_2 & p_3 \end{pmatrix} \mathcal{L} \begin{pmatrix} \psi_1 \\ \psi_2 \\ \psi_3 \end{pmatrix} - M \alpha h \right] dx dt \\
& = \int_Q \left[\begin{pmatrix} p_1 & p_2 & p_3 \end{pmatrix} \begin{pmatrix} hu_1 \int_{\Omega} \frac{u_3}{1+u_3} dy \\ -hu_2 \int_{\Omega} \frac{u_3}{1+u_3} dy \\ hu_3 \int_{\Omega} \left(\frac{u_1}{1+u_1} - \frac{u_2}{1+u_2} \right) dy \end{pmatrix} - M \alpha h \right] dx dt \\
& = \int_Q h \left[(p_1 u_1 - p_2 u_2) \int_{\Omega} \frac{u_3}{1+u_3} dy + p_3 u_3 \int_{\Omega} \left(\frac{u_1}{1+u_1} - \frac{u_2}{1+u_2} \right) dy - M \alpha \right] dx dt.
\end{aligned}$$

Hence, we have

$$\int_Q h \left[(p_1 u_1 - p_2 u_2) \int_{\Omega} \frac{u_3}{1+u_3} dy + p_3 u_3 \int_{\Omega} \left(\frac{u_1}{1+u_1} - \frac{u_2}{1+u_2} \right) dy - M \alpha \right] dx dt \leq 0.$$

Consider the following three cases.

(i) On the set $\{(x, t) \in Q \mid \alpha^*(x, t) = -\overline{M}\}$, the variation h with support on that set must be non-negative, and we have

$$\left[(p_1 u_1 - p_2 u_2) \int_{\Omega} \frac{u_3}{1+u_3} dy + p_3 u_3 \int_{\Omega} \left(\frac{u_1}{1+u_1} - \frac{u_2}{1+u_2} \right) dy - M \alpha \right] \leq 0,$$

which gives

$$\frac{1}{\overline{M}} \left[(p_1 u_1 - p_2 u_2) \int_{\Omega} \frac{u_3}{1+u_3} dy + p_3 u_3 \int_{\Omega} \left(\frac{u_1}{1+u_1} - \frac{u_2}{1+u_2} \right) dy \right] \leq \alpha = -\overline{M}.$$

(ii) On the set $\{(x, t) \in Q \mid \alpha(x, t) = \overline{M}\}$, the variation h must be non-positive, which gives

$$\frac{1}{M}[(p_1 u_1 - p_2 u_2) \int_{\Omega} \frac{u_3}{1 + u_3} dy + p_3 u_3 \int_{\Omega} (\frac{u_1}{1 + u_1} - \frac{u_2}{1 + u_2}) dy] \geq \alpha^* = \overline{M}.$$

(iii) On the set $\{(x, t) \in Q \mid -\overline{M} < \alpha(x, t) < \overline{M}\}$, the sign of variation h is arbitrary, and

$$[(p_1 u_1 - p_2 u_2) \int_{\Omega} \frac{u_3}{1 + u_3} dy + p_3 u_3 \int_{\Omega} (\frac{u_1}{1 + u_1} - \frac{u_2}{1 + u_2}) dy - M\alpha] = 0,$$

gives

$$\frac{1}{M}[(p_1 u_1 - p_2 u_2) \int_{\Omega} \frac{u_3}{1 + u_3} dy + p_3 u_3 \int_{\Omega} (\frac{u_1}{1 + u_1} - \frac{u_2}{1 + u_2}) dy] = \alpha.$$

Putting the three cases together,

$$\alpha = \min\{\max\{\frac{1}{M}(p_1 u_1 - p_2 u_2) \int_{\Omega} \frac{u_3}{1 + u_3} dx + \frac{p_3 u_3}{M} \int_{\Omega} (\frac{u_1}{1 + u_1} - \frac{u_2}{1 + u_2}) dx, -\overline{M}\}, \overline{M}\}$$

□

2.5 Uniqueness of the Optimality System

The optimality system consists of the state system (2.1)-(2.4) and the adjoint system(2.31)-(2.32) coupled with the characterization of the optimal control (2.33). We now prove that solutions of the optimality system are unique, which gives a characterization of the unique optimal control in terms of the unique solution of the optimality system. We know that the solution of the optimality system exists by Theorem 5.

Theorem 6. *The solution of the optimality system is unique for sufficiently small T .*

Proof. Suppose $(u_1, u_2, u_3, p_1, p_2, p_3)$ and $(\bar{u}_1, \bar{u}_2, \bar{u}_3, \bar{p}_1, \bar{p}_2, \bar{p}_3)$ are two solutions of the optimality system. Let

$$\alpha = \min\{\max\{\frac{1}{M}(p_1 u_1 - p_2 u_2) \int_{\Omega} \frac{u_3}{1+u_3} dx + \frac{p_3 u_3}{M} \int_{\Omega} (\frac{u_1}{1+u_1} - \frac{u_2}{1+u_2}) dx, -\bar{M}\}, \bar{M}\}$$

$$\bar{\alpha} = \min\{\max\{\frac{1}{M}(\bar{p}_1 \bar{u}_1 - \bar{p}_2 \bar{u}_2) \int_{\Omega} \frac{\bar{u}_3}{1+\bar{u}_3} dx + \frac{\bar{p}_3 \bar{u}_3}{M} \int_{\Omega} (\frac{\bar{u}_1}{1+\bar{u}_1} - \frac{\bar{u}_2}{1+\bar{u}_2}) dx, -\bar{M}\}, \bar{M}\}$$

We change the variables

$$u_i = e^{\lambda t} w_i, p_i = e^{-\lambda t} z_i, \bar{u}_i = e^{\lambda t} \bar{w}_i, \bar{p}_i = e^{-\lambda t} \bar{z}_i$$

where $\lambda > 0$ is to be chosen later. We subtract the bilinear forms of w_i and \bar{w}_i , p_i and \bar{p}_i .

The equation for $w_1 - \bar{w}_1$ is illustrated below.

$$\begin{aligned} & \int_Q ((w_1 - \bar{w}_1)_t \phi + \sum_{i,j=1}^n a_{ij}^1 (w_1 - \bar{w}_1)_{x_i} \phi_{x_j} + \sum_{i=1}^n b_i^1 (w_1 - \bar{w}_1)_{x_i} \phi + (c^1 + \lambda)(w_1 - \bar{w}_1) \phi) dx dt \\ &= - \int_Q (w_1 \int_{\Omega} \frac{w_2}{e^{-\lambda t} + w_2} dy - \bar{w}_1 \int_{\Omega} \frac{\bar{w}_2}{e^{-\lambda t} + \bar{w}_2} dy) \phi dx dt \\ & \quad + \int_Q (\alpha w_1 \int_{\Omega} \frac{w_3}{e^{-\lambda t} + w_3} dy - \bar{\alpha} \bar{w}_1 \int_{\Omega} \frac{\bar{w}_3}{e^{-\lambda t} + \bar{w}_3} dy) \phi dx dt \\ &= - \int_Q ((w_1 - \bar{w}_1) (\int_{\Omega} \frac{w_2}{e^{-\lambda t} + w_2} dy + \bar{w}_1 \int_{\Omega} \frac{e^{-\lambda t} (w_2 - \bar{w}_2)}{(e^{-\lambda t} + w_2)(e^{-\lambda t} + \bar{w}_2)} dy) \\ & \quad + (\alpha w_1 - \bar{\alpha} \bar{w}_1) \int_{\Omega} \frac{w_3}{e^{-\lambda t} + w_3} dy - \bar{\alpha} \bar{w}_1 \int_{\Omega} \frac{e^{-\lambda t} (w_3 - \bar{w}_3)}{(e^{-\lambda t} + w_3)(e^{-\lambda t} + \bar{w}_3)} dy) \phi dx dt \\ &\leq \int_Q [C_1 |w_1 - \bar{w}_1| + |\bar{w}_1| \int_{\Omega} |w_2 - \bar{w}_2| e^{\lambda t} dy + C_2 |\alpha w_1 - \bar{\alpha} \bar{w}_1| \\ & \quad + |\bar{\alpha} \bar{w}_1| \int_{\Omega} |w_3 - \bar{w}_3| e^{\lambda t} dy] |\phi| dx dt \end{aligned}$$

where $\phi \in L^2(0, T; H_0^1(\Omega))$.

We can get similar expressions for $w_2 - \bar{w}_2, w_3 - \bar{w}_3, z_1 - \bar{z}_1, z_2 - \bar{z}_2$ and $z_3 - \bar{z}_3$. By using test functions $w_i - \bar{w}_i, z_i - \bar{z}_i$ in the corresponding equations and adding the weak

formulations, we get the following:

$$\begin{aligned}
& \frac{1}{2} \int_{\Omega \times \{t=T\}} (|w_1 - \bar{w}_1|^2 + |w_2 - \bar{w}_2|^2 + |w_3 - \bar{w}_3|^2) dx \\
& + \theta \int_Q (|\nabla (w_1 - \bar{w}_1)|^2 + |\nabla (w_2 - \bar{w}_2)|^2 + |\nabla (w_3 - \bar{w}_3)|^2) dx dt \\
& + \int_Q ((c^1 + \lambda)|w_1 - \bar{w}_1|^2 + (c^2 + \lambda)|w_2 - \bar{w}_2|^2 + (c^3 + \lambda)|w_3 - \bar{w}_3|^2) dx dt \\
& \leq C_1 \int_Q e^{\lambda t} (|w_1 - \bar{w}_1| \int_{\Omega} |w_2 - \bar{w}_2| dy + |w_2 - \bar{w}_2| \int_{\Omega} |w_1 - \bar{w}_1| dy) dx dt \\
& + C_2 \int_Q (|\alpha w_1 - \bar{\alpha} \bar{w}_1| |w_1 - \bar{w}_1| + |\alpha w_2 - \bar{\alpha} \bar{w}_2| |w_2 - \bar{w}_2| + |\alpha w_3 - \bar{\alpha} \bar{w}_3| |w_3 - \bar{w}_3|) dx dt \\
& + C_3 \int_Q e^{\lambda t} (\bar{w}_1 |\bar{\alpha}| |w_1 - \bar{w}_1| + \bar{w}_2 |\bar{\alpha}| |w_2 - \bar{w}_2|) \left(\int_{\Omega} |w_3 - \bar{w}_3| dy \right) dx dt \\
& + \int_Q \bar{w}_3 |\bar{\alpha}| |w_3 - \bar{w}_3| e^{\lambda t} \left[\int_{\Omega} (|w_1 - \bar{w}_1| + |w_2 - \bar{w}_2|) dy \right] dx dt \\
& + \frac{1}{2} \theta \int_Q (|\nabla (w_1 - \bar{w}_1)|^2 + |\nabla (w_2 - \bar{w}_2)|^2 + |\nabla (w_3 - \bar{w}_3)|^2) dx dt \\
& + C_4 \int_Q (|w_1 - \bar{w}_1|^2 + |w_2 - \bar{w}_2|^2 + |w_3 - \bar{w}_3|^2) dx dt
\end{aligned}$$

We illustrate the estimates of two specific terms from the right-hand side. The terms of the form

$$\int_Q e^{\lambda t} |w_i - \bar{w}_i| \int_{\Omega} |w_j - \bar{w}_j| dy dx dt$$

or from the adjoint equations

$$\int_Q e^{\lambda t} |z_i - \bar{z}_i| \int_{\Omega} |z_j - \bar{z}_j| dy dx dt$$

where $i \neq j$, are estimated by using the Hölder's inequality and the Cauchy inequality as

follows:

$$\begin{aligned}
C_1 \int_Q e^{\lambda t} |w_1 - \bar{w}_1| \int_{\Omega} |w_2 - \bar{w}_2| dy dx dt &= C_1 e^{\lambda T} \int_0^T \left(\int_{\Omega} |w_1 - \bar{w}_1| dx \right) \left(\int_{\Omega} |w_2 - \bar{w}_2| dy \right) dt \\
&\leq C_2 e^{\lambda T} \int_0^T \left(\int_{\Omega} |w_1 - \bar{w}_1|^2 dx \right)^{\frac{1}{2}} \left(\int_{\Omega} |w_2 - \bar{w}_2|^2 dy \right)^{\frac{1}{2}} dt \\
&\leq C_3 e^{\lambda T} \int_0^T \left(\int_{\Omega} |w_1 - \bar{w}_1|^2 dx \right) + \left(\int_{\Omega} |w_2 - \bar{w}_2|^2 dy \right) dt.
\end{aligned}$$

The terms of the form

$$\int_Q |\alpha w_i - \bar{\alpha} \bar{w}_i| |w_j - \bar{w}_j| dx dt$$

or

$$\int_Q |\alpha z_i - \bar{\alpha} \bar{z}_i| |z_j - \bar{z}_j| dx dt$$

are estimated as follows:

$$\begin{aligned}
C_2 \int_Q |\alpha w_1 - \bar{\alpha} \bar{w}_1| |w_1 - \bar{w}_1| dx dt &= C_2 \int_Q |\alpha w_1 - \alpha \bar{w}_1 + \alpha \bar{w}_1 - \bar{\alpha} \bar{w}_1| |w_1 - \bar{w}_1| dx dt \\
&\leq C_2 \int_Q |\alpha(w_1 - \bar{w}_1) + \bar{w}_1(\alpha - \bar{\alpha})| |w_1 - \bar{w}_1| dx dt \\
&\leq C_2 \int_Q |\alpha| |w_1 - \bar{w}_1|^2 + |\bar{w}_1| |\alpha - \bar{\alpha}| |w_1 - \bar{w}_1| dx dt.
\end{aligned}$$

In order to estimate the second term of the above integral, we estimate $|\alpha - \bar{\alpha}|$.

Using (2.33), we obtain

$$\begin{aligned}
|\alpha - \bar{\alpha}| &\leq \left| \frac{1}{M} (z_1 w_1 \int_{\Omega} \frac{w_3}{e^{-\lambda t} + w_3} dx - \bar{z}_1 \bar{w}_1 \int_{\Omega} \frac{\bar{w}_3}{e^{-\lambda t} + \bar{w}_3} dx - z_2 w_2 \int_{\Omega} \frac{w_3}{e^{-\lambda t} + w_3} dx \right. \\
&\quad + \bar{z}_2 \bar{w}_2 \int_{\Omega} \frac{\bar{w}_3}{e^{-\lambda t} + \bar{w}_3} dx + z_3 w_3 \int_{\Omega} \frac{w_1}{e^{-\lambda t} + w_1} dx - \bar{z}_3 \bar{w}_3 \int_{\Omega} \frac{\bar{w}_1}{e^{-\lambda t} + \bar{w}_1} dx \\
&\quad \left. - z_3 w_3 \int_{\Omega} \frac{w_2}{e^{-\lambda t} + w_2} dx + \bar{z}_3 \bar{w}_3 \int_{\Omega} \frac{\bar{w}_2}{e^{-\lambda t} + \bar{w}_2} dx) \right| \\
&\leq \frac{1}{M} (|z_1 w_1 - \bar{z}_1 \bar{w}_1| \int_{\Omega} \frac{|w_3|}{|e^{-\lambda t} + w_3|} dx + |\bar{z}_1 \bar{w}_1| \int_{\Omega} \frac{e^{-\lambda t} |w_3 - \bar{w}_3|}{|e^{-\lambda t} + w_3| |e^{-\lambda t} + \bar{w}_3|} dx \\
&\quad + |z_2 w_2 - \bar{z}_2 \bar{w}_2| \int_{\Omega} \frac{|w_3|}{|e^{-\lambda t} + w_3|} dx + |\bar{z}_2 \bar{w}_2| \int_{\Omega} \frac{e^{-\lambda t} |w_3 - \bar{w}_3|}{|e^{-\lambda t} + w_3| |e^{-\lambda t} + \bar{w}_3|} dx \\
&\quad + |z_3 w_3 - \bar{z}_3 \bar{w}_3| \int_{\Omega} \frac{|w_1|}{|e^{-\lambda t} + w_1|} dx + |\bar{z}_3 \bar{w}_3| \int_{\Omega} \frac{e^{-\lambda t} |w_1 - \bar{w}_1|}{|e^{-\lambda t} + w_1| |e^{-\lambda t} + \bar{w}_1|} dx \\
&\quad + |z_3 w_3 - \bar{z}_3 \bar{w}_3| \int_{\Omega} \frac{|w_2|}{|e^{-\lambda t} + w_2|} dx + |\bar{z}_3 \bar{w}_3| \int_{\Omega} \frac{e^{-\lambda t} |w_2 - \bar{w}_2|}{|e^{-\lambda t} + w_2| |e^{-\lambda t} + \bar{w}_2|} dx) \\
&\leq \frac{1}{M} (C_1 |z_1 w_1 - \bar{z}_1 \bar{w}_1| + |\bar{z}_1 \bar{w}_1| \int_{\Omega} e^{\lambda t} |w_3 - \bar{w}_3| dx \\
&\quad + C_2 |z_2 w_2 - \bar{z}_2 \bar{w}_2| + |\bar{z}_2 \bar{w}_2| \int_{\Omega} e^{\lambda t} |w_3 - \bar{w}_3| dx \\
&\quad + C_3 |z_3 w_3 - \bar{z}_3 \bar{w}_3| + |\bar{z}_3 \bar{w}_3| \int_{\Omega} e^{\lambda t} (|w_1 - \bar{w}_1| + |w_2 - \bar{w}_2|) dx) \\
&\leq \frac{C_4}{M} (|z_1 w_1 - \bar{z}_1 \bar{w}_1| + |z_2 w_2 - \bar{z}_2 \bar{w}_2| + |z_3 w_3 - \bar{z}_3 \bar{w}_3| \\
&\quad + e^{\lambda t} \int_{\Omega} (|w_1 - \bar{w}_1| + |w_2 - \bar{w}_2| + |w_3 - \bar{w}_3|) dx)
\end{aligned}$$

using L^∞ bounds on the state and the adjoint variables.

To illustrate, we substitute this estimate into a particular term.

$$\begin{aligned}
& C_2 \int_Q |\bar{w}_1| |\alpha - \bar{\alpha}| |w_1 - \bar{w}_1| dx dt \\
& \leq \frac{C_5}{M} \left[\int_Q (|z_1 w_1 - \bar{z}_1 \bar{w}_1| + |z_2 w_2 - \bar{z}_2 \bar{w}_2| + |z_3 w_3 - \bar{z}_3 \bar{w}_3|) |w_1 - \bar{w}_1| dx dt \right. \\
& \quad \left. + \int_Q e^{\lambda t} |w_1 - \bar{w}_1| \int_{\Omega} (|w_1 - \bar{w}_1| + |w_2 - \bar{w}_2| + |w_3 - \bar{w}_3|) dy dx dt \right] \\
& = \frac{C_5}{M} \int_Q (|z_1 w_1 - z_1 \bar{w}_1 + z_1 \bar{w}_1 - \bar{z}_1 \bar{w}_1| |w_1 - \bar{w}_1| + |z_2 w_2 - z_2 \bar{w}_2 + z_2 \bar{w}_2 - \bar{z}_2 \bar{w}_2| |w_1 - \bar{w}_1| \\
& \quad + |z_3 w_3 - z_3 \bar{w}_3 + z_3 \bar{w}_3 - \bar{z}_3 \bar{w}_3| |w_1 - \bar{w}_1|) dx dt \\
& \quad + \int_Q e^{\lambda t} |w_1 - \bar{w}_1| \int_{\Omega} (|w_1 - \bar{w}_1| + |w_2 - \bar{w}_2| + |w_3 - \bar{w}_3|) dy dx dt \\
& \leq \frac{C_5}{M} \int_Q (|z_1| |w_1 - \bar{w}_1|^2 + |\bar{w}_1| |z_1 - \bar{z}_1| |w_1 - \bar{w}_1| + |z_2| |w_2 - \bar{w}_2| |w_1 - \bar{w}_1| \\
& \quad + |z_2 - \bar{z}_2| |\bar{w}_2| |w_1 - \bar{w}_1| + |z_3| |w_3 - \bar{w}_3| |w_1 - \bar{w}_1| + |z_3 - \bar{z}_3| |\bar{w}_3| |w_1 - \bar{w}_1|) dx dt \\
& \quad + \int_Q e^{\lambda t} |w_1 - \bar{w}_1| \int_{\Omega} (|w_1 - \bar{w}_1| + |w_2 - \bar{w}_2| + |w_3 - \bar{w}_3|) dy dx dt.
\end{aligned}$$

By using that w_i, z_i are L^∞ bounded and Hölder's and Cauchy's inequalities as before, we have,

$$\begin{aligned}
& C_2 \int_Q |\bar{w}_1| |\alpha - \bar{\alpha}| |w_1 - \bar{w}_1| dx dt \\
& \leq C_6 \left(\int_Q (|w_1 - \bar{w}_1|^2 + |w_2 - \bar{w}_2|^2 + |w_3 - \bar{w}_3|^2) dx dt \right) \\
& \quad + C_7 \left(\int_Q (|z_1 - \bar{z}_1|^2 + |z_2 - \bar{z}_2|^2 + |z_3 - \bar{z}_3|^2) dx dt \right) \\
& \quad + C_8 e^{\lambda T} \int_Q (|w_1 - \bar{w}_1|^2 + |w_2 - \bar{w}_2|^2 + |w_3 - \bar{w}_3|^2) dx dt.
\end{aligned}$$

The combined estimate becomes

$$\begin{aligned}
& \frac{1}{2} \int_{\Omega \times \{t=T\}} (|w_1 - \bar{w}_1|^2 + |w_2 - \bar{w}_2|^2 + |w_3 - \bar{w}_3|^2) dx \\
& + \frac{1}{2} \int_{\Omega \times \{t=0\}} (|z_1 - \bar{z}_1|^2 + |z_2 - \bar{z}_2|^2 + |z_3 - \bar{z}_3|^2) dx \\
& + \theta \int_Q (|\nabla (w_1 - \bar{w}_1)|^2 + |\nabla (w_2 - \bar{w}_2)|^2 + |\nabla (w_3 - \bar{w}_3)|^2 \\
& + |\nabla (z_1 - \bar{z}_1)|^2 + |\nabla (z_2 - \bar{z}_2)|^2 + |\nabla (z_3 - \bar{z}_3)|^2) dx dt \\
& + \int_Q ((c^1 + \lambda)(|w_1 - \bar{w}_1|^2 + |z_1 - \bar{z}_1|^2) + (c^2 + \lambda)(|w_2 - \bar{w}_2|^2 + |z_2 - \bar{z}_2|^2) \\
& + (c^3 + \lambda)(|w_3 - \bar{w}_3|^2 + |z_3 - \bar{z}_3|^2)) dx dt \\
& \leq C_3 \left(\int_Q (|w_1 - \bar{w}_1|^2 + |w_2 - \bar{w}_2|^2 + |w_3 - \bar{w}_3|^2 + |z_1 - \bar{z}_1|^2 + |z_2 - \bar{z}_2|^2 + |z_3 - \bar{z}_3|^2) dx dt \right. \\
& + e^{\lambda T} \int_Q (|w_1 - \bar{w}_1|^2 + |w_2 - \bar{w}_2|^2 + |w_3 - \bar{w}_3|^2 + |z_1 - \bar{z}_1|^2 + |z_2 - \bar{z}_2|^2 + |z_3 - \bar{z}_3|^2) dx dt \\
& \left. + \frac{1}{2} \theta \int_Q (|\nabla (w_1 - \bar{w}_1)|^2 + |\nabla (w_2 - \bar{w}_2)|^2 + |\nabla (w_3 - \bar{w}_3)|^2) dx dt \right).
\end{aligned}$$

By combining like terms, we have,

$$\begin{aligned}
& \frac{1}{2} \int_{\Omega \times \{t=T\}} (|w_1 - \bar{w}_1|^2 + |w_2 - \bar{w}_2|^2 + |w_3 - \bar{w}_3|^2) dx \\
& + \frac{1}{2} \int_{\Omega \times \{t=0\}} (|z_1 - \bar{z}_1|^2 + |z_2 - \bar{z}_2|^2 + |z_3 - \bar{z}_3|^2) dx \\
& + \frac{1}{2} \theta \int_Q (|\nabla (w_1 - \bar{w}_1)|^2 + |\nabla (w_2 - \bar{w}_2)|^2 + |\nabla (w_3 - \bar{w}_3)|^2 \\
& + |\nabla (z_1 - \bar{z}_1)|^2 + |\nabla (z_2 - \bar{z}_2)|^2 + |\nabla (z_3 - \bar{z}_3)|^2) dx dt \\
& + \int_Q ((-C_4 + \lambda - C_3(1 + e^{\lambda T}))(|w_1 - \bar{w}_1|^2 + |w_2 - \bar{w}_2|^2 + |w_3 - \bar{w}_3|^2 \\
& + |z_1 - \bar{z}_1|^2 + |z_2 - \bar{z}_2|^2 + |z_3 - \bar{z}_3|^2)) dx dt \\
& \leq 0
\end{aligned}$$

where $-C_4$ is a lower bound on c^i for $i = 1, 2, 3$.

First, choose λ to be a positive number satisfying

$$-C_4 + \lambda - C_3 > C_3$$

i.e.,

$$\lambda > 2C_3 + C_4.$$

Therefore, if we choose T such that

$$\frac{\ln \frac{\lambda - (C_3 + C_4)}{C_3}}{\lambda} > T$$

we have

$$-C_4 + \lambda - C_3(1 + e^{\lambda T}) > 0.$$

Therefore, we obtain $w_i = \bar{w}_i$ and $z_i = \bar{z}_i$. Thus, $u_i = \bar{u}_i$ and $p_i = \bar{p}_i$ for $i = 1, 2, 3$. \square

This result gives a characterization of the unique optimal control in terms of the unique solution of the optimality system.

2.6 Numerical Results - Control Function $\alpha(t)$

In Theorem 8, we showed that the optimal control is characterized in terms of state and adjoint variables for the control function of the form $\alpha(x, t)$ as follows.

$$\alpha = \min\{\max\{\frac{1}{M}(p_1 u_1 - p_2 u_2) \int_{\Omega} \frac{u_3}{1 + u_3} dx + \frac{p_3 u_3}{M} \int_{\Omega} (\frac{u_1}{1 + u_1} - \frac{u_2}{1 + u_2}) dx, -\bar{M}\}, \bar{M}\}.$$

If the control is a function of time only, then the above characterization becomes

$$\alpha = \min\{\max\{\frac{1}{M} \int_{\Omega} [(p_1 u_1 - p_2 u_2) \int_{\Omega} \frac{u_3}{1 + u_3} dx + p_3 u_3 \int_{\Omega} (\frac{u_1}{1 + u_1} - \frac{u_2}{1 + u_2}) dx] dy, -\bar{M}\}, \bar{M}\}.$$

We numerically solve the simplified version of our problem in one spatial dimension using different values of scaling constants in the objective functional and initial populations. For

simplicity, we set all source terms and the coefficients b_1^k and c_1^k to be zero for all $k = 1, 2, 3$.

Then, the state system (2.1)-(2.4) becomes

$$\begin{aligned}
(u_1)_t - a_1^1(u_1)_{xx} &= -u_1 \int_{\Omega} \frac{u_2}{1+u_2} dx + \alpha u_1 \int_{\Omega} \frac{u_3}{1+u_3} dx \\
(u_2)_t - a_1^2(u_3)_{xx} &= -u_2 \int_{\Omega} \frac{u_1}{1+u_1} dx - \alpha u_2 \int_{\Omega} \frac{u_3}{1+u_3} dx \\
(u_3)_t - a_1^3(u_3)_{xx} &= \alpha u_3 \int_{\Omega} \frac{u_1}{1+u_1} dx - \alpha u_3 \int_{\Omega} \frac{u_2}{1+u_2} dx
\end{aligned} \tag{2.34}$$

Initial Conditions:

$$u_k(x, 0) = u_{k0}(x) \text{ for } x \in \Omega, k = 1, 2, 3 \tag{2.35}$$

Boundary Conditions:

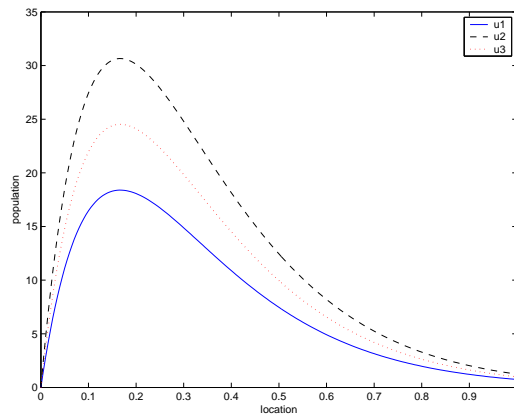
$$u_k = 0 \text{ on } \partial\Omega \times (0, T), k = 1, 2, 3 \tag{2.36}$$

where $\Omega = [0, 1]$ and $T = 0.0375$.

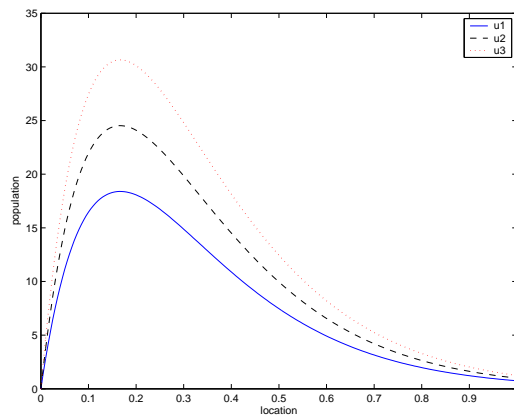
Numerical solutions for the three populations and the optimal control have been generated iteratively using the finite difference method with central differences for second derivative terms. First, with the initial guess for the control, the state system is solved forward in time. Using these state solutions, we solve the adjoint system backward in time. We repeat the iteration with the updated control until the solutions converge.

We examined how the difference in the weight constants in the objective functional (2.5) affect the optimal control and final time population distribution. In this section, we discuss the results using three different initial population distributions (A, B and C) shown in Figure 2.1 and four different settings of weight constants and control bounds as the following.

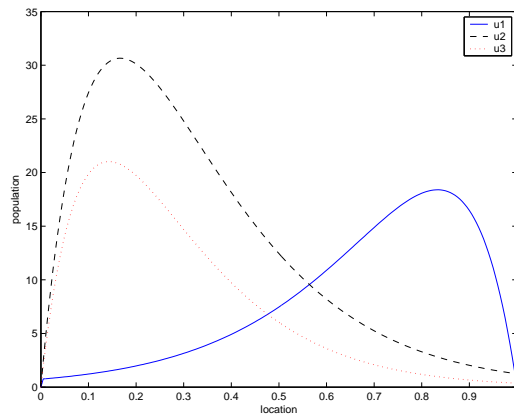
1. $K = 1, L = 1, M = 0.1$ and $\overline{M} = 5$
2. $K = 1, L = 0.1, M = 0.1$ and $\overline{M} = 5$
3. $K = 1, L = 0.1, M = 0.01$ and $\overline{M} = 5$
4. $K = 1, L = 0.01, M = 0.1$ and $\overline{M} = 5$
5. $K = 1, L = 0.1, M = 0.01$ and $\overline{M} = 20$.



(a) Initial population A



(b) Initial population B



(c) Initial population C

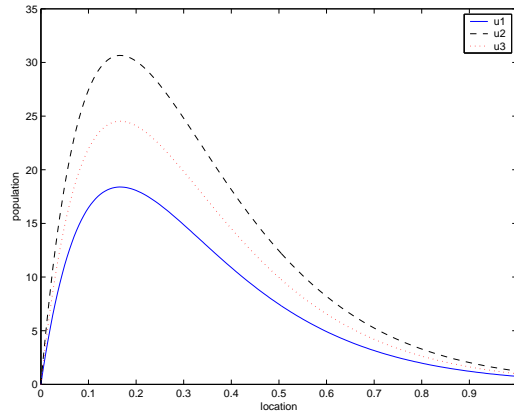
Figure 2.1: Initial population distribution A, B and C.

We set $a_1^1 \equiv a_1^2 \equiv a_1^3 \equiv 0.6$, i.e., all populations have the same diffusivity, except in a few cases. Since there is no source terms and individuals die at the both boundaries ($x = 0$ and $x = 1$), all populations eventually die out if T is long enough.

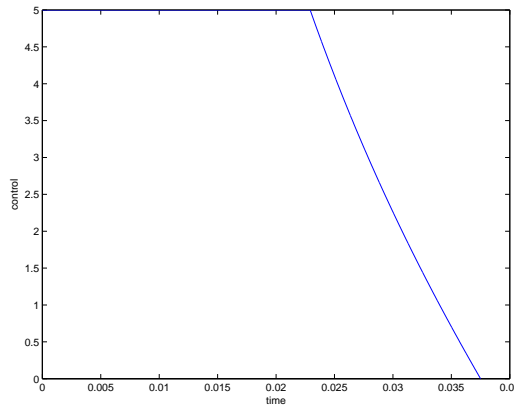
Figure 2.2 and Figure 2.3 show the two solutions with the same initial population distribution (Initial population A) but different sets of weight constants. In initial population distribution A, u_3 is between u_1 and u_2 , and the u_2 is the largest of all. Figure 2.2(b) shows the optimal control with $K = 1$, $L = 1$, $M = 0.1$ and $\bar{M} = 5$ and Figure 2.3(b) shows the optimal control with $K = 1$, $L = 0.1$, $M = 0.1$ and $\bar{M} = 5$. In both cases, population 3 cooperates with population 1 all the time, however, population 3 cooperates with population 1 more strongly in the case of $L = 1$. Figure 2.2(c) and Figure 2.3(c) show that the difference between the competing populations 1 and 2 is smaller for $L = 1$ than for $L = 0.1$. The objective functional values, $J(\alpha^*)$ for $L = 1$ and $L = 0.1$ are 3.6033 and 4.2259 respectively. Population 3 maximizes the objective functional value by decreasing the alliance with population 1 when L gets smaller since the increased difference between populations 1 and 2 does not have a strong effect.

Now, we also change the value M from 0.1 to 0.01. The weight constant setting is $K = 1$, $L = 0.1$, $M = 0.1$ and $\bar{M} = 5$. Smaller M means the cost associated with the alliance is less. Thus, we would expect that population 3 tries to cooperate with population 1 more strongly. In fact, Figure 2.4(b) shows population 3 strengthens the alliance much more when compared with Figure 2.3(b). Consequently, the difference of the two competing populations 1 and 2 becomes smaller and the objective functional value is 4.23.

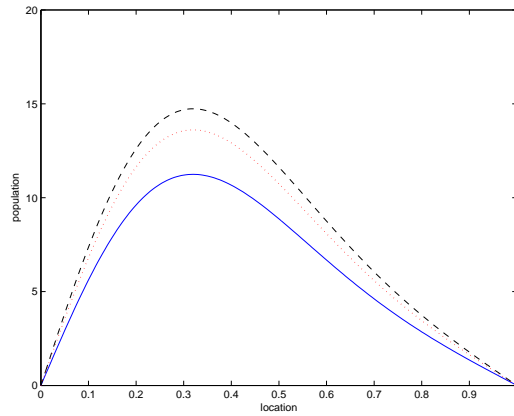
Next, we modify the scaling constant L to 0.01 and set $M = 0.1$. This means that the difference between the competing populations 1 and 2 becomes much less important, while the size of population 3 becomes more important. In this new setting, the optimal control is quite different from the previous examples with $L = 1$ or $L = 0.1$. Population 3 cooperates with population 2 all the time. The optimal control and the final time population distribution are given in Figures 2.5(b) and 2.5(c). Since population 2 is more dominant than population 1, population 3 gets more benefit by cooperating with the higher population. In this setting, $J(\alpha^*) = 4.3257$. It is interesting to see that the final time distribution for



(a) Initial population

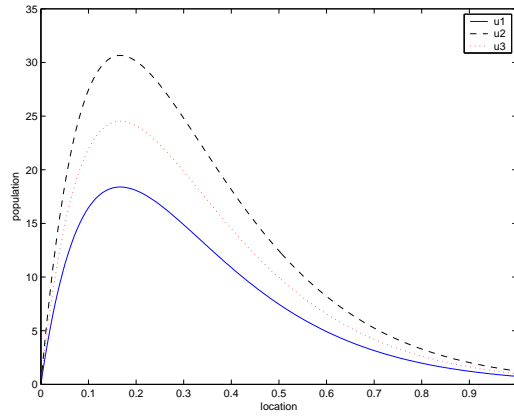


(b) Optimal control

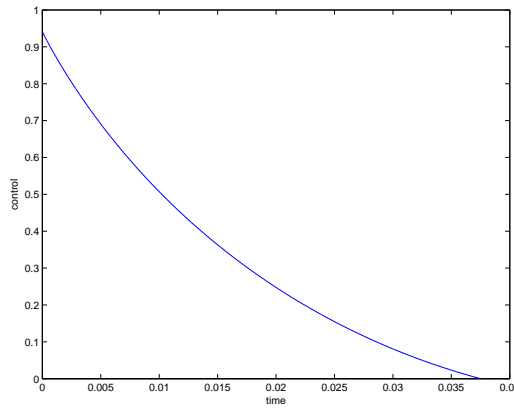


(c) Population at final time T

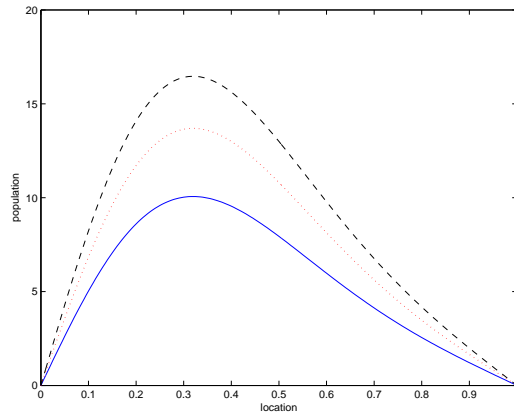
Figure 2.2: Population distribution and optimal control $\alpha(t)$ with $K = 1, L = 1, M = 0.1, \bar{M} = 5$.



(a) Initial population

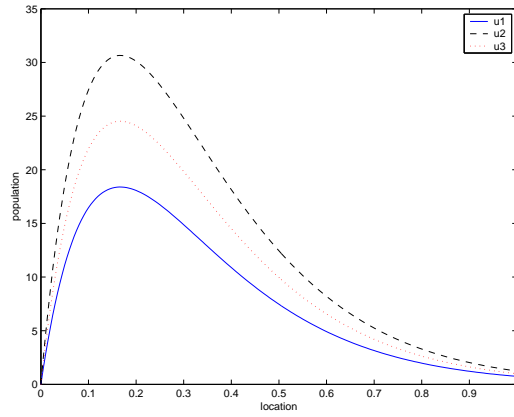


(b) Optimal control

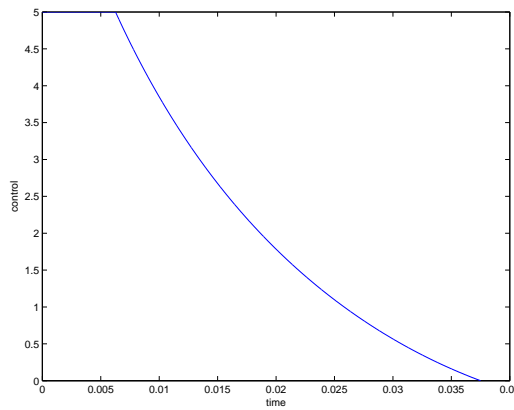


(c) Population at final time T

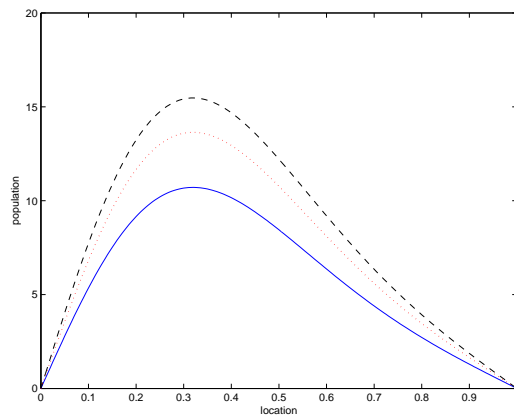
Figure 2.3: Population distribution and optimal control $\alpha(t)$ with $K = 1, L = 0.1, M = 0.1, \bar{M} = 5$.



(a) Initial population

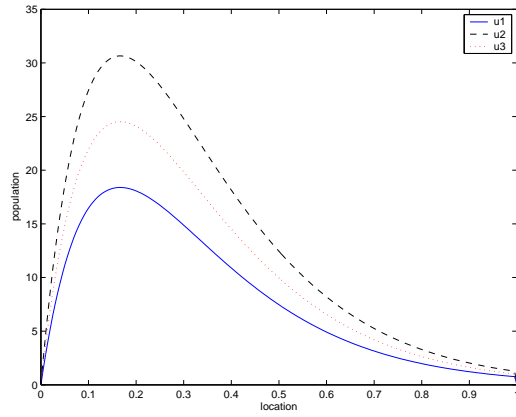


(b) Optimal control

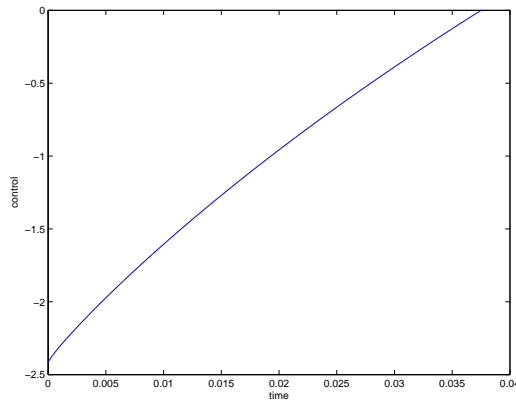


(c) Population at final time T

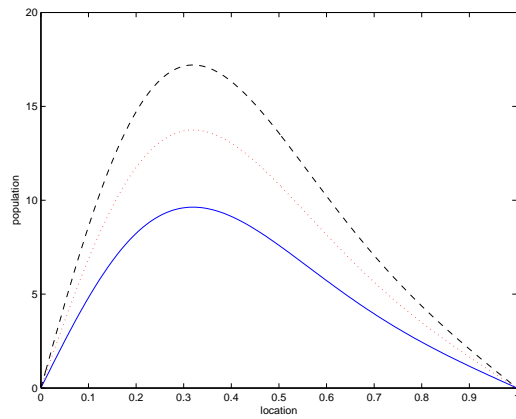
Figure 2.4: Population distribution and optimal control $\alpha(t)$ with $K = 1, L = 0.1, M = 0.01, \bar{M} = 5$.



(a) Initial population



(b) Optimal control



(c) Population at final time T

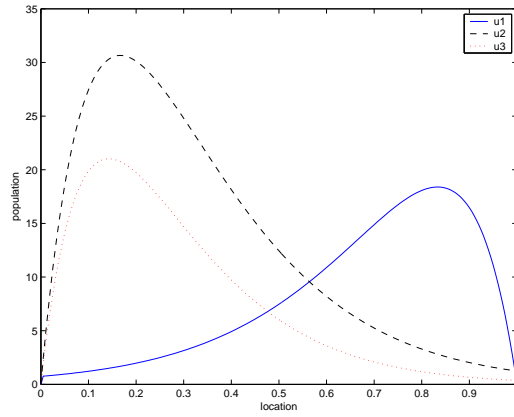
Figure 2.5: Population distribution and optimal control $\alpha(t)$ with $K = 1, L = 0.01, M = 0.1, \bar{M} = 5$.

population 3 is almost the same but the objective functional value is increased. Moreover, the final time populations 1 and 2 are much greater than the cases with $L = 1$ and $L = 0.1$. Since the magnitude of the control is less than the previous example with $L = 1$ (see Figure 2.2(b) and Figure 2.5(b)), the cost associated with the alliance is smaller. Moreover, the small value of the weight constant L allows the large difference of populations 1 and 2 without lowering the objective functional value.

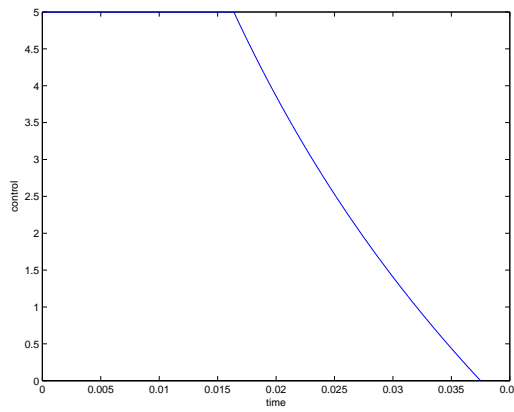
Next, we examined the outcome with the same weight constant setting: $K = 1$, $L = 0.1$, $M = 0.01$ and $\bar{M} = 5$ but changed the initial population distribution from A to C (see Figure 2.1(a) and 2.1(c)). In initial population distribution C, the peaks of u_1 and u_2 are at different locations. The optimal control starting with the initial population C is given in Figure 2.6(b) and the final time population distribution is given in Figure 2.6(c). The sign of the optimal control is positive all the time, i.e., population 3 cooperates with the population 1. Since the cost of the alliance is small, population 3 tries to maximize the objective functional value by cooperating with smaller population 1 and minimizing the difference between the competing populations 1 and 2. The objective functional value $J(\alpha^*)$ is 2.0086 in this setting.

When we start with the initial population B with u_3 being the largest with the setting $K = 1$, $L = 1$, $M = 0.1$ and $\bar{M} = 5$ (Figure 2.7), the population 3 always cooperates with the weaker population 1 and maximizes the objective functional value by reducing the difference of the populations 1 and 2. Compare with Figure 2.2.

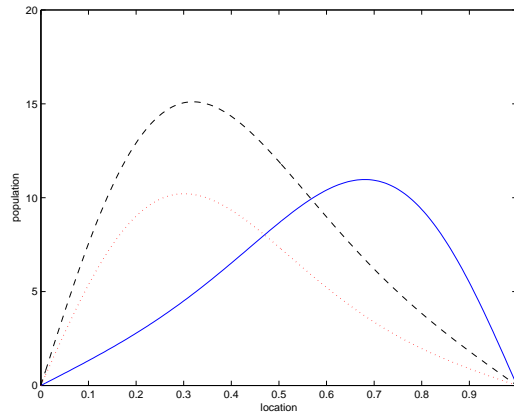
So far, we analyzed the cases in which all the diffusivity constants for the three populations are equal. Now, we start with the same initial population A (Figure 2.1(a)) with the setting: $K = 1$, $L = 1$, $M = 0.1$ and $\bar{M} = 5$ but set the diffusivity constants to $a^1 = 0.8$, $a^2 = 0.6$, $a^3 = 0.4$. This means population 1 diffuses more quickly and dies at the boundaries faster than the other two. The optimal control with this setting is given in Figure 2.8(b), slightly different from the one with the same diffusivity constants setting. However, the final time population distribution is different (see Figure 2.2(c) and 2.8(c)). Population 3 cooperates with population 1 all the time but for a little longer duration in the new setting. Since population 1 decreases in size more rapidly than population 2, the



(a) Initial population

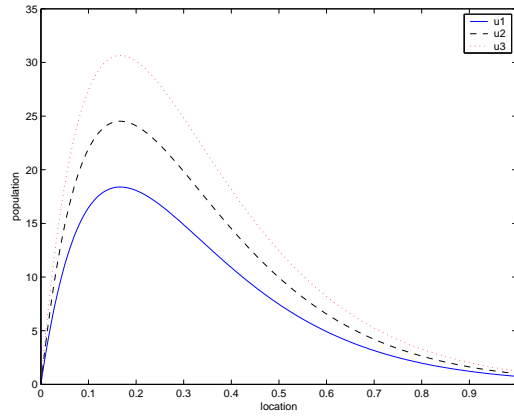


(b) Optimal control

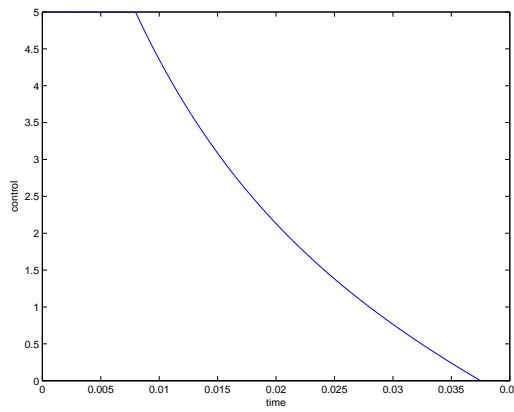


(c) Population at final time T

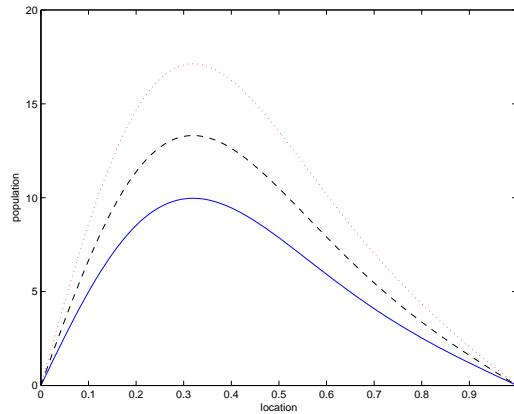
Figure 2.6: Population distribution and optimal control $\alpha(t)$ with initial population C , $K = 1, L = 0.1, M = 0.01, \bar{M} = 5$.



(a) Initial population

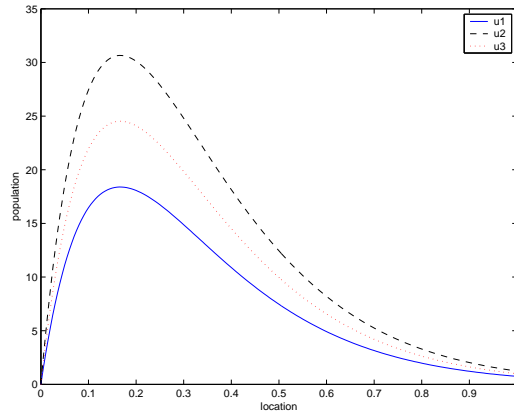


(b) Optimal control

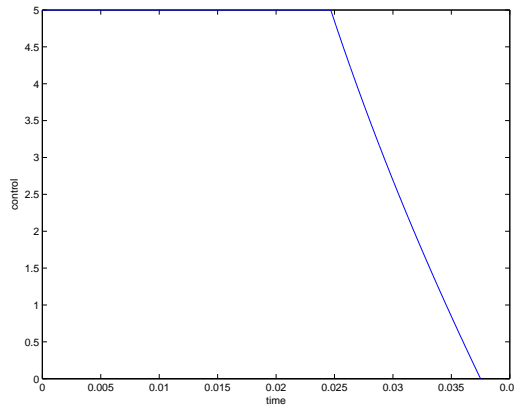


(c) Population at final time T

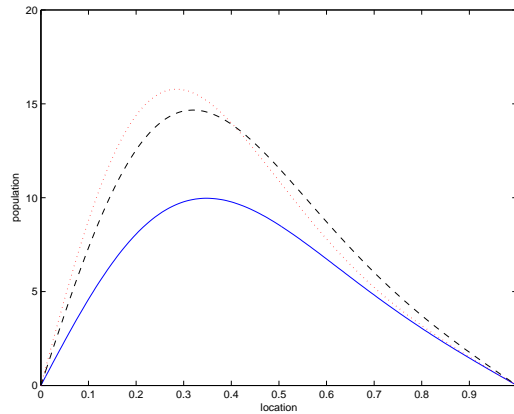
Figure 2.7: Population distribution and optimal control $\alpha(t)$ with initial population B , $K = 1, L = 1, M = 0.1, \bar{M} = 5$.



(a) Initial population



(b) Optimal control



(c) Population at final time T

Figure 2.8: Population distribution and optimal control $\alpha(t)$ with $K = 1, L = 1, M = 0.1, \bar{M} = 5, a^1 = 0.8, a^2 = 0.6, a^3 = 0.4$.

difference between the two populations tends to increase, therefore, population 3 tries to help the smaller population to improve the objective functional. The objective functional value is 4.0166, which is slightly larger than the equal diffusivity case.

In the next section, we consider a more general form of the control function, $\alpha(x, t)$. Now, the control function depends on both space and time.

2.7 Numerical Results - Control Function $\alpha(x, t)$

In the previous section, the control function only depends on time, but now we consider the control function which depends on both time and space.

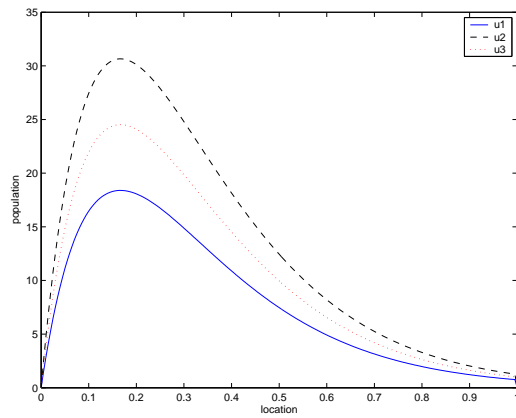
First, we examined how the solutions are different with the same initial population distribution and the weight constants when we allow the control function to depend on both time and space. We generated the solutions with the following settings.

1. $K = 1, L = 1, M = 0.1$ and $\bar{M} = 5$ with initial population distribution A
2. $K = 1, L = 0.01, M = 0.1$ and $\bar{M} = 5$ with initial population distribution A
3. $K = 1, L = 0.1, M = 0.01$ and $\bar{M} = 5$ with initial population distribution C

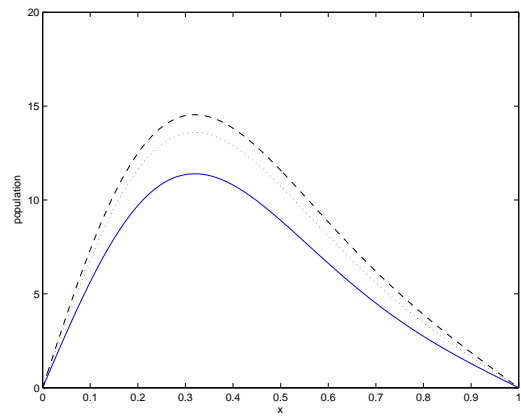
In addition to the graphs of the optimal control and the final time distribution, the cross sectional view of the optimal control at different times is given for each setting.

Consider the case with $K = 1, L = 1, M = 0.1$ and $\bar{M} = 5$ with initial population distribution A. In initial population distribution A, u_3 is between u_1 and u_2 , and the u_2 is the largest of all. Figure 2.9 represents the results with the optimal control function $\alpha(x, t)$ and the corresponding results with the optimal control $\alpha(t)$ is shown in Figure 2.2. The final time population distributions are almost the same for both cases. Figure 2.9(c) shows that population 3 cooperates with population 1 all the time at any location. The alliance is stronger where the difference between populations 1 and 2 are larger and smaller at both ends where the size of all the populations are small. The objective functional value with the control $\alpha(x, t)$ is 3.6208, which is slightly larger than the case of $\alpha(t)$ cases.

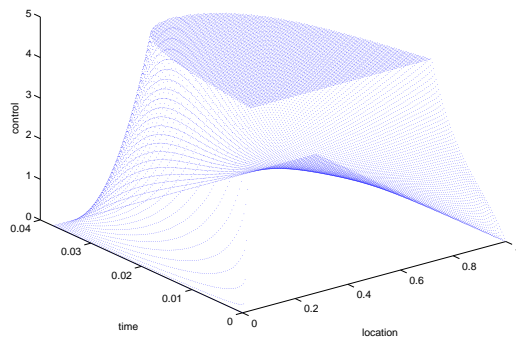
When we change the value of L from 1 to 0.01 with the same initial population distribution, the sign of the optimal control was reversed from positive to negative and the



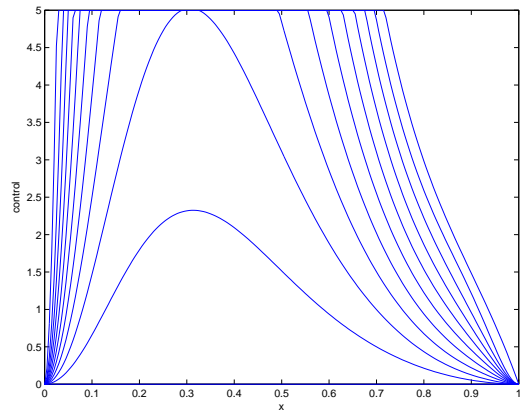
(a) Initial population



(b) Population at final time T



(c) Optimal control



(d) Optimal control for different time t , $0 < t \leq T$

Figure 2.9: Population distribution and optimal control $\alpha(x, t)$ with $K = 1, L = 1, M = 0.1, \bar{M} = 5$.

magnitude of the optimal control decreased (Figure 2.10(c), 2.10(d)). This means that population 3 cooperates with population 2 instead. Since the importance of the difference in the size of the populations 1 and 2 becomes less important, population 3 could improve the objective functional value by reducing the strength of the alliance. The objective functional value increased from 3.6208 with $L = 1$ to 4.3303 in this new setting with smaller L . In this setting, the final time population distributions are almost identical for both $\alpha(x, t)$ and $\alpha(t)$ (2.10(b) and 2.5(c)). The objective functional value is 4.3303, which is slightly larger than the case with $\alpha(t)$ with the same weight constant setting.

Next, we examined the case with the setting $K = 1, L = 0.1, M = 0.01, \overline{M} = 5$ and the initial population distribution C. In initial population distribution C, the peaks of u_1 and u_2 are at different locations. In comparison with the case of $\alpha(t)$, we see a big difference in the pattern of the optimal control. When the control function depends only on time, population 3 always cooperates with the larger population 2 at any location (Figure 2.6(b)). Figure 2.11(c) shows that population 3 cooperates with both populations 1 and 2 at the same time in different spatial locations. Population 3 cooperates with the smaller population to minimize the difference of the others. For example, population 2 is more dominant than the population 1 on the locations between $x = 0$ and $x = 0.6$ (Figure 2.11(d)). In this range of x , population 3 cooperates with population 1. When we compare the final time population distributions for cases $\alpha(x, t)$ and $\alpha(t)$, the size of population 1 is smaller with the case $\alpha(x, t)$. Since the control function can change sign across the spatial domain, more refined adjustment is possible to improve the objective functional value. In fact, although the difference is small, $J(\alpha^*) = 4.3303$ for the case $\alpha(x, t)$ and the corresponding value for the case $\alpha(t)$ is 4.3257.

Finally, we compared the results using different diffusivity constants. We generated the numerical solutions using the initial population C with the setting: $K = 1, L = 0.1, M = 0.01, \overline{M} = 5$. In all examples presented above in this section, we set all the diffusivity constants equal to 0.6. Now, we examine two other combinations. The first one is $a_1^1 = 0.8, a_1^2 = 0.6, a_1^3 = 0.4$ and the other one is $a_1^1 = 0.8, a_1^2 = 0.4, a_1^3 = 0.6$. The difference in the optimal control is more clearly seen in the cross sectional view of the optimal control

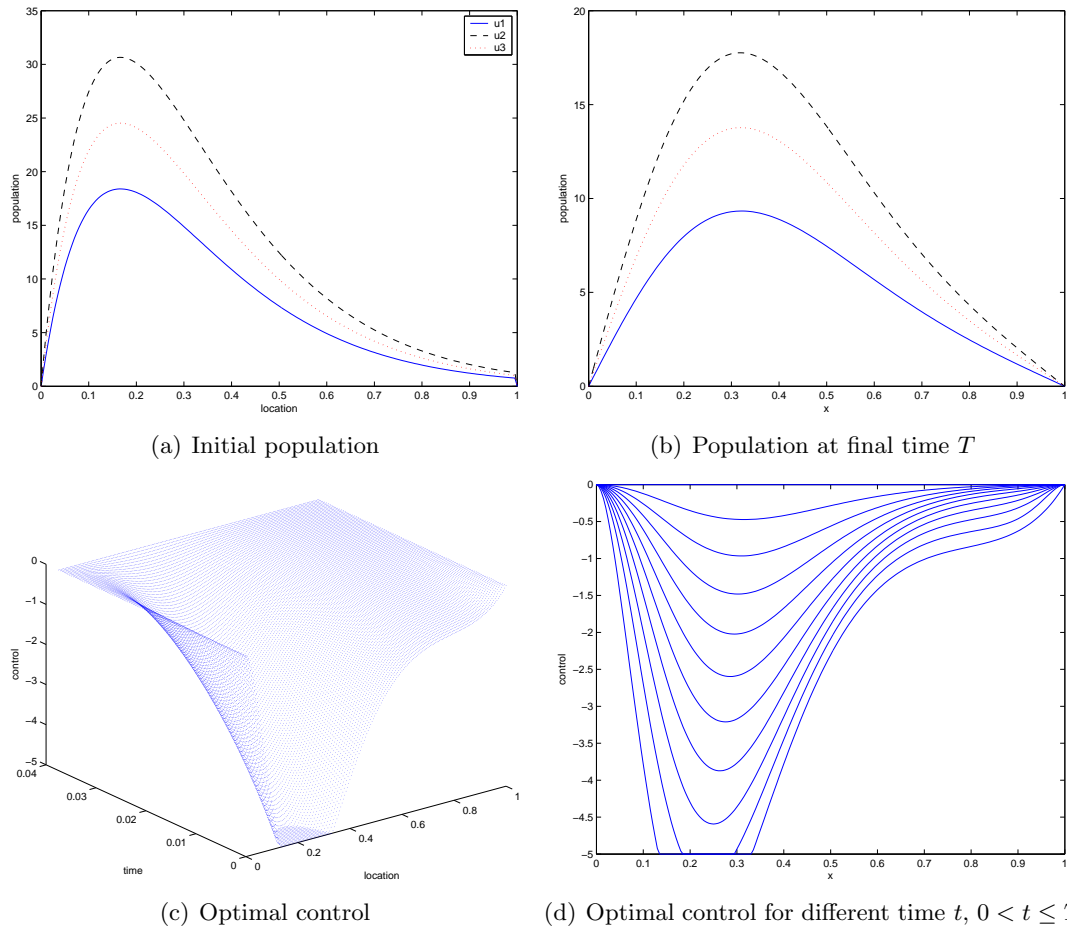


Figure 2.10: Population distribution and optimal control $\alpha(x, t)$ with $K = 1, L = 0.01, M = 0.1, \bar{M} = 5$.

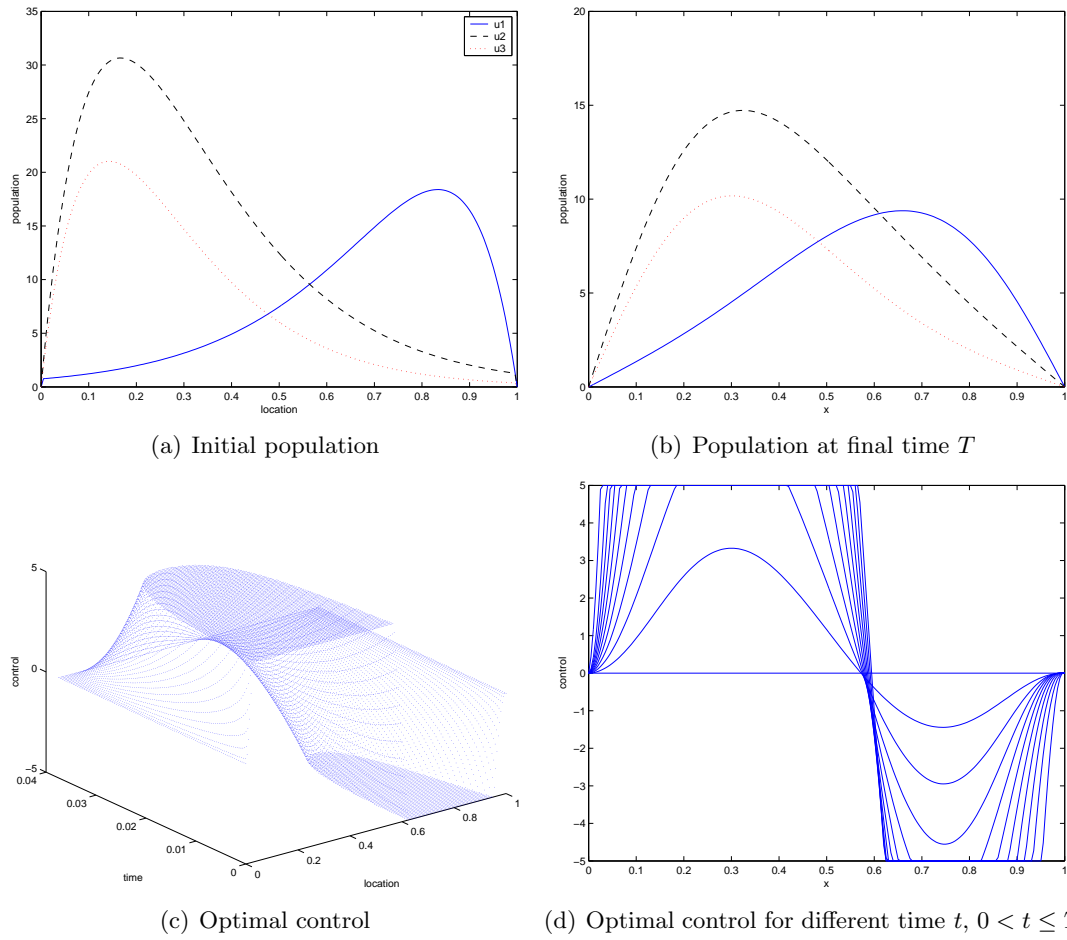


Figure 2.11: Population distribution and optimal control $\alpha(x, t)$ with initial population C , $K = 1$, $L = 0.1$, $M = 0.01$, $\bar{M} = 5$.

curves shown in Figure 2.12(d) and Figure 2.13(d). Note each curve shown in Figures 2.12(d) and 2.13(d) are obtained by slicing the graph in Figures 2.12(c) and 2.13(c) at different time respectively. The peaks of the curves are decreasing over time in both cases. When the difference in the diffusivity constants for populations 1 and 2 is larger, i.e., the case when $a_1^1 = 0.8, a_1^2 = 0.4$, the difference in the size of the two populations is larger and the difference is more obvious in the range between $x = 0$ and $x = 0.6$. When we compare the cross sectional view of the optimal control for this spatial location, the alliance between population 3 and population 1 is stronger for the case $a_1^1 = 0.8, a_1^2 = 0.4$. In both Figures 2.12(d) and 2.13(d), the curve with the smallest peak(i.e., the innermost curve) corresponds to the optimal control curve at the penultimate time slice. At any given time, the optimal control value is higher for the case $a_1^1 = 0.8, a_1^2 = 0.4$. This is because population 3 tries to minimize the difference in the size of the other two population to improve the objective functional value.

2.8 Conclusions

This work introduces a new feature of spatial-temporal control that can switch the structure of interaction terms. The control can switch an interaction from cooperative to competitive and vice-versa. Balancing the strengths of the two competing populations with an alliance involving the third population is a reasonable scenario in today's global community.

We first proved the existence of solutions to the state system and then we obtained the existence and uniqueness results for the optimal control. This gives a characterization of the unique optimal control in terms of the unique solution of the optimality system(OS). Using the characterization of OS, we numerically solved the problem to illustrate how the weight constants in the objective functional and the control bounds affect the outcome. The following are conclusions from the numerical results.

When the reversal in the order of the size of the three populations exists across the spatial domain, the opportunistic population 3 can improve the objective functional better with the control function $\alpha(x, t)$ than the control function $\alpha(t)$. When the control function depends on both time and space, $\alpha(x, t)$ can have different signs, i.e., the opportunistic

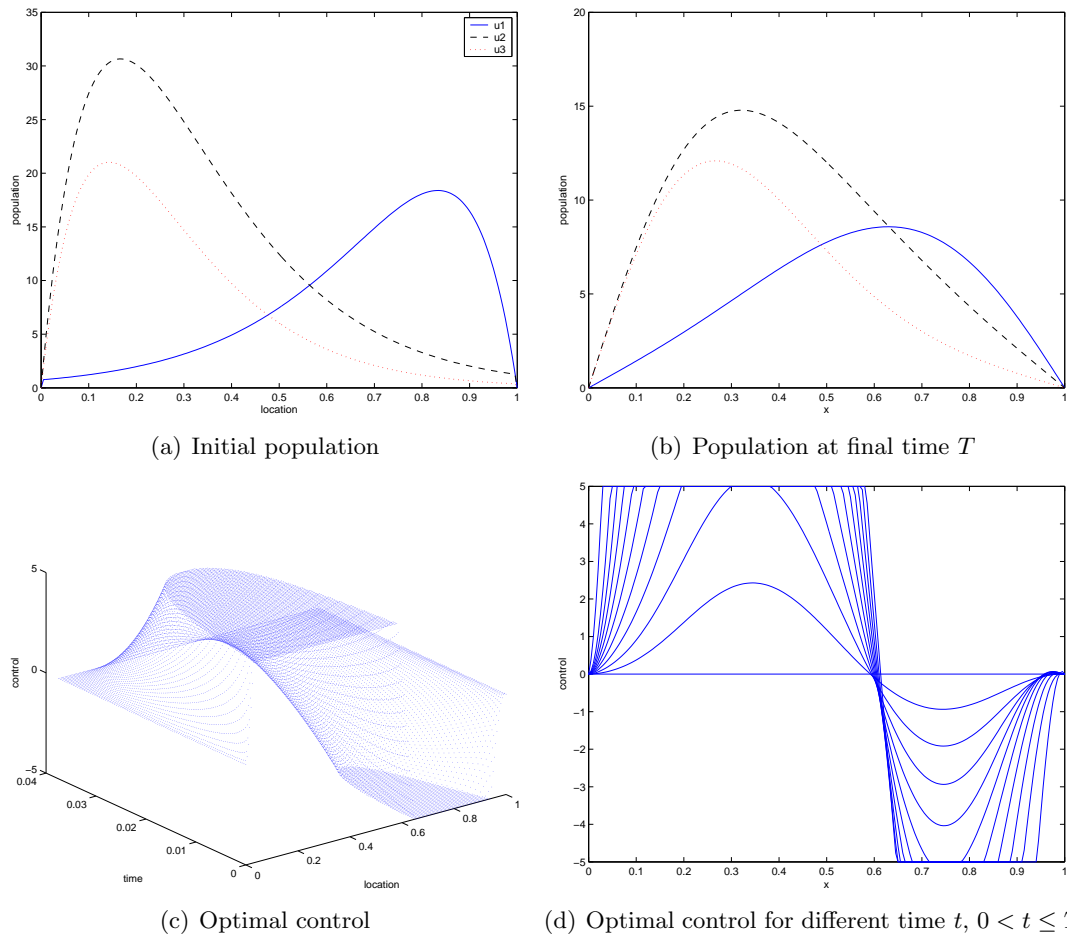


Figure 2.12: Population distribution and optimal control $\alpha(x, t)$ with initial population C , $K = 1$, $L = 0.1$, $M = 0.01$, $\bar{M} = 5$, $a_1^1 = 0.8$, $a_1^2 = 0.6$, $a_1^3 = 0.4$.

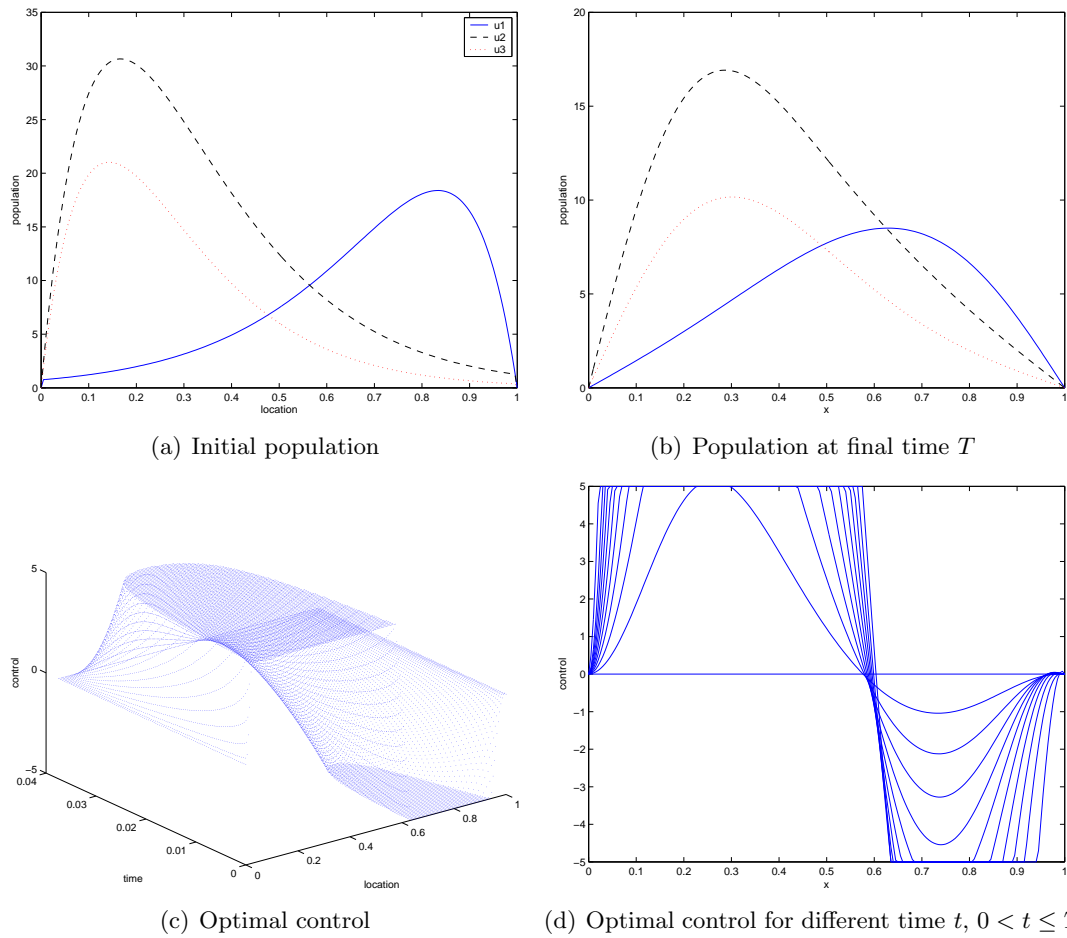


Figure 2.13: Population distribution and optimal control $\alpha(x, t)$ with initial population C , $K = 1$, $L = 0.1$, $M = 0.01$, $\bar{M} = 5$, $a_1^1 = 0.8$, $a_1^2 = 0.4$, $a_1^3 = 0.6$.

population can cooperate with different populations at different locations at the same time. This feature was only seen for the case with $\alpha(x, t)$, thus the spatial dependence in the control can cause switches in alliances. For the case of $\alpha(t)$, the sign of the control is always the same at different locations. This means population 3 cooperates with the same population everywhere.

If we had used much smaller diffusivity constants and compared the final time population distribution, the sign of the control might have been changed at some time in the interval $[0, T]$.

Since the time interval we used is very short, the final time population distribution for population 3 was almost identical regardless of the difference in the settings of the weight constants and the control bounds. Therefore, the changes in the objective functional values were mainly caused by either minimizing the difference in the size of the two competing populations 1 and 2 when the importance of the cost associated with the alliance is low, or minimizing the cost associated with the alliance when the importance of the size difference of populations 1 and 2 is small. This result was common to both cases $\alpha(x, t)$ and $\alpha(t)$.

Finally, since the interaction terms in the state equations are symmetric with respect to populations 1 and 2, we may add some constants in front of the non-local interaction terms on the right hand side of the state equations to break this symmetry. The strength of the alliance may be the same but the degree of the benefit from cooperation with different populations may not be the same. Also adding first derivative or source terms may be more realistic and lead to some unexpected behavior.

Chapter 3

Rabies Metapopulation Model

3.1 Introduction

Rabies is one of the oldest known viral diseases. The most common mode of rabies virus transmission is through the bites of an infected animal. In infected animals, rabies virus migrates through the nervous system to the brain. When rabies virus reaches the brain, it replicates rapidly and passes to the salivary glands and the infected animal starts to show signs of disease. Time between the initial infection and death is variable among species and the location or severity of wound when they were bitten by a rabid animal, but the infected animal dies approximately one week after it shows the symptoms of disease.

Although rabies vaccinations have been available for domestic animals for many years, until recently no preventive action existed to control the spread of rabies in wildlife. Wild animals accounted for 93% of reported cases of rabies in 2001. In the United States, several distinct rabies virus variants have been identified in wildlife such as raccoons, skunks, foxes, coyotes and bats. Among these wild animals, raccoons have been the most frequently reported rabid wildlife species (37.2% of all animal cases during 2001) and they are the primary vector for rabies in the eastern United States [47].

As a measure of the importance of controlling the spread of rabies, currently 15 states distribute oral rabies vaccination (ORV) for raccoons in the US. For raccoons, the vaccine is encased within a plastic package coated in fish meal and oil. When the raccoon eats the

bait, there is an immune response to the rabies antigen which creates antibodies to fight off the disease. Baits are distributed by airplanes in rural areas and by hand in urban and suburban areas. In 2003, more than 10 million baits were distributed in the United States and Canada [58].

Analytic results for optimal control applied to a simple SIR epidemic model including vaccination, quarantine and health promotion campaign were obtained by Behncke [2]. Greenhalgh considers control of an epidemic spreading in a homogeneously mixing population, which is controlled by both immunizing susceptibles and isolating infecteds [25]. For epidemics in heterogeneous populations in which the optimal vaccination policy is linked to the changing growth rate, see the work by Cairns [5]. For deterministic and stochastic models with discrete time describing an epidemic in an university setting, see the work by Martin et.al.[?]. Clancy treated optimal intervention policies for general stochastic epidemic models [7]. See a paper by Francis [24] which gives an economic viewpoint for a vaccination model in a flu season. See the works by Sethi, Morton and Wickwire for some survey and fundamental work on control of epidemics [44, 60, 67]. Ögren and Martin studied optimal vaccination patterns for a rapidly spreading disease in an urbanized highly mobile population setting [48]. Their model is similar to ours but with a different spatial arrangement.

The modeling of rabies spread and control has been widely studied by ecologists and mathematical biologists. The paper by Murray, Stanley and Brown [45] studied the spatial spread of rabies among foxes in England. In their PDE model, the fox population was divided into three classes: susceptible, infected but non-infectious and infectious rabid [45]. Evans and Pritchard extended this model as a nonlinear time-varying control system described by partial differential equations (feedback control to drive the system toward a desired profile [19]). Coyne, Smith and McAllister developed a model which makes explicit the development of natural immunity to rabies and used this to evaluate culling and vaccination elimination strategies [11]. In this model, six classes are considered: susceptible raccoons, infected but noninfectious raccoons that develop rabies, infected but noninfectious raccoons that eventually develop immunity, rabid raccoons, raccoons that are immune as a

result of natural infection, and vaccinated raccoons. Both discrete-time deterministic and stochastic models were analyzed by Allen, Flores, Tatnayake and Herbold [1]. Their models are structured with respect to space (m patches), age (juvenile and adults) and three disease states: susceptible, infected and vaccinated. An SEIR (susceptible, exposed, infectious, and recovered) model was developed to describe the spatial and temporal patterns of raccoon rabies epizootic in [6]. Optimal control has not been previously applied to an epidemic model for rabies in raccoons, thus this work is the first optimal control application in this area.

Our goal is to investigate optimal vaccination strategies to control the spread of rabies using a metapopulation SIR model with a system of ODEs. In Section 2, the assumptions of our model and definitions of parameters are stated. Then we give a description of our metapopulation SIR model and objective functional to be minimized. In Section 3, we apply Pontryagin's Maximum Principle to find the necessary conditions for the optimal control. We show simulation results to illustrate the population dynamics with the rate of vaccination as a control in Section 4.

3.2 Metapopulation Model

We consider a population consists of n subpopulations which are connected to each other via immigration or emigration. Figure 3.1 represents the flow diagram of our model. Subpopulation i is divided into three classes; the susceptibles, S_i , who can be infected with the rabies; the infecteds, I_i , who are infected with rabies and can transmit the disease; and the removed class, R_i , who are vaccinated and become immune to the rabies. Since we only consider the population dynamics for a short time period, we assume that the individuals in class R_i do not lose the immunity once they are vaccinated. Individuals in class R_i are removed from the system only when they die, with mortality rate μ_R . The mortality rate for the class I_i is much higher compared to the mortality caused by natural causes or factors other than the disease. We only include the mortality due to rabies for the class I_i . Moreover, since the rabid animals usually die within a few weeks after the symptoms of the disease appear, individuals in I_i do not enter the class R_i . Only the individuals in S_i

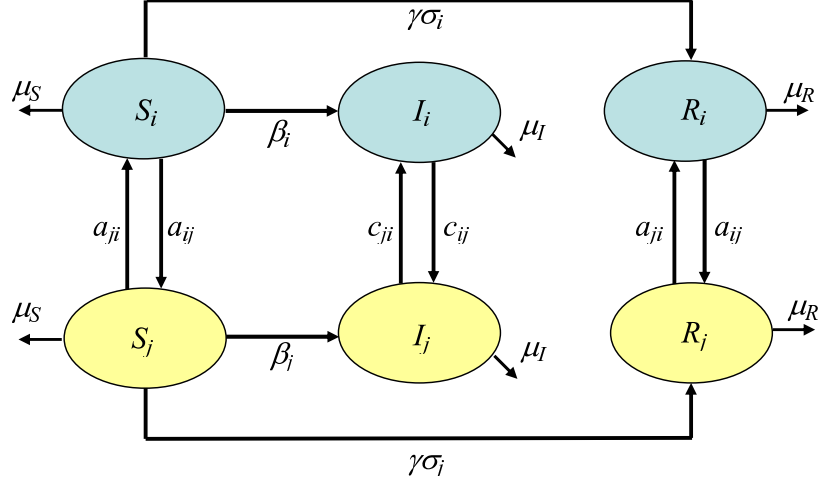


Figure 3.1: Flow diagram

can enter R_i when they are vaccinated. We do not consider the case that infected animals recover from the disease and become immune to it. Thus, once individuals are infected, they die and are removed from the system. In Figure 3.1, the symbol a_{ij} represents the rate of geographic movement of noninfecteds (susceptible and immune classes) and c_{ij} represents the rate of geographic movement of infecteds. Depending on the spatial orientation of subpopulations, a_{ij} may not be the same as a_{ji} and similarly for c_{ij} and c_{ji} . The values are assumed to be inversely proportional to the distance between the subpopulations i and j . It has been observed that infected animals change their behavior and becomes aggressive and move much more rapidly than uninfected ones. On the other hand, we assume the vaccine does not alter the behavior of raccoons. The definition of the parameters used is summarized in Table 3.1.

Key assumptions for our model are listed below.

Assumptions

- Infected animals move more actively than the animals in both susceptible and immune classes, i.e., $a_{ij} < c_{ij}$.
- The mortality rates for susceptible and immune classes are the same, i.e., $\mu_S = \mu_R$.
- The magnitude of the rates of geographic movement, a_{ij} and c_{ij} , reflects the distance between the subpopulations i and j . For instance, Figure 3.2 shows two examples

Table 3.1: Nomenclature

| Symbol | Definition |
|-----------------------|--|
| a_{ij} | the rate of geographic movement of noninfecteds (susceptible and immune classes) from subpopulation i to subpopulation j |
| c_{ij} | the rate of geographic movement of infecteds from subpopulation i to subpopulation j |
| β_i | the rate of transmission in subpopulation i |
| μ_S, μ_I, μ_R | the mortality rate in each class: S, I and R |
| σ_i | the rate of removal (control) of susceptibles from subpopulation i due to vaccination |
| γ | the efficacy of vaccination |
| S_i | the number of susceptibles in subpopulation i |
| I_i | the number of infecteds in subpopulation i |
| R_i | the number of individuals immune to the disease in subpopulation i |

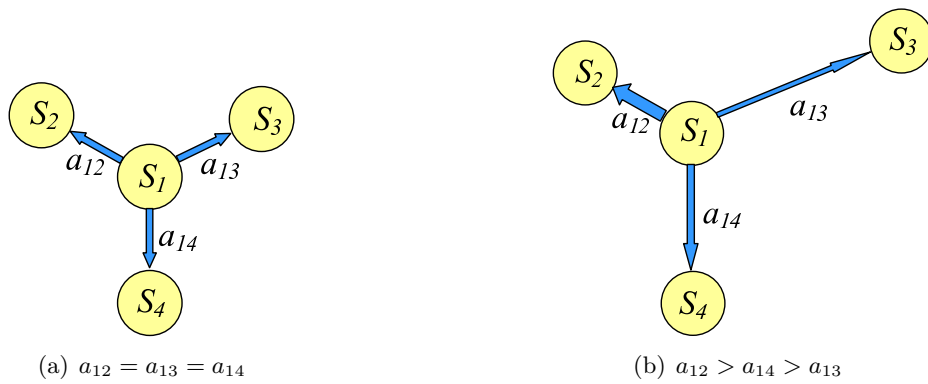


Figure 3.2: Rate of geographic movement a_{ij}

of possible spatial configurations of four subpopulations. In the first example shown in Figure 3.2(a), the subpopulation 1 is located at the same distance from the other subpopulations 2, 3 and 4. In this case, the rates of geographic movement from S_1 to the other three, S_2 , S_3 and S_4 are the same. However, if the distance between the subpopulation 3 and the subpopulation 1 is largest, as shown in Figure 3.2(b), then the rate a_{13} is smallest.

- If raccoons consume the baits containing the vaccine and the vaccine is working, they instantly become immune to the disease.

The state system is:

$$\begin{aligned}
\frac{dS_i}{dt} &= -\beta_i S_i I_i - \gamma \sigma_i S_i + \sum_{j, j \neq i}^n a_{ji} S_j - \sum_{j, j \neq i}^n a_{ij} S_i - \mu_S S_i \\
\frac{dI_i}{dt} &= \beta_i S_i I_i + \sum_{j, j \neq i}^n c_{ji} I_j - \sum_{j, j \neq i}^n c_{ij} I_i - \mu_I I_i \\
\frac{dR_i}{dt} &= \gamma \sigma_i S_i + \sum_{j, j \neq i}^n a_{ji} R_j - \sum_{j, j \neq i}^n a_{ij} R_i - \mu_R R_i
\end{aligned} \tag{3.1}$$

$$\begin{aligned}
S(0) &= S_0 \\
I(0) &= I_0 \\
R(0) &= R_0 \\
S(T), I(T), R(T) & \text{ free.}
\end{aligned} \tag{3.2}$$

The control set is defined as

$$\begin{aligned}
U &= \{ \sigma = (\sigma_1, \dots, \sigma_n) \mid \sigma_i \text{ is Lebesgue measurable,} \\
& \quad 0 \leq \sigma_i(t) \leq \sigma_{\max} \text{ a.e. for } i = 1, 2, \dots, n \},
\end{aligned}$$

We wish to minimize the total number of infecteds and the cost associated with vaccination. We consider the following optimal control problem, over $\sigma \in U$.

$$\text{Minimize } J(\sigma) = \sum_{i=1}^n \int_0^T (I_i + \frac{\alpha}{2} \sigma_i^2) dt \tag{3.3}$$

where $\alpha > 0$ is the weight factor in the cost of control. We choose a quadratic cost on the control for analysis convenience for this prototype problem. One can easily choose a combination of quadratic and linear cost, $A\sigma_i + B\sigma_i^2$ where $A > 0, B > 0$, or other convex functions.

In next section, we show the existence and derive necessary conditions for the optimal control.

3.3 Necessary Conditions for the Optimal Control

Theorem 7. *There exists an optimal control σ in U that minimizes the objective functional $J(\sigma)$.*

Proof. To prove the existence of an optimal control to our problem, we use a result from [23]. By Lukes [42], note that solutions to the state system exist and are L^∞ a priori bounded (independent of the control).

For existence, the following required conditions are satisfied.

1. For each $i = 1, \dots, n$, the class of all initial conditions with a control σ_i such that σ_i is a Lebesgue integrable function on $[0, T]$ with values in the admissible control set and such that the state system is satisfied, is not empty.
2. The admissible control set U is closed and convex.
3. The right hand side of the state system is continuous and is bounded above by a sum of the bounded control and the state, and can be written as a linear function of σ_i with coefficients depending on time and the state variables.
4. The integrand of the objective functional is convex on the admissible control set. The structure of the integrand of our objective functional gives a required bound of the type:

$$\sum_{i=1}^n [I_i + \frac{\alpha}{2}\sigma_i^2] \geq -c_2 + \frac{\alpha}{2} \sum_{i=1}^n \sigma_i^2$$

□

By using Pontryagin's Maximum Principle [51], we derive the necessary conditions for optimality. We form the Hamiltonian with adjoint variables λ_{1i} , λ_{2i} and λ_{3i} for $i = 1, 2, \dots, n$.

$$H(t, S, I, R, \sigma) = \sum_{i=1}^n [I_i + \frac{\alpha}{2}\sigma_i^2 + \lambda_{1i}S'_i + \lambda_{2i}I'_i + \lambda_{3i}R'_i], \quad (3.4)$$

where λ_{1i} is multiplied by the right hand side of the S_i ODE and similarly for λ_{2i} and λ_{3i}

Theorem 8. *Given an optimal control $\sigma = (\sigma_1, \sigma_2, \dots, \sigma_n)$ and corresponding state solutions $S = (S_1, S_2, \dots, S_n)$, $I = (I_1, I_2, \dots, I_n)$, and $R = (R_1, R_2, \dots, R_n)$, there exist $\lambda_1 = (\lambda_{11}, \lambda_{12}, \dots, \lambda_{1n})$, $\lambda_2 = (\lambda_{21}, \lambda_{22}, \dots, \lambda_{2n})$ and $\lambda_3 = (\lambda_{31}, \lambda_{32}, \dots, \lambda_{3n})$ satisfying the adjoint system:*

$$\begin{aligned} \lambda'_{1i} &= -\frac{\partial H}{\partial S_i} \\ &= \lambda_{1i}(\beta_i I_i + \gamma \sigma_i + \sum_{k=1, k \neq i}^n a_{ik} + \mu_S) - \lambda_{2i} \beta_i I_i - \lambda_{3i} \gamma \sigma_i - \sum_{k=1, k \neq i}^n \lambda_{1k} a_{ik} \\ \lambda'_{2i} &= -\frac{\partial H}{\partial I_i} \\ &= -1 + \lambda_{2i}(-\beta_i S_i + \sum_{k=1, k \neq i}^n c_{ik} + \mu_I) + \lambda_{1i} \beta_i S_j - \sum_{k=1, k \neq i}^n \lambda_{2k} c_{ik} \\ \lambda'_{3i} &= -\frac{\partial H}{\partial R_i} \\ &= \lambda_{3i}(\sum_{k=1, k \neq i}^n a_{ik} + \mu_R) - \sum_{k=1, k \neq i}^n \lambda_{3k} a_{ik} \end{aligned} \quad (3.5)$$

and

$$\lambda_{1i}(T) = \lambda_{2i}(T) = \lambda_{3i}(T) = 0 \quad \text{for } i = 1, 2, \dots, n.$$

Furthermore we conclude

$$\sigma = (\sigma_1, \sigma_2, \sigma_i, \dots, \sigma_n)$$

where

$$\sigma_i = \min\{\max\{0, \frac{\gamma S_i(\lambda_{1i} - \lambda_{3i})}{\alpha}\}, \sigma_{max}\} \quad \text{for } i = 1, 2, \dots, n. \quad (3.6)$$

Proof. Suppose $\sigma = (\sigma_1, \sigma_2, \dots, \sigma_n)$ is an optimal control and $S = (S_1, S_2, \dots, S_n)$, $I = (I_1, I_2, \dots, I_n)$, and $R = (R_1, R_2, \dots, R_n)$ are corresponding solutions, Using the result of

Pontryagin's Maximum Principle [51], there exists adjoint variables λ_{3i} , λ_{2i} and λ_{1i} satisfying: For $i = 1, 2, \dots, n$

$$\begin{aligned}\lambda'_{1i} &= -\frac{\partial H}{\partial S_i} \\ \lambda'_{2i} &= -\frac{\partial H}{\partial I_i} \\ \lambda'_{3i} &= -\frac{\partial H}{\partial R_i}\end{aligned}\tag{3.7}$$

where H is the Hamiltonian, with the transversality conditions

$$\lambda_{1i}(T) = \lambda_{2i}(T) = \lambda_{3i}(T) = 0.\tag{3.8}$$

For example, λ'_{1i} for $i = 1, \dots, n$ is given by

$$\begin{aligned}\lambda'_{11} &= -\frac{\partial H}{\partial S_1} \\ &= \lambda_{11}(\beta_1 I_1 + \gamma \sigma_1 + \sum_{k=2}^n a_{1k} + \mu_S) - \lambda_{21} \beta_1 I_1 - \lambda_{31} \gamma \sigma_1 - \sum_{k=2}^n \lambda_{1k} a_{1k}\end{aligned}\tag{3.9}$$

⋮

$$\begin{aligned}\lambda'_{1i} &= -\frac{\partial H}{\partial S_i} \\ &= \lambda_{1i}(\beta_i I_i + \gamma \sigma_i + \sum_{k=1, k \neq i}^n a_{ik} + \mu_S) - \lambda_{2i} \beta_i I_i - \lambda_{3i} \gamma \sigma_i - \sum_{k=1, k \neq i}^n \lambda_{1k} a_{ik}\end{aligned}\tag{3.10}$$

⋮

$$\begin{aligned}\lambda'_{1n} &= -\frac{\partial H}{\partial S_n} \\ &= \lambda_{1n}(\beta_n I_n + \gamma \sigma_n + \sum_{k=1}^{n-1} a_{nk} + \mu_S) - \lambda_{2n} \beta_n I_n - \lambda_{3n} \gamma \sigma_n - \sum_{k=1}^{n-1} \lambda_{1k} a_{nk}\end{aligned}\tag{3.11}$$

Similarly, λ'_{2i} and λ'_{3i} are given by the following formulas:

$$\begin{aligned}\lambda'_{21} &= -\frac{\partial H}{\partial I_1} \\ &= -1 + \lambda_{21}(-\beta_1 S_1 + \sum_{k=2}^n c_{1k} + \mu_I) + \lambda_{11} \beta_1 S_1 - \sum_{k=2}^n \lambda_{2k} c_{1k}\end{aligned}\tag{3.12}$$

⋮

$$\begin{aligned}\lambda'_{2i} &= -\frac{\partial H}{\partial I_i} \\ &= -1 + \lambda_{2i}(-\beta_i S_i + \sum_{k=1, k \neq i}^n c_{ik} + \mu_I) + \lambda_{1i} \beta_i S_j - \sum_{k=1, k \neq i}^n \lambda_{2k} c_{ik}\end{aligned}\quad (3.13)$$

⋮

$$\begin{aligned}\lambda'_{2n} &= -\frac{\partial H}{\partial I_n} \\ &= -1 + \lambda_{2n}(-\beta_n S_n + \sum_{k=1}^{n-1} c_{nk} + \mu_I) + \lambda_{1n} \beta_n S_n - \sum_{k=1}^{n-1} \lambda_{2k} c_{nk}\end{aligned}\quad (3.14)$$

$$\begin{aligned}\lambda'_{31} &= -\frac{\partial H}{\partial R_1} \\ &= \lambda_{31}(\sum_{k=2}^n a_{1k} + \mu_R) - \sum_{k=2}^n \lambda_{3k} a_{1k}\end{aligned}\quad (3.15)$$

⋮

$$\lambda'_{3i} = -\frac{\partial H}{\partial R_i} = \lambda_{3i}(\sum_{k=1, k \neq i}^n a_{ik} + \mu_R) - \sum_{k=1, k \neq i}^n \lambda_{3k} a_{ik}\quad (3.16)$$

⋮

$$\begin{aligned}\lambda'_{3n} &= -\frac{\partial H}{\partial R_n} \\ &= \lambda_{3n}(\sum_{k=1}^{n-1} a_{nk} + \mu_R) - \sum_{k=1}^{n-1} \lambda_{3k} a_{nk}\end{aligned}\quad (3.17)$$

The general form for the optimality condition is given by

$$\frac{\partial H}{\partial \sigma_i} = \alpha \sigma_i - \gamma S_i (\lambda_{1i} - \lambda_{3i}) = 0, \text{ at } \sigma_i^* \quad (3.18)$$

on the set $\{t \mid 0 < \sigma_i^*(t) < \sigma_{max}, i = 1, 2, \dots, n\}$. By solving (3.18) for $\sigma_i^*(t)$ for $i = 1, 2, \dots, n$ on the interior of the control set, we have

$$\sigma_i^*(t) = \frac{\gamma S_i (\lambda_{1i} - \lambda_{3i})}{\alpha} \quad (3.19)$$

Using the control bounds, we obtain the optimal characterization (3.6). \square

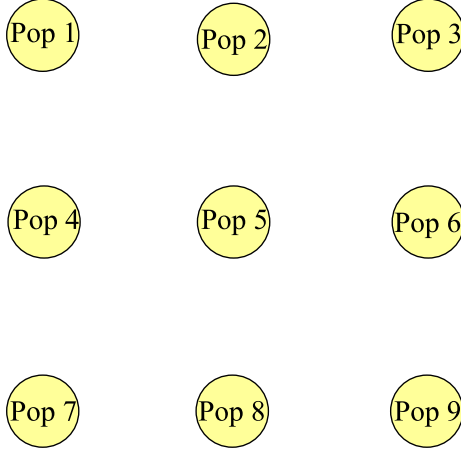


Figure 3.3: Spatial arrangement of subpopulations used in numerical simulation

Since the solutions of the state and adjoint systems are L^∞ bounded, the right hand side of these ODEs are *Lipschitz* in the state and adjoint variables, which guarantees the uniqueness of the optimality system consisting of (3.1), (3.2), (3.5) and (3.6). This *Lipschitz* property implies, for T sufficiently small, the solutions of the optimality system are unique [22].

3.4 Numerical Results

In this section, we consider a population consisting of 9 subpopulations whose geographical orientation is given by Figure 3.3.

Since we have three state variables: susceptibles (S_i), infected (I_i) and removed (immune) (R_i) for each subpopulation $i = 1, \dots, 9$, our state system given by (3.1) consists of 27 ODEs. There is a corresponding system of adjoint variable consisting of 27 ODEs.

We numerically solved the optimality system, consisting of 54 ODEs from the state and adjoint equations. Each subpopulation and the optimal control (vaccination rate) have been generated iteratively. First, we solve the state equations with a guess for the control, the state system is solved forward in time with a fourth order Runge-Kutta method. Using these state solutions, we solve the adjoint system backward in time. We repeat the iteration with the updated control (convex combination of the previous control and the value from the characterizations given by (3.6)) until the solutions converge.

The following is the default setting for the values of initial condition and parameters. We used these values unless specified. Note that

$$\alpha = 100$$

$$\beta_i = 0.01 \quad \text{for all } i$$

$$\gamma = 0.122$$

$$\mu_S = \mu_R = 0.00236, \mu_I = 0.1818.$$

$$S_i(0) = 100 \quad \text{for } i \neq 9, \quad S_9(0) = 90$$

$$I_i(0) = 0 \quad \text{for } i \neq 9 \quad I_9(0) = 10$$

$$\sigma_{max} = 1$$

$$A = (a_{ij}) = 10^{-4} \times \begin{pmatrix} 0 & 3.83 & 1.92 & 3.83 & 2.71 & 1.71 & 1.92 & 1.71 & 1.36 \\ 3.27 & 0 & 3.27 & 2.31 & 32.7 & 2.31 & 1.46 & 1.64 & 1.46 \\ 1.92 & 3.83 & 0 & 1.71 & 2.71 & 3.83 & 1.36 & 1.71 & 1.92 \\ 3.27 & 2.31 & 1.46 & 0 & 3.27 & 16.4 & 3.27 & 2.31 & 1.46 \\ 1.97 & 2.78 & 1.97 & 2.78 & 0 & 27.8 & 1.97 & 2.78 & 1.97 \\ 1.46 & 2.31 & 3.27 & 1.64 & 3.27 & 0 & 1.46 & 2.31 & 3.27 \\ 1.92 & 1.71 & 1.36 & 3.83 & 2.71 & 1.71 & 0 & 3.83 & 1.92 \\ 1.46 & 1.64 & 1.46 & 2.31 & 3.27 & 2.31 & 3.27 & 0 & 3.27 \\ 1.36 & 1.71 & 1.92 & 1.71 & 2.71 & 3.83 & 1.92 & 3.83 & 0 \end{pmatrix}$$

$$C = (c_{ij}) = 1.5A$$

where the element, (a_{ij}) , in the matrix A is the rate of movement for non-infected (susceptibles and removed (immune)) from subpopulation i to subpopulation j and similarly for (c_{ij}) for the infecteds.

The A values were determined in the following way. First, we assume that the population exponentially decay without birth. We determine the exponent for a simple decay model such that approximately 50% of animals will move to another subpopulation in one year (=

365 days). This can be done by solving the following equation for k .

$$0.5S_1(0) = S_1(0)e^{-365k}$$

After simple calculation, we have

$$k = \frac{\ln 2}{365} \approx 1.899 \times 10^{-3}. \quad (3.20)$$

Next, we find the ratios of the spatial distances between subpopulation 1 and the others. Let l_{ij} denote the spatial distance between subpopulation i and j . From Figure 3.3, the ratios of spatial distances between subpopulation 1 and the rest of subpopulations are

$$\begin{aligned} l_{12} : l_{14} : l_{15} : l_{13} : l_{17} : l_{15} : l_{16} : l_{18} : l_{19} \\ = 1 : 1 : \sqrt{2} : 2 : 2 : \sqrt{5} : \sqrt{5} : 2\sqrt{2}. \end{aligned}$$

The rates of geographic movement, a_{ij} (for noninfected), c_{ij} (for infected), are assumed to be inversely proportional to the distances between the subpopulations i and j . The ratios of a_{1j} for $j = 1, \dots, 9$ are obtained by taking the reciprocal of the ratios for l_{1j} above.

$$\begin{aligned} a_{12} : a_{14} : a_{15} : a_{13} : a_{17} : a_{16} : a_{18} : a_{19} \\ = 1 : 1 : 1/\sqrt{2} : 1/2 : 1/2 : 1/\sqrt{5} : 1/\sqrt{5} : 1/2\sqrt{2}. \end{aligned} \quad (3.21)$$

For simplicity, we take the proportionality constant to be 1. Distributing the value of k in (3.20) using the ratios in (3.21), we obtain

$$\begin{aligned} a_{12} : a_{14} : a_{15} : a_{13} : a_{17} : a_{16} : a_{18} : a_{19} \\ = 10^{-4} \times (3.83 : 3.83 : 2.71 : 1.92 : 1.92 : 1.71 : 1.71 : 1.36). \end{aligned}$$

Note that $\sum_{j=2}^{j=9} a_{1j} = k \approx 1.899 \times 10^{-3}$. Note also that A is not necessarily symmetric depending on the spatial configuration of each subpopulation with respect to each other.

By default, the initial fraction of infecteds is set to 10% of subpopulation. In other words, if the total number in subpopulation 9 is 100, and the infection started from this

subpopulation, $I_1(0) = 10$ and $S_1(0) = 90$. There are no removed (immune) individuals present at the beginning.

First, we examine the outcome of changing the weight constant for the control, α , which measures the cost of vaccination.

Example 1) $\alpha = 50$. The numbers in each class (susceptibles (solid line), infected (dotted line) and removed (dashed line)) are shown in Figure 3.4(a) and the optimal control (vaccination rate) is shown in Figure 3.4(b). The numbers in each class for the whole population are shown in Figure 3.5.

Example 2) $\alpha = 100$ (default). The numbers in each class (susceptibles, infected and removed) are shown in Figure 3.6(a) and the optimal control (vaccination rate) is shown in Figure 3.6(b). The numbers in each class for the whole population are shown in Figure 3.7.

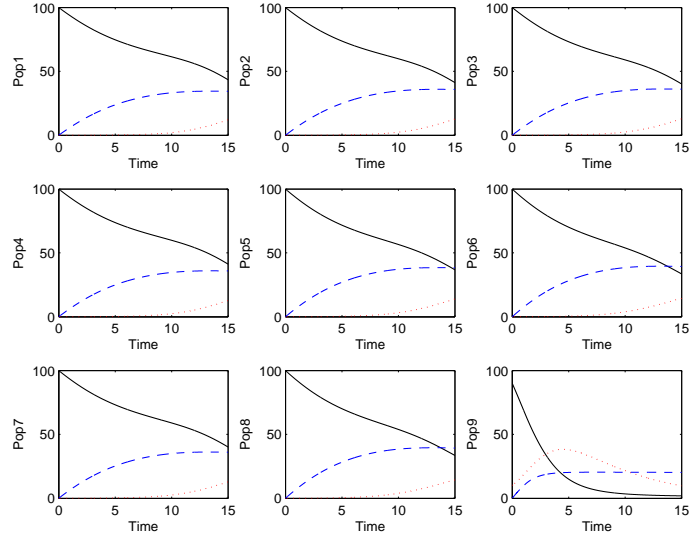
Example 3) $\alpha = 200$. The numbers in each class (susceptibles, infected and removed) are shown in Figure 3.8(a) and the optimal control (vaccination rate) is shown in Figure 3.8(b). The numbers in each class for the whole population are shown in Figure 3.9.

Due to the spatial symmetry of the subpopulations, both the final time population distribution and the optimal control are symmetric. For example, the results for the subpopulations 2 and 4 are the same. Similar results were found for the pairs of subpopulations 3 and 7, and subpopulations 6 and 8.

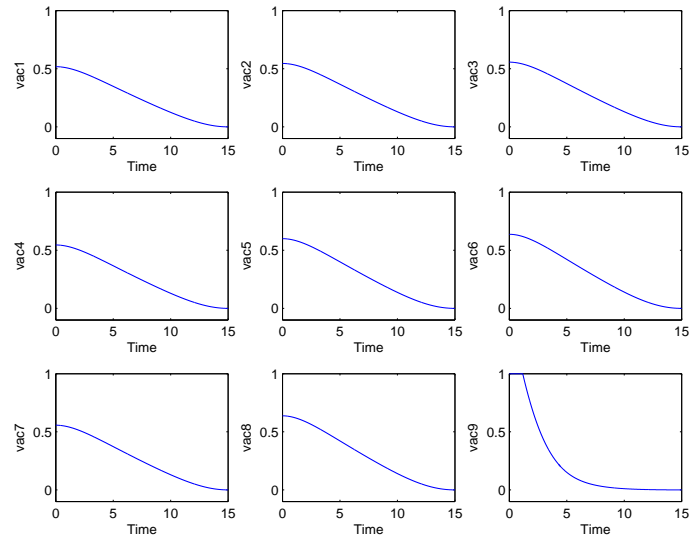
Larger values of α means the cost associated with vaccination is larger, thus we expect that less control(vaccination) will be applied for larger α . In fact, the maximum control is applied in the subpopulation 9 for the case $\alpha = 50$ (see Figure 3.4(b)). For all three cases, the infecteds in the subpopulation 1 die out, since there are not enough susceptible raccoons present.

For reference, the numbers in the susceptible and infected classes starting with the same initial populations without control is shown in Figure 3.10(a). The numbers in each class for the whole population are shown in Figure 3.10(b). There are no removed in this case. Without vaccination, rabies spreads quickly to wipe out the population.

Next, we examined varying the initial population as follows.



(a) Population



(b) Optimal control $\alpha = 50$

Figure 3.4: Population distribution and optimal control with $\alpha = 50$, $I_9(0) = 10$.

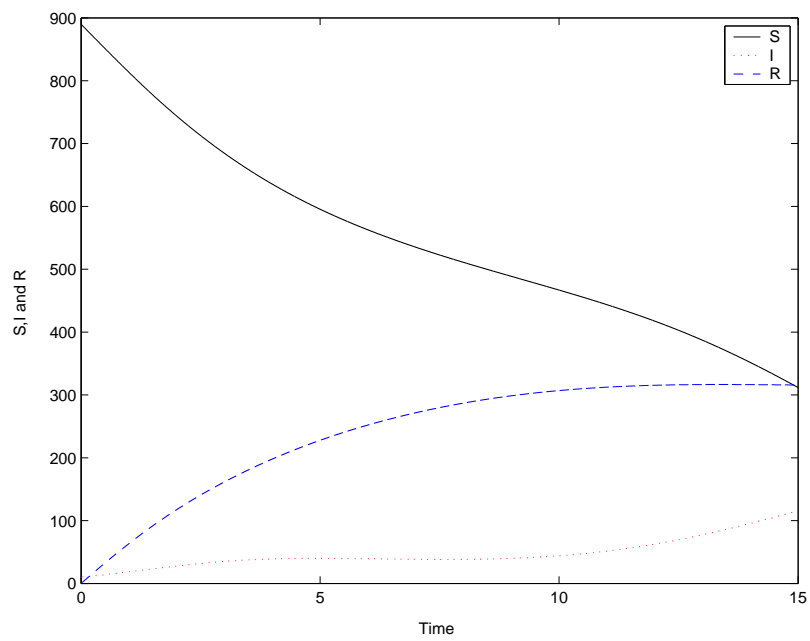
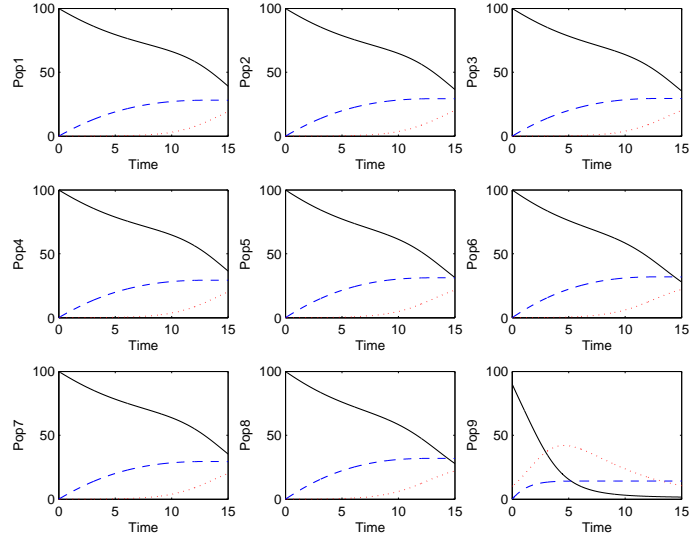
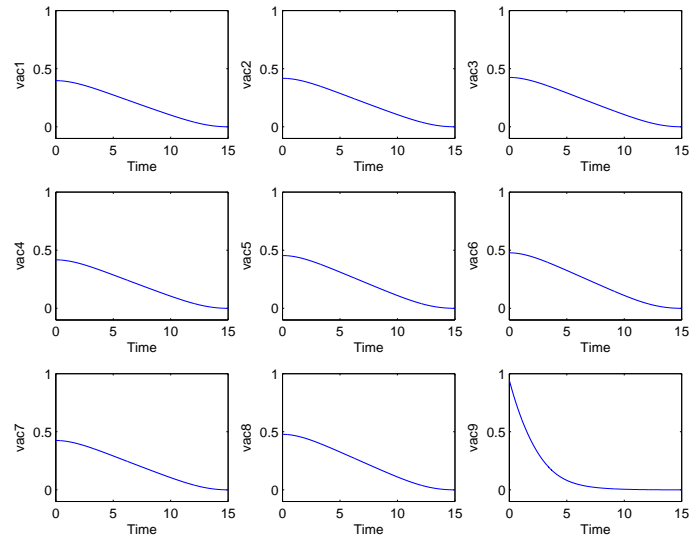


Figure 3.5: Total population with $\alpha = 50$, $I_9(0) = 10$.



(a) Population



(b) Optimal control $\alpha = 100$

Figure 3.6: Population distribution and optimal control with $\alpha = 100$, $I_9(0) = 10$ (Example 2).

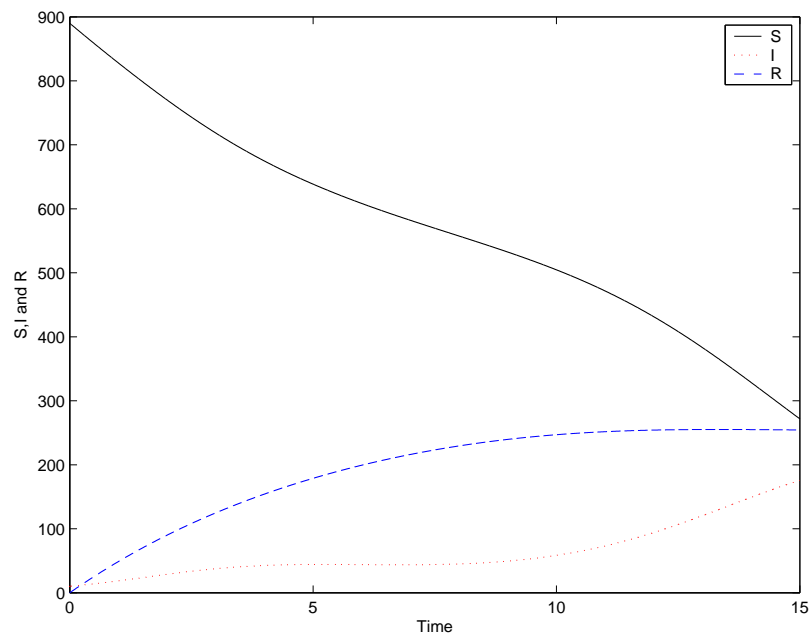
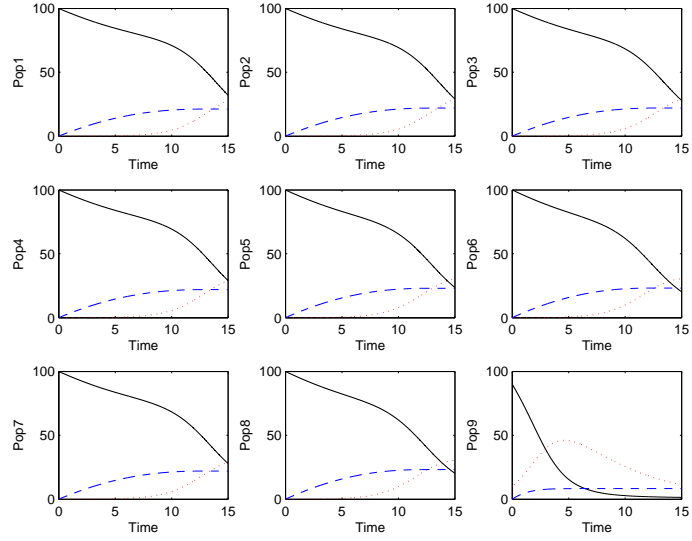
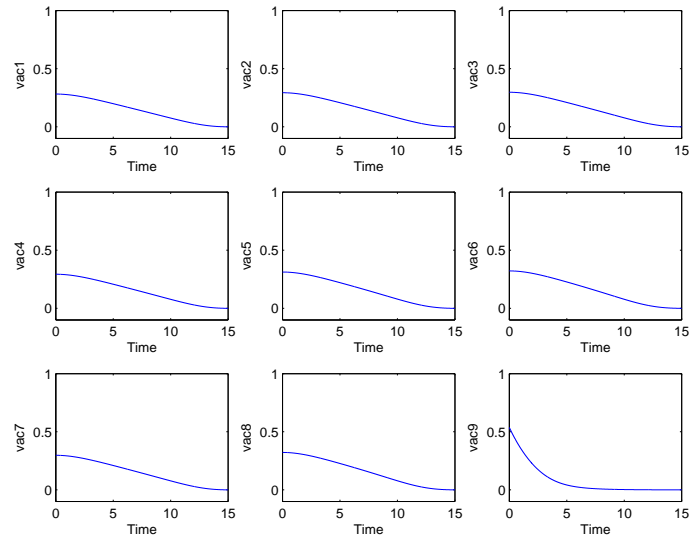


Figure 3.7: Total population with $\alpha = 100$, $I_9(0) = 10$.



(a) Population



(b) Optimal control $\alpha = 200$

Figure 3.8: Population distribution and optimal control with $\alpha = 200$, $I_9(0) = 10$ (Example 3).

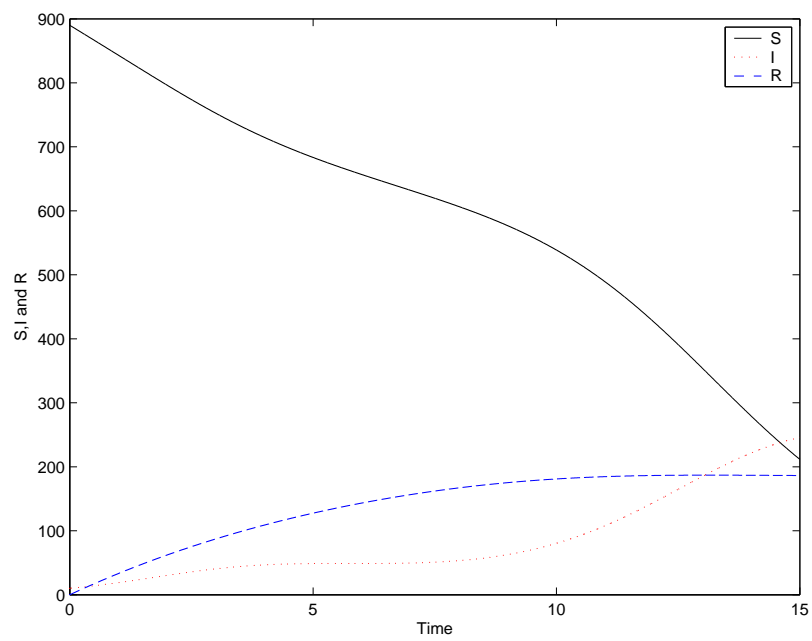
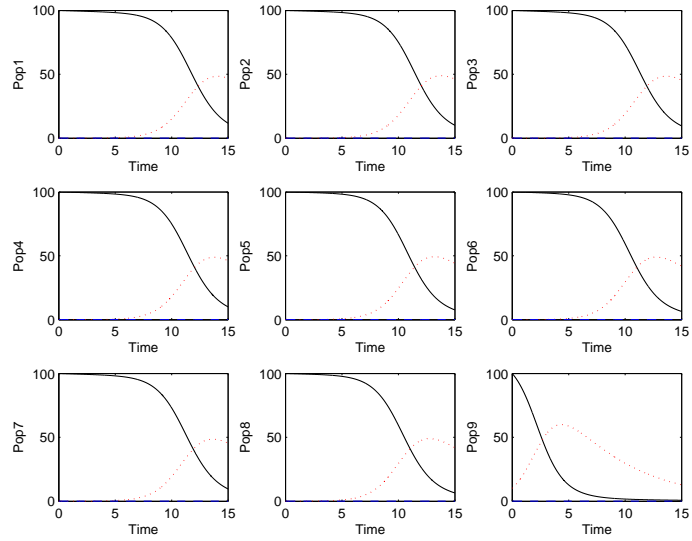
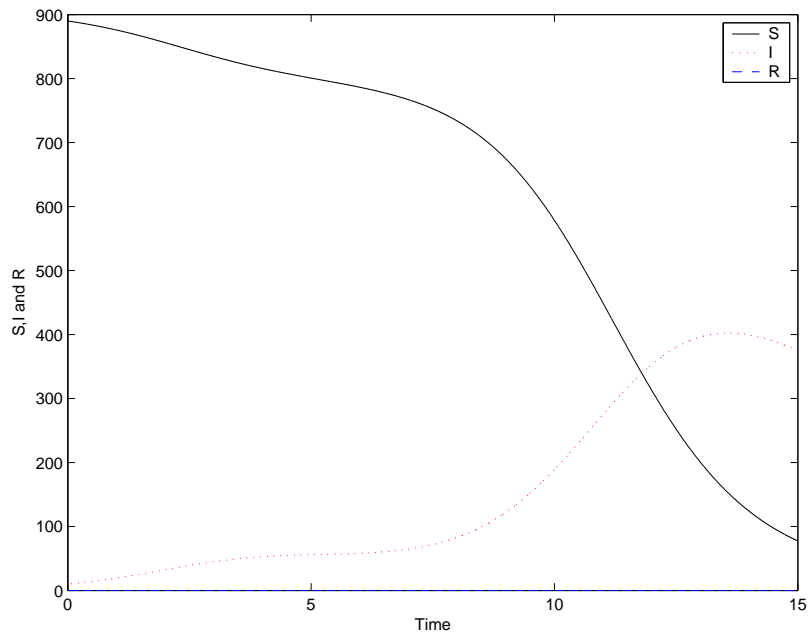


Figure 3.9: Total population with $\alpha = 200$, $I_9(0) = 10$.



(a) Population distribution



(b) Total population distribution

Figure 3.10: Population distribution without control(Examples 1, 2 and 3) .

Example 4) $\alpha = 100$.

$$S_1(0) = S_6(0) = S_9(0) = 100,$$

$$S_2(0) = S_5(0) = 50, S_3(0) = 150, S_4(0) = 45,$$

$$S_7(0) = 250, S_8(0) = 200,$$

$$I_4(0) = 5.$$

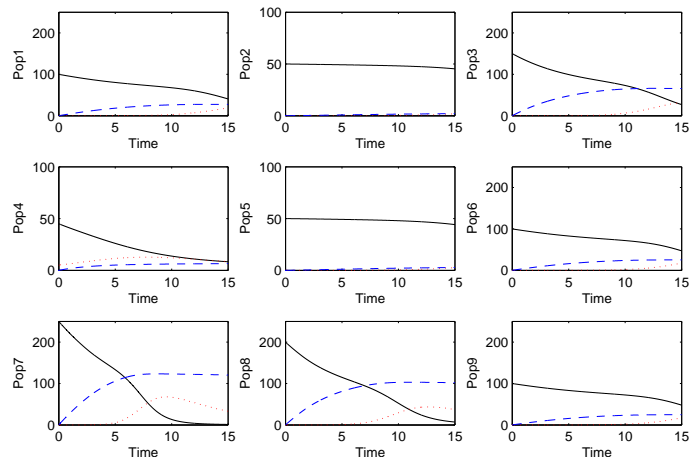
The origin of the spread is the subpopulation 4. The numbers in each class (susceptibles, infected and removed) are shown in Figure 3.11(a). The onset of the spread is much faster in large populations. In this example, five infected are introduced in the subpopulation 4. The animals move out to either subpopulation 1 or subpopulation 7 with equal rates. However, the number of infecteds in the larger subpopulation 7 started increasing earlier than that in subpopulation 1. Moreover, subpopulation 5 is closer to the origin of the spread, subpopulation 4, than the subpopulation 3, but the spread is faster in subpopulation 3, where more susceptibles are present. The numbers in each class for the whole population are shown in Figure 3.12.

Now, when we examine the optimal control shown in Figure 3.11(b), more control (vaccination) is applied in larger subpopulations, such as subpopulations 3, 7 and 8. Almost no control is applied for much smaller populations such as 2 and 5. The reference for this setting (with no control) is given in Figure 3.13. As before, without control, the population will eventually die out without any growth.

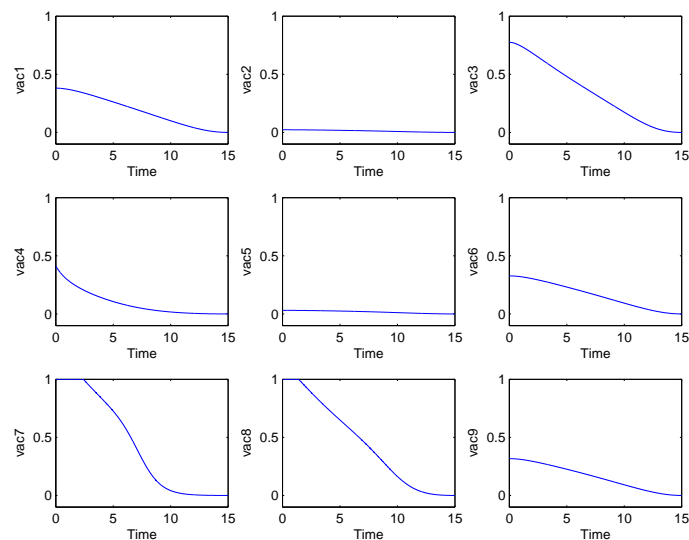
Example 5) $\alpha = 100$. In this example, only the origin of the spread is changed. Instead of subpopulation 4, we started with the infected individuals in subpopulation 7. Note that the number of infected is 25 (10% of the total number). The only change from the last example is the following.

$$S_4(0) = 50, S_7(0) = 225, I_7(0) = 25.$$

The results are shown in Figures 3.14 and 3.15. As in the last example, the strategy to minimize the objective functional is to vaccinate the populations large in size. In this



(a) Population



(b) Optimal control $\alpha = 100$

Figure 3.11: Population distribution and optimal control with $\alpha = 100$, $I_4(0) = 5$.

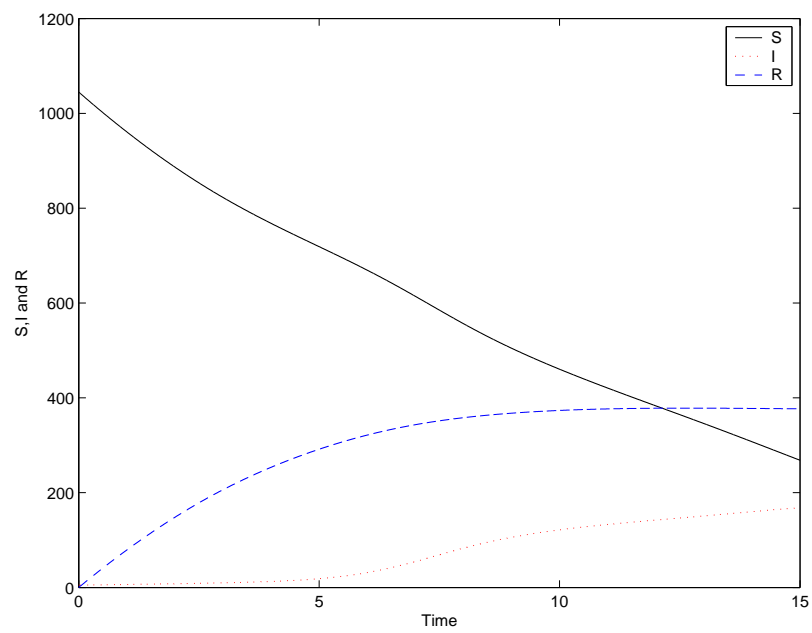
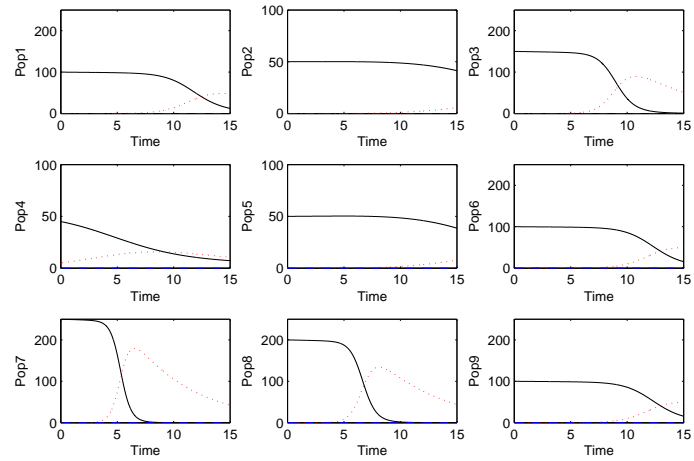
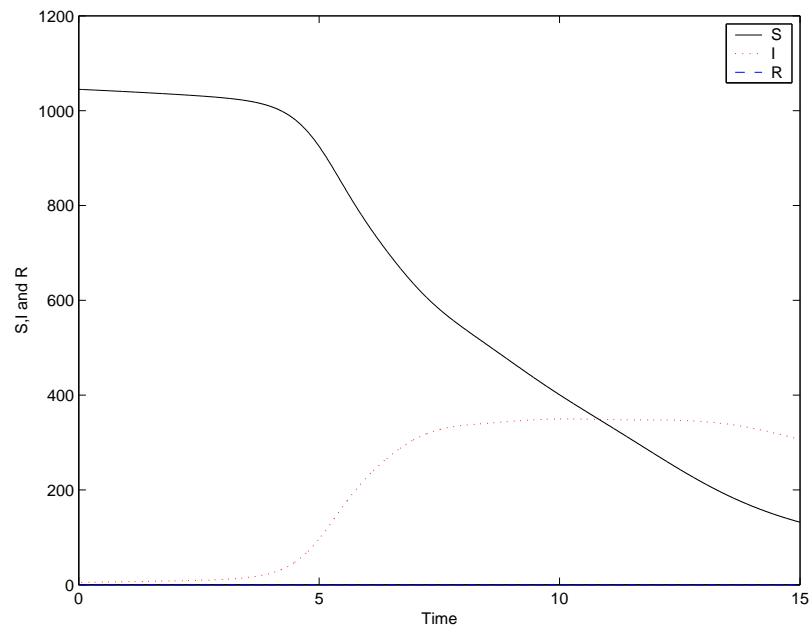


Figure 3.12: Total population with $\alpha = 100$, $I_4(0) = 5$.

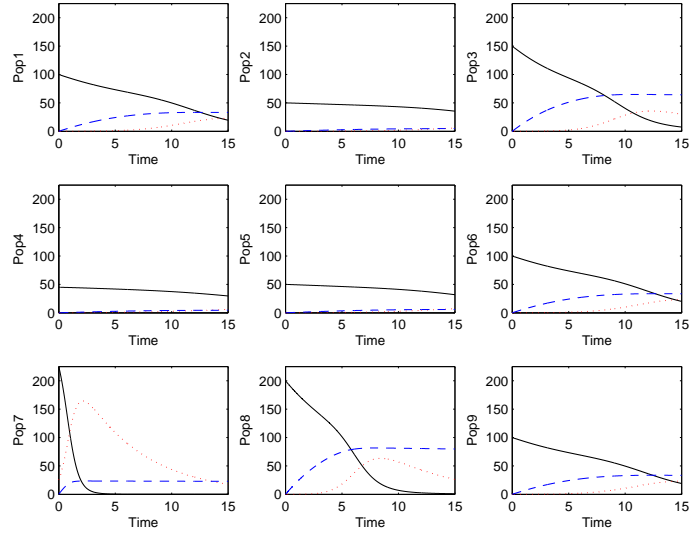


(a) Population distribution

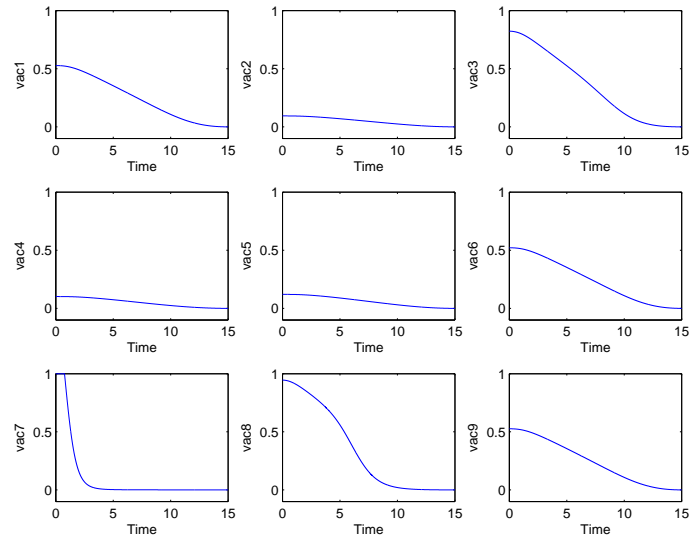


(b) Total population distribution

Figure 3.13: Population distribution without control(example 4) .



(a) Population



(b) Optimal control $\alpha = 100$

Figure 3.14: Population distribution and optimal control with $\alpha = 100$, $I_7(0) = 25$.

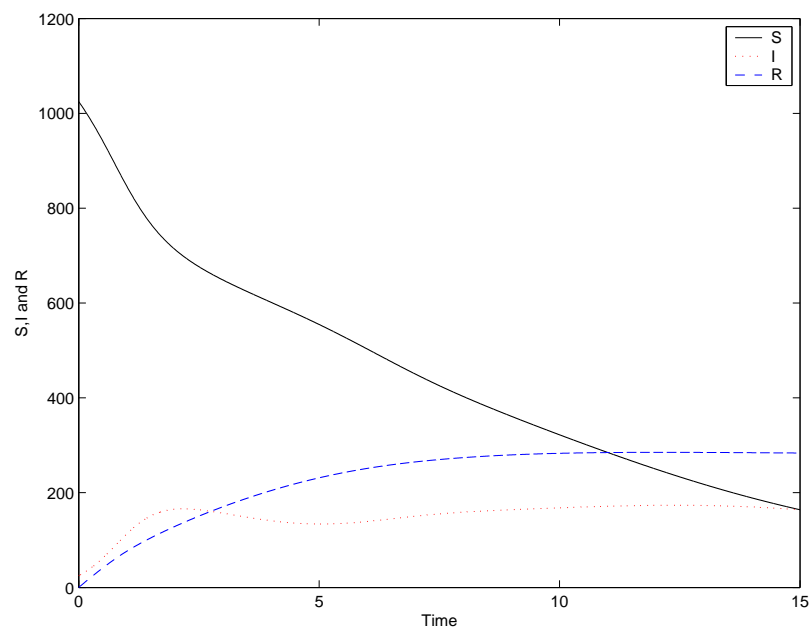


Figure 3.15: Total population with $\alpha = 100$, $I_7(0) = 25$

example, the infection started in subpopulation 7, which is the largest of all. Since the susceptibles in subpopulation 7 are quickly infected, the intensity of the control is much less than that of the previous example. The reference for this setting (with no control) is given in Figure 3.16. Again, if the population size is relatively large, the vaccination rate is very high.

3.5 Conclusions

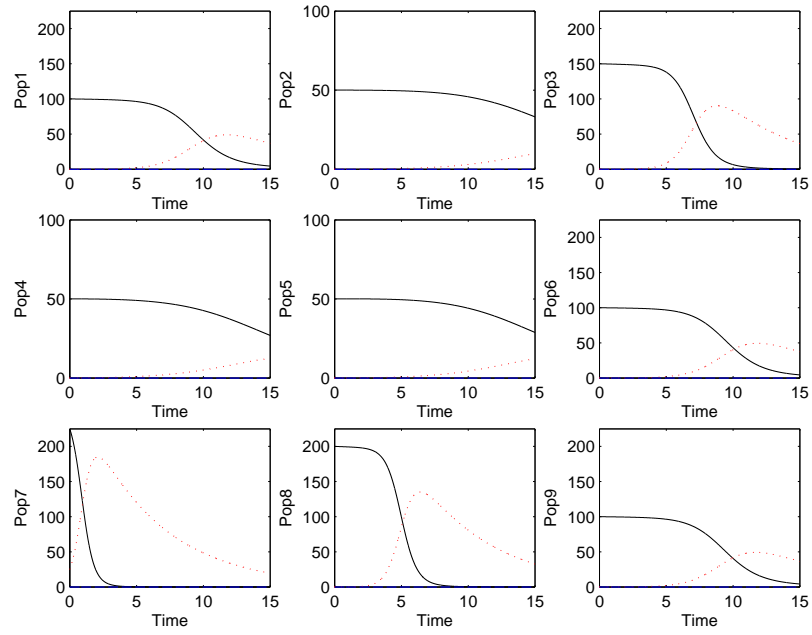
We constructed a metapopulation SIR (susceptible, infected and removed(immune)) model to investigate optimal vaccination strategies to control rabies among raccoons for a short-term time scale. It is a system of $3n$ ODEs (n is the number of subpopulations). While this application to a rabies epidemic is new, this model and control techniques could easily be adapted to other epidemic scenarios. This work provides a useful tool for analyzing optimal control in metapopulation epidemic models.

We have shown the existence/uniqueness of the optimal control and the necessary conditions for the optimal control using the Pontryagin's Maximum Principle. Using the state and adjoint system together with the characterization of the optimal control, we solved the problem numerically with preliminary parameter values.

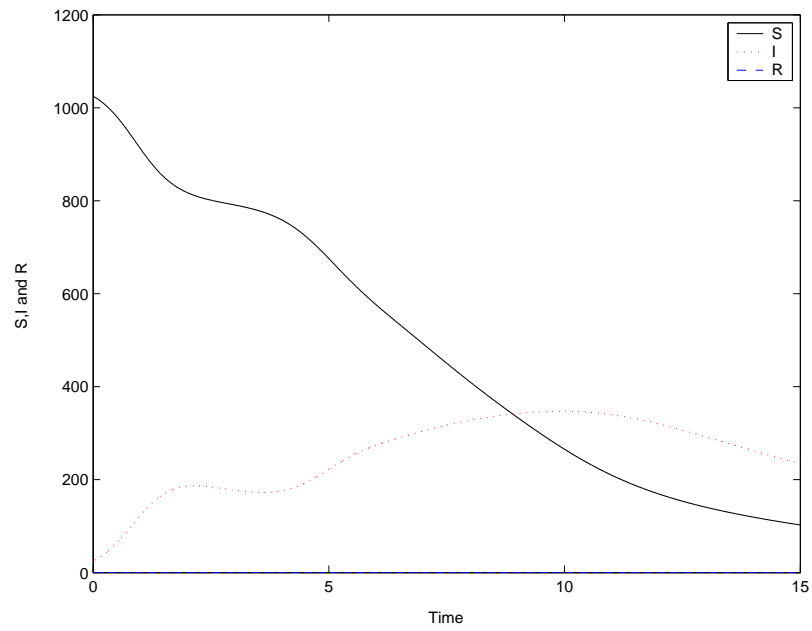
For the case of 9 subpopulations, the optimal strategy is to vaccinate at a larger rate in larger populations. When the cost of applying the vaccine is higher, as expected, the amount of effort devoted to vaccination is lower. This aspect can also be seen in the graphs involving the total population. These control results illustrate how the spatial arrangement and the location of the initial infecteds can affect the optimal vaccination strategy.

When we compare the numbers of each class for the whole populations in Examples 1 through 3 (different α values), the difference in the number of infecteds is not so significant during the first 7-8 days. However, the number of infecteds increases more rapidly when the cost of vaccinations is high (corresponds to the higher value of α).

When the initial number of each subpopulation is different (Examples 4 and 5), the pattern of the change in the number of infecteds depends on the size of the subpopulation where the initial infected animals were introduced. In Example 4 (see Figure 3.12), the



(a) Population distribution



(b) Total population distribution

Figure 3.16: Population distribution without control(example 5) .

number of infecteds gradually increases as seen in Example 2 (see Figure 3.7). Even though the initial number of infecteds in Example 4 is less than the one in Example 2, the rate of increase in the number of infecteds is faster between the day 5 and day 10. When the initial infecteds are placed in relatively large size subpopulation as in Example 5, the number of infecteds increases quickly at the beginning and does not change much after that (see Figure 3.15).

Note also that convergence of the iterative method was quick (taking only a few seconds) and this indicates that problems with even more refined spatial grids could be handled.

The following is a list of some features which can be added to our model in the future to make it more realistic.

- Introduce another state variable to add the dynamics of the bait, since the baits are delivered at different spatial locations and may decay over time or be consumed by other animals.
- Add another class, exposed (latently infected), E , which represents the group of individuals who are infected but do not transmit the disease yet.
- Include birth and growth terms, including possibly a birth pulse function or maturity movement function, in the state equations.
- Add more constraints such as a limit on the amount of vaccine to be used.
- Add age or gender structures(adult/juvenile/male/female).
- Use more realistic parameter values and geographic layout.

Chapter 4

Eurasian Collared Dove Model

4.1 Introduction

The Eurasian collared dove's place of origin is believed to be in south-central Asia (the region of India, Sri Lanka, and Myanmar [13]). They spread across Europe from Turkey and the Balkans during the 1920s. The collared dove now occupies most of Europe from Turkey to Spain, as far west as Britain, and north to southern Scandinavia and parts of Russia [28, 29]. The Eurasian collared dove has been introduced in the U.S. and continued spreading across the U.S. In next section, we describe the history of collared dove invasion in the U.S. in more detail.

Our main interest is how the difference in the breeding season affects the growth rate of the collared dove and thus affects the spread. If the breeding season is too short, the doves cannot produce successfully. On the other hand, if the breeding season is long enough, it is possible that the dove can reproduce multiple clutches during the same breeding season. Our goal is to construct a model which takes into account the spatial variation in the breeding season length and investigate the effect of such variation on the spread of the invasion. Using data on the number of frost free days provided by National Climatic Data Center (NCDC) and data on the dispersal distance (banding data) from [29], we construct an integrodifference equation model for the growth and the dispersal. The format of the growth function uses ideas from [66].

We describe when and where the collared dove was introduced in the U.S. in Section 2. Then, we briefly describe dove ecology in Section 3. The general background on integrodifference equations is addressed in Section 4. In Section 5, we give a detailed description of our model. In Sections 6 and 7, we explain how we estimated our dispersal kernel and the breeding season length function. In Sections 8 and 9, we describe various parameters and bird data used in our model and simulation. In Sections 10 and 11, we present the numerical results using our one spatial dimension model and provide conclusions.

4.2 History of Dove Invasion in the U.S.

The Eurasian collared dove (*Streptopelia decaocto*), a species that is raised and bred by dove fanciers, was introduced to North America several times since the 1980s [56]. The source of the earliest introduction is thought to be captives from the Bahama Islands that escaped or were released in 1974. As the Bahama populations grew and expanded, they reached southern Florida by the early 1980s without human assistance. Independent releases of captive collared doves by local breeders have also been reported from California, Colorado, Missouri, Tennessee, and Texas, and it is suspected to have been released in Illinois, Louisiana, Maryland, and New Jersey [54, 56]. Since its earliest introduction to Florida, the collared dove has spread rapidly, particularly along the eastern seaboard and Gulf of Mexico.

The independent releases of this species in different parts of the US makes it difficult to determine the precise nature of its invasion dynamics. Each release potentially acts as a separate satellite population that can speed the rate of invasion. However, the independent releases that have occurred periodically represent small numbers of individuals (< 50), whereas the movement of the doves from the Bahamas and surrounding islands represents the expansion by dispersal of established populations. Therefore, we assume that the westward and northward spread of the species from the southeastern US represents mainly the expansion of the Florida population.

There is evidence that the spread of the collared dove in North America frequently involves long-distance “jump” dispersal. In a series of papers, Romagosa and her colleagues

describe in detail the biology and life history of the collared dove, and documents its colonization and spread in North America. Using data from the Christmas Bird Count program (National Audubon Society 2004), Romagosa describes the expansion of the collared dove using annual distribution maps [54, 55, 56]. Their analysis indicates that the species can travel long distances in a short amount of time. Banding studies in Europe also document long-distance dispersal for the collared dove.

4.3 Dove Ecology

Eurasian collared doves form breeding pairs as soon as weather and food availability permit reproduction. Breeding is year-round where weather permits, and as many as 6 broods have been reported from a single pair during a single breeding season [12]. Pairs formed in the beginning of the breeding season are maintained until the following winter, and may be maintained over multiple years. Most often (97 percent in one study) the doves lay 2 eggs per clutch but from 1 to 4 eggs per clutch have been recorded [12].

In its native range, the doves inhabit open arid country, including cultivated groves of trees and natural acacia savanna from sea level to 2400 m or more [12]. However, doves in Europe and the US are found nesting in buildings as well as trees. In northern temperate areas the species tends to prefer cultivated areas where grain is available, and is therefore found in association with agricultural, rural, and suburban settings [12].

4.4 Integrodifference Equations

A reaction-diffusion equation has been frequently used to model the spread of invasive organisms. Reaction-diffusion models are continuous in time and space. The growth and dispersal of a population take place simultaneously. They assume that dispersal distances are normally distributed and predict a constant speed of traveling waves of invasion. Reaction-diffusion models predict the rate of invasion quite well for certain organisms, however, sometimes the speed of invading organisms is underestimated [33].

Integrodifference equation (IDE) models have been used to model the spread of invasive

organisms as well. In IDE models, the time variable is discrete and the spatial variable is continuous. IDE models are suitable for populations with distinct growth and dispersal phases [39]. In our case, note that individuals produce offspring during each growth period but the offspring do not start reproducing in the same growth period.

In next section, we describe our IDE model for Eurasian collared dove invasion in North America.

4.5 Model Description

During each breeding season, individuals mate and produce offspring. At the end of the breeding season, some individuals die but their offspring and surviving adults either stay at the same location or move to a new location. Our integrodifference equation model for the density of collared doves is

$$N_{t+1}(x) = \int_{\Omega} k(x, y) f[N_t(y)] dy. \quad (4.1)$$

The variable $N_t(x)$ represents the density of potential breeders (adult individual doves) at location x in year t . The functions $f[N_t(y)]$ and $k(x, y)$ represent the growth rate at location y and the dispersal kernel, respectively. Our growth function $f[N_t(y)]$ has two components.

$$f[N_t(y)] = sN_t(y) + g(N_t(y)). \quad (4.2)$$

The first term in the growth function (4.2) represents the fraction of the individuals who survive until the next breeding season with the probability of survival s . The second term represents the offspring produced during the breeding season in year t . By substituting (4.2) into (4.1), we have

$$N_{t+1}(x) = \int_{\Omega} k(x, y) [sN_t(y) + g(N_t(y))] dy \quad (4.3)$$

Since the dispersal kernel, $k(x, y)$ is a probability density function for the dispersal distance z , we have

$$\int_{-\infty}^{\infty} k(x, y) dy = 1 \quad \text{for all } x.$$

For simplicity, we assume that the dispersal kernel is symmetric, i.e., surviving individuals and their offspring disperse in all directions with the same probability at the end of each breeding season. For the one dimensional domain, we assume that the collared-dove disperse either south or north. For a two dimensional domain, the dispersion is radially symmetric.

As we mentioned earlier in Sec 4.2, we assume that the westward and northward spread of the collared doves from the southeastern US started mainly from the Florida population. We assume that there is no dispersal toward either the Gulf of Mexico or the Atlantic Ocean. Instead, we assume that once the birds dispersing toward the ocean reach the boundary, they change direction and fly the same distance back toward the land. If we set the southern most point of the one-dimensional domain to be our reference point (corresponding to $x = 0$), then our dispersal kernel $k(|x - y|)$ is defined on a semi-infinite domain ($x, y \geq 0$). However, this is mathematically equivalent to using the dispersal kernel $\hat{k}(|x - y|)$ defined on an infinite domain with reflective boundary condition at $x = 0$.

Figure 4.1 shows a dispersal kernel with reflective boundary condition for two different locations, x_1 and x_2 . In Figure 4.1, the dashed curve represents the dispersal kernel $\hat{k}(|x - y|)$ defined on an infinite domain and the dotted curve represents the reflection of $\hat{k}(|x - y|)$ about the y -axis. The kernel $k(|x - y|)$ used in our model is shown as the solid curve in Figure 4.1. Notice the difference in the shape of two kernels corresponding to two different locations, $k(|x - x_1|)$ and $k(|x - x_2|)$. Since the location x_1 is closer to the boundary than x_2 , the difference in the shape of the two curves, $k(|x - x_1|)$ and $\hat{k}(|x - x_1|)$ is greater.

In order to choose an appropriate dispersal kernel, $\hat{k}(|x - y|)$, we analyzed European banding data. We will describe in more detail how we estimated our dispersal kernel in Section 4.6.

To derive the growth function in our model (4.2), we modified the model proposed by Veit and Lewis [66] for the invasion of the house finch of Eastern North America. First, we briefly describe their model. They consider density dependent competition among the

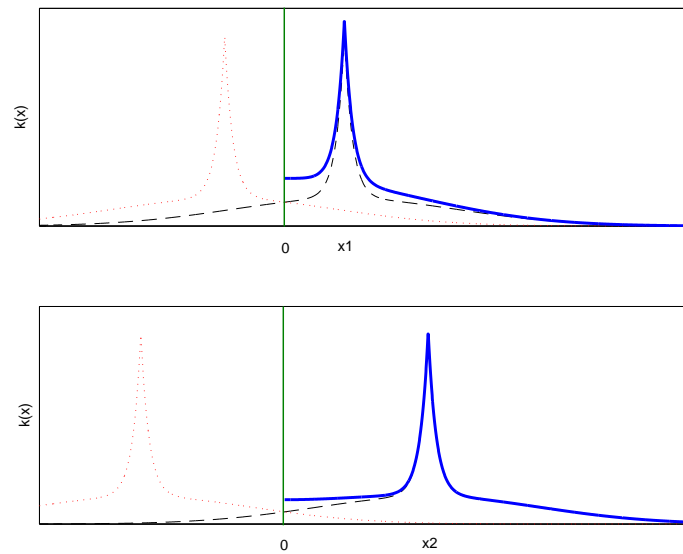
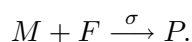


Figure 4.1: Dispersal kernel $k(x)$ with reflective boundary at $x = 0$

breeding pairs for suitable breeding sites. In order to derive the density of pairs in each breeding season, Veit and Lewis assumed that the sex ratio of a population is 1:1 and that no pairs exist at the beginning of each breeding season, i.e., the density of birds that have not found mates at the beginning of breeding season in year t is equal to N_t .

Unmated males (M) and females (F) mate randomly to form pairs (P) at a rate σ :



By applying the law of mass action, we have

$$-\frac{d[M]}{d\tau} = \sigma[M][F] \quad (4.4)$$

where $[M]$ and $[F]$ denote the density of unmated or unpaired males and females, respectively. Let $n(\tau)$ be the density of unmated birds at time τ within a breeding season, where τ is a time variable within a breeding season, i.e., $0 \leq \tau \leq T$, where T is the length of breeding season at this location. Given a 1:1 sex ratio, we have

$$[M] = [F] = \frac{1}{2}n. \quad (4.5)$$

By substituting equation (4.5) into equation (4.4), we get

$$\frac{d[\frac{1}{2}n]}{d\tau} = -\frac{1}{4}\sigma n^2.$$

Solving for $\frac{dn}{d\tau}$, the rate of change in the density of unmated birds is expressed as

$$\frac{dn}{d\tau} = -\frac{\sigma}{2}n(\tau)^2, \quad n(0) = N_t, \quad 0 \leq \tau \leq T. \quad (4.6)$$

Using $P(\tau) = \frac{N_t - n(\tau)}{2}$, the rate of change in the density of pairs is given by

$$\frac{dP}{d\tau} = -\frac{1}{2}\frac{dn}{d\tau}, \quad P(0) = 0, \quad 0 \leq \tau \leq T \quad (4.7)$$

By separation of variables, we can easily solve the equation (4.6) for $n(\tau)$, then use the equation (4.7) to find the solution $P(\tau)$:

$$P(\tau; N_t) = \frac{N_t^2}{\frac{4}{\sigma\tau} + 2N_t} \quad (4.8)$$

Veit and Lewis assumed constant breeding season length, say, T_1 , then the density of potential breeding pairs at the end of breeding season of length T_1 is simply a function of the density of population, N_t :

$$P[N_t] = \frac{N_t^2}{\frac{4}{\sigma T_1} + 2N_t} \quad (4.9)$$

If all the pairs formed can successfully nest and breed, and all offspring survive, then the growth function is obtained by equation (4.9) times the average number of offspring born to a breeding pair. However, it is reasonable to consider the possibility that a breeding pair may not find an appropriate nesting site due to limited availability of nests. For limited numbers of nesting sites, Veit and Lewis considered density-dependent resource competition among breeding pairs. Unless pairs find suitable breeding sites, they will not be able to produce offspring.

To estimate the density of successful breeding pairs given the density of potential breeding pairs, $P(N_t)$, we want a function, $h(P)$, with the following properties. Here “successful” means “finding a nest.”

$$\lim_{P \rightarrow \infty} h(P) = \delta \quad (4.10)$$

$$h(P) \leq P \quad \text{for all } P \geq 0 \quad (4.11)$$

$$\frac{dh}{dP} \geq 0 \quad \text{and} \quad (4.12)$$

$$\frac{d^2h}{dP^2} \leq 0 \quad \text{for all } P \geq 0 \quad (4.13)$$

where δ in (4.10) represents the density of available nesting sites at the current time. If the number of pairs is sufficiently large, eventually all available nests will be occupied. The second property (4.11) is required because the density of pairs finding nests is always less than or equal to the density of potential breeding pairs. The third property (4.12) is

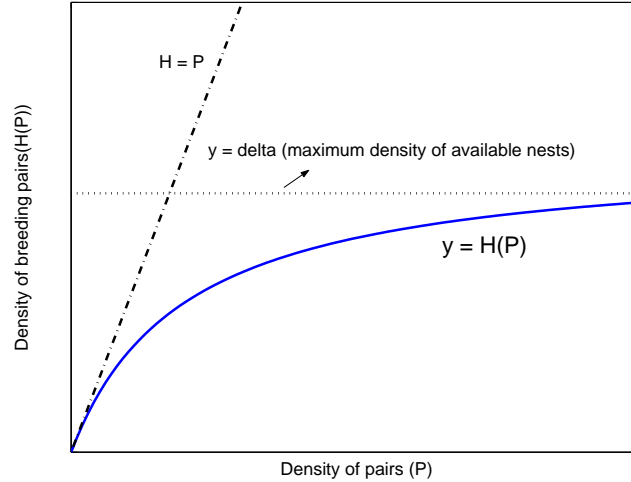


Figure 4.2: Normalized Beverton-Holt function

obvious. The last property (4.13) means that the rate of change at which nests are occupied is decreasing as the density of pairs increases. Suppose there are 30 nests available and 28 pairs are serially formed. For the first pair, it will take a relatively short time to find an empty site. On the other hand, even though there are enough nesting sites for all pairs, it will take more time for the last pair to find an unoccupied site.

Veit and Lewis used the normalized Beverton-Holt stock recruitment function, $H(P)$, to estimate the density of successful breeding pairs. This function satisfies all properties (4.10)-(4.13) and the formula for $H(P)$ is

$$H[P] = \frac{P}{1 + \frac{P}{\delta}} \quad (4.14)$$

where the parameter δ represents the density of available nesting sites. A typical shape of this curve with arbitrary parameter δ is given in Figure 4.2.

The Beverton-Holt stock recruitment function depicts density dependent resource competition in which the resource is not shared equally. In this type of competition, each individual gets some of the resources (e.g. nesting site), or not at all. By substituting the equation (4.9) into (4.14), Veit and Lewis derived the function which estimates the density

of offspring produced in year t :

$$g(N_t; x) = \frac{cN_t^2}{\frac{4}{\sigma T_1} + 2N_t + \frac{N_t^2}{\delta}} \quad (4.15)$$

where c is the average number of surviving offspring produced per pair.

In their model, the length of breeding period is considered to be spatially uniform. However, the breeding season lasts longer at lower latitude or altitude regions due to the warm climate. For example, breeding takes place almost year round in South Florida. The longer the breeding period, T , the higher the possibility that pairs can produce more than one clutch per breeding season. Moreover, more offspring are produced by pairs that mated and found their nest at earlier times during breeding season than the ones mated at a time close to the end of breeding season. However, the number of clutches a breeding pair can produce in a finite period will be limited. We extend the Veit and Lewis model by adding spatial variation in the length of breeding season and allow multiple clutches during one breeding season. We take into account that both the number of clutches that a breeding pair can produce and the number of available nests decreases as the time they start producing offspring gets closer to the end of breeding season.

For example, suppose that a maximum of m clutches are possible per year and the breeding season at some location x is $T(x)$. Then, on average, it takes $1/m$ years to produce a clutch. Therefore, at most $k = [mT(x)]$ clutches can be produced at this location, where $[u]$ is the greatest integer which does not exceed u . At the end of the first time interval, the first clutch is produced. By the end of the second time interval, $\tau = 2/m$, the same pairs can produce the second clutch and the i^{th} clutch will be produced by the end of i^{th} time interval, $\tau = i/m$ for $i = 1, 2, \dots, k$. At the same time, new pairs are formed during each time interval and they can produce offspring every $1/m$ years until the breeding season ends. To estimate the total number of offspring produced in year t , we need to calculate carefully how many and in which time interval pairs are formed and start producing offspring within a breeding season.

Next, we derive our growth function which allows multiple clutches in one breeding

season. Again, assume that the maximum number of clutches per year is m , and the length of one breeding season is $T(x)$ (spatially dependent). As described above, the number of clutches a pair can produce during the breeding length of $T(x)$ is at most $k = [mT(x)]$. Now, we partition each breeding season into k time intervals of length $1/m$ i.e.,

$$[0, T(x)) = \bigcup_{i=1}^k I_i \quad (4.16)$$

where

$$I_i = \left[\frac{i-1}{m}, \frac{i}{m} \right)$$

for $i = 1, 2, \dots, k$.

Define:

$N_{t,i}(x)$ the density of unmated adult birds at the beginning of each time interval I_i at location x .

$P_{t,i}(x)$ the density of potential breeding pairs newly formed in time interval I_i at location x .

$Q_{t,i}(x)$ the density of pairs that nest and produce offspring during time interval I_i at location x .

$R_{t,i}(x)$ the density of pairs that have not found nests by the end of time interval I_i at location x .

$\delta_{t,i}(x)$ the density of available nests in time interval I_i at location x .

$O_{t,i}(x)$ the total number of offspring produced by pairs that started breeding in time interval I_i at location x .

$O_t(x)$ the total number of offspring produced in year t at location x .

Note $N_{t,1} = N_t$.

First, consider the case $i = 1$. Since we assume that no pairs are formed at the beginning of each breeding season, by using the formula (4.9) with $T_1 = 1/m$ and $N_t(x) = N_{t,1}(x)$,

the number of pairs formed during the first period is given by

$$P_{t,1}(x) = P[N_{t,1}(x)] = \frac{N_{t,1}^2}{\frac{4m}{\sigma} + 2N_{t,1}} \quad (4.17)$$

and by using the formula (4.14), the density of pairs that actually produce offspring is

$$Q_{t,1}(x) = H[P_{t,1}(x)] = \frac{P_{t,1}}{1 + \frac{P_{t,1}}{\delta_{t,1}}} = \frac{N_{t,1}^2}{\frac{4m}{\sigma} + 2N_{t,1} + \frac{N_{t,1}^2}{\delta_{t,1}}} \quad (4.18)$$

Since the pairs formed in time interval I_1 can have the maximum number of clutches, m , the total number of offspring by these pairs is

$$O_{t,1}(x) = mcQ_{t,1}(x) \quad (4.19)$$

where c is the average number of surviving offspring.

We assume that once they form pairs, the doves remained paired during the entire breeding season and continue looking for a suitable nest site during next time interval if they could not find one during the first time interval. Therefore, the density of pairs that have not found nests is

$$R_{t,1}(x) = P_{t,1}(x) - Q_{t,1}(x). \quad (4.20)$$

Similarly, in the next time interval I_2 , more pairs are formed and produce offspring. However, at the beginning of next period, the number of unmated birds is reduced by twice the number of pairs formed, and newly formed pairs must compete for nests with the pairs that are formed earlier but still need to find a nest. Moreover, the density of available nests is reduced by the number of nests occupied, so we need to update δ in (4.14) after each time interval. Therefore, the expressions for $N_{t,2}(x)$, $P_{t,2}(x)$, $Q_{t,2}(x)$, $R_{t,2}(x)$ and $\delta_{t,2}$ are

$$N_{t,2}(x) = N_{t,1}(x) - 2P_{t,1}(x) \quad (4.21)$$

$$P_{t,2}(x) = P[N_{t,1}(x)] \quad (4.22)$$

$$Q_{t,2}(x) = H[P_{t,2}(x) + R_{t,1}(x)] \quad (4.23)$$

$$R_{t,2}(x) = P_{t,2}(x) - Q_{t,2}(x) + R_{t,1}(x) \quad (4.24)$$

$$\delta_{t,2}(x) = \delta_{t,1}(x) - Q_{t,2}(x) \quad (4.25)$$

The pairs that started breeding during the second time interval can produce at most $m - 1$ clutches before the breeding season ends. The number of clutches produced by these pairs is one less than that of the previous group of pairs, therefore

$$O_{t,2}(x) = (m - 1)cQ_{t,2}(x) \quad (4.26)$$

In general, the formulas for $N_{t,i}(x)$, $P_{t,i+1}(x)$, $Q_{t,i+1}(x)$, $R_{t,i+1}(x)$, $\delta_{t,i+1}(x)$ and $O_{t,i+1}(x)$ for $1 \leq i \leq k - 1$ are as follows.

$$N_{t,i+1}(x) = N_{t,i}(x) - 2P_{t,i}(x) \quad (4.27)$$

$$P_{t,i+1}(x) = P[N_{t,i+1}(x)] \quad (4.28)$$

$$Q_{t,i+1}(x) = H[P_{t,i+1}(x) + R_{t,i}(x)] \quad (4.29)$$

$$R_{t,i+1}(x) = P_{t,i+1}(x) - Q_{t,i+1}(x) + R_{t,i}(x) \quad (4.30)$$

$$\delta_{t,i+1}(x) = \delta_{t,i}(x) - Q_{t,i}(x) \quad (4.31)$$

$$O_{t,i+1}(x) = (k - i)cQ_{t,i+1}(x) \quad (4.32)$$

In order to calculate the total number of offspring produced during the breeding season in year t , we need to sum over $O_{t,i}$ for $i = 1, \dots, k$, i.e.,

$$O_t(x) = \sum_{i=1}^k O_{t,i}(x) \quad (4.33)$$

Our growth function, a modified version of the growth function of Veit and Lewis, is spatially dependent:

$$f(N_t(x)) = sN_t(x) + O_t(x). \quad (4.34)$$

The next step is to choose an appropriate dispersal kernel in our model (4.1).

4.6 Dispersal Kernel

In this section, we explain how we selected our dispersal kernel, $k(x)$. We have data on the dispersal distance of the collared doves (banding data) from North America provided by USGS Pawtuxent Wildlife Research Center Bird Banding Lab. However, out of 117 birds that were caught and banded between 1994-2004, only seven doves were recovered, which is approximately a 6% recovery rate. Moreover, three of the captured doves did not move from their initial banding site. Therefore, we decided to use the European banding data (Table 4.1[29]) to find the best fitting kernel using the least-squares method. We are aware that using European data for the dispersal in U.S. is a source of error. Table 4.1 shows the number of ring recoveries in various distance classes from the place of marking for the collared dove in Europe. Although there is evidence that once offspring disperse from their parent's nest, they tend to settle down [50], for simplicity, we assume that doves disperse regardless of their ages. In Table 4.1, the number of ring recoveries is given for different ranges of dispersal, but we used the lower bound of the range and corresponding number of ring recoveries to find the best fitting curves. For example, we assume that 38 doves out of 72 did not disperse at all. Since there is evidence of long dispersal, we used a distribution kernel with a fat-tail relative to a normal distribution. We also consider some combination of two distributions to produce spread patterns to fit the data.

We found the best fitting kernel among those kernels in Table 4.2. Using the banding data from Table 4.1, we estimated the parameters in the kernels.

The best parameter values with adjusted R^2 (coefficient of determination) are given in Table 4.3 and the corresponding curves with the data are shown in Figure 4.3 and Figure 4.4.

We chose the dispersal kernel with the highest R^2 value, i.e., a combination of two kernels, namely, Laplace and normal distributions, for our model and our simulation.

Table 4.1: Number of ring recoveries for the Eurasian collared dove

| Class boundary(km) | Number of recoveries |
|--------------------|----------------------|
| 0-50 | 38 |
| 50-100 | 8 |
| 100-150 | 5 |
| 150-200 | 3 |
| 200-250 | 6 |
| 250-300 | 1 |
| 400-450 | 1 |
| 450-500 | 1 |
| 550-600 | 1 |
| 600-650 | 2 |
| total | 72 |

Source: R. Hengeveld. *Dynamics of Biological Invasions*,1989

Table 4.2: Kernels used to estimate $k(x)$

| Function | Formula | Parameters |
|-------------------------------------|--|----------------------|
| Bivariate Student t | $K(x) = \frac{a}{\pi b(1+ x ^2/b)(a+1)}$ | a, b |
| Cauchy | $K(x) = \frac{ab}{b^2+ x ^2}$ | a, b |
| Laplace(Double-Exponential) | $K(x) = abe^{-a x }$ | a, b |
| Normal(Gaussian) | $f(x) = ae^{- \frac{x}{b} ^2}$ | a, b |
| Normal 1 + Normal 2 (combination) | $K(x) = a_1e^{- \frac{x}{b_1} ^2} + a_2e^{- \frac{x}{b_2} ^2}$ | a_1, a_2, b_1, b_2 |
| Laplace 1 + Laplace 2 (combination) | $K(x) = a_1b_1e^{-a_1 x } + a_2b_2e^{-a_2 x }$ | a_1, a_2, b_1, b_2 |
| Laplace + Normal | $K(x) = a_1b_1e^{-a_1 x } + a_2e^{- \frac{x}{b_2} ^2}$ | a_1, a_2, b_1, b_2 |

Table 4.3: Best fitting curves for dispersal kernels

| Function | Parameters | Adjusted R^2 |
|-------------------------------------|--------------------|----------------|
| Bivariate Student t | $a = 0.1815$ | 0.9213 |
| | $b = 0.1098$ | |
| Cauchy | $a = 0.1585$ | 0.9298 |
| | $b = 0.3014$ | |
| Laplace(Double-Exponential) | $a = 2.583,$ | 0.9112 |
| | $b = 0.2022$ | |
| Normal(Gaussian) | $a = 0.5273$ | 0.8907 |
| | $b = 0.4039$ | |
| Normal 1 + Normal 2 (combination) | $a_1 = 0.08124$ | 0.9708 |
| | $a_2 = 0.4365$ | |
| | $b_1 = 3.355$ | |
| | $b_2 = 0.0373$ | |
| Laplace 1 + Laplace 2 (combination) | $a_1 = -0.0002991$ | 0.7897 |
| | $a_2 = 1.291$ | |
| | $b_1 = -20.74$ | |
| | $b_2 = 0.344$ | |
| Laplace + Normal (combination) | $a_1 = 0.3199$ | 0.975 |
| | $a_2 = 0.4252$ | |
| | $b_1 = 0.3205$ | |
| | $b_2 = 0.2943$ | |

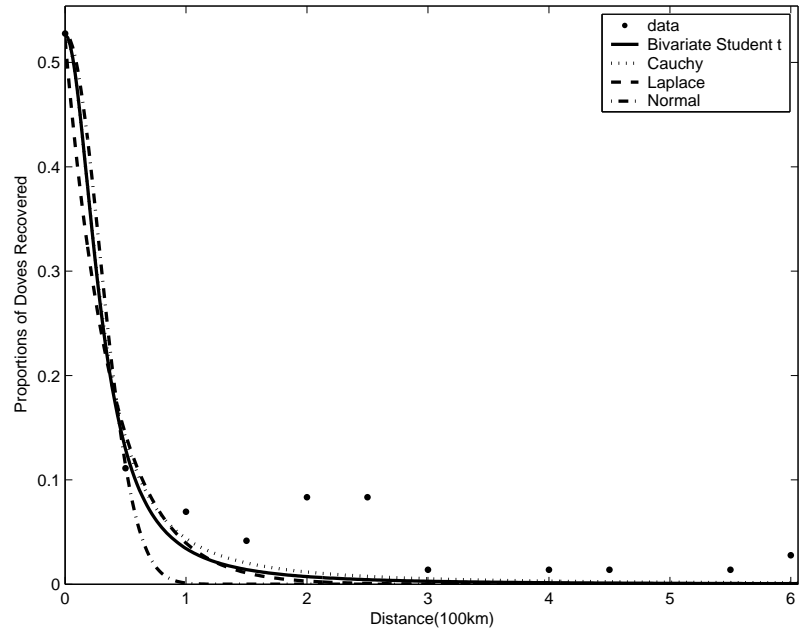


Figure 4.3: Dispersal kernel using a single distribution

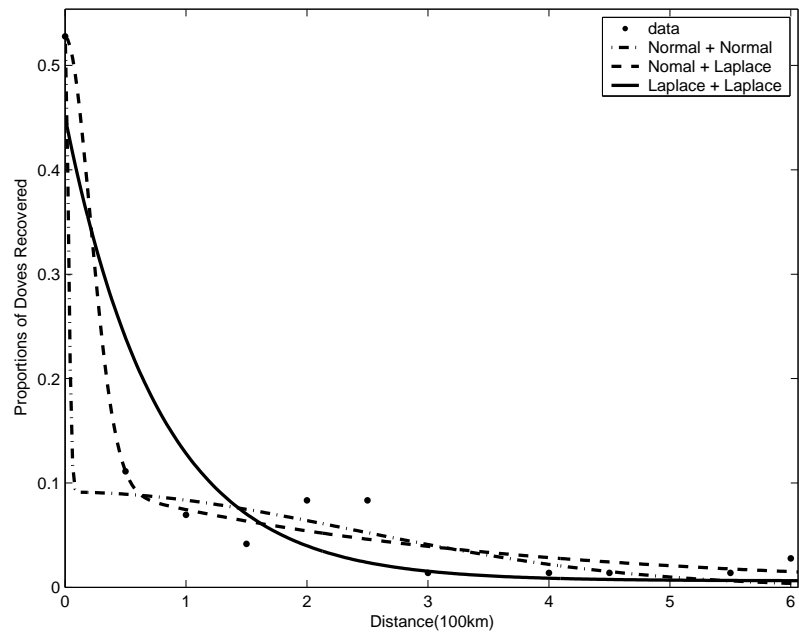


Figure 4.4: Dispersal kernel using two distributions

Since the dispersal kernel must satisfy the condition (4.5), our kernel used in the simulation is given by

$$\begin{aligned}
 k(x, y) &= k(|x - y|) = \frac{1}{A}K(|x - y|) \\
 \text{where } A &= \int_{-\infty}^{\infty} K(|x - y|)dy \quad \text{and} \\
 K(|x - y|) &= a_1b_1e^{-a_1|x-y|} + a_2e^{-\left(\frac{x-y}{b_2}\right)^2} \quad \text{with parameter values given in Table 4.3.}
 \end{aligned}
 \tag{4.35}$$

4.7 Breeding Season Length Function

In order to estimate the breeding season length, $T(x)$, in our model, we use the data set 9712C (DSI-9712C) provided by National Climatic Data Center (NCDC). This is a collection of data on probability levels for freeze dates and growing season lengths. The computations of these statistics was performed for 4,346 weather stations in the United States (including Alaska and Hawaii) for the 1971-2000 period. The number of frost-free days are computed at different temperature thresholds with specified probability levels (10, 50 and 90 percent). For example, suppose that at the 0.1 probability level, the frost-free days is computed to be 250 days at the 32-degree Fahrenheit threshold. This means that the chance of having a longer frost-free period than 250 days at this location is only ten percent. Since the length of the breeding period is strongly influenced by the availability of resources such as food, it is reasonable that the breeding season length is proportional to number of frost-free days. Therefore, we used these data to estimate the breeding season length function, $T(x)$, in our model. We used the number of frost-free days computed at the 32-degree threshold with the 0.1 probability level. First we converted the computed number of frost-free days into years by dividing the number by 365. For some locations, the computed number of frost-free days were not specified but it is only indicated that they are greater than 365 days. Since the maximum breeding season length is one (i.e., breeding takes place year-round) in our model, we set the breeding length to be 1 for such cases.

The number of frost-free days is likely to be affected by many factors including latitude, elevation, cloud cover, humidity and the distance to bodies of large water (rivers, lakes,

oceans). Across the US, we selected five vertical geographic zones with width 1.75 degrees longitude (approximately 168.73 km) as shown in Table 4.4 and Figure 4.5. We chose the southern most weather station located at $24^{\circ}33'N$ and $24^{\circ}33'W$ to be our reference location. This station is the southern most of all weather stations listed in the data set 9712C (DSI-9712C). To estimate the breeding length function in one dimension, we calculated the north-south distance between each station and the reference latitudinal line at $24^{\circ}33'N$ using the Great Circle formula. Note that this north-south distance is not the distance between two weather stations.

Figures 4.6 through 4.10 show the change of the number of frost-free days (in years) and the elevation level as we move toward north. In zones 1, 2 and 3, there is negative correlation between the number of frost-free days and the distance. For zone 2 and zone 3, the elevational change across the domain is moderate, ranging from 0 to 0.75km (Figure 4.7 and Figure 4.8) On the other hand, for zone 4 and zone 5, the effect of the change in elevation due to mountain ranges is strong (Figure 4.9 and Figure 4.10). Moreover, since the stations in zone 5 are located very close to the Pacific ocean, the number of frost-free days is significantly greater compared to other stations located at similar latitudinal distance but further inland from the corresponding coastline.

For our one spatial dimension model, we consider the collared dove advances toward north along the north-south latitudinal straight path from the origin of the spread in South Florida. Moreover, as more points are available in zone 1, we used the frost-free days data in zone 1 to estimate the breeding length function, $T(x)$. We use the MATLAB curve fitting toolbox to find the best fit curve using the least-squares method. The functions used to estimate our $T(x)$ and the results are shown in Table 4.5. We chose the exponential function

Table 4.4: Zone description for the frost-free days data

| Zone | Longitude(center) in degrees | Number of data points |
|------|------------------------------|-----------------------|
| 1 | -81.5 | 179 |
| 2 | -90.5 | 198 |
| 3 | -98.25 | 220 |
| 4 | -110 | 119 |
| 5 | -121 | 144 |

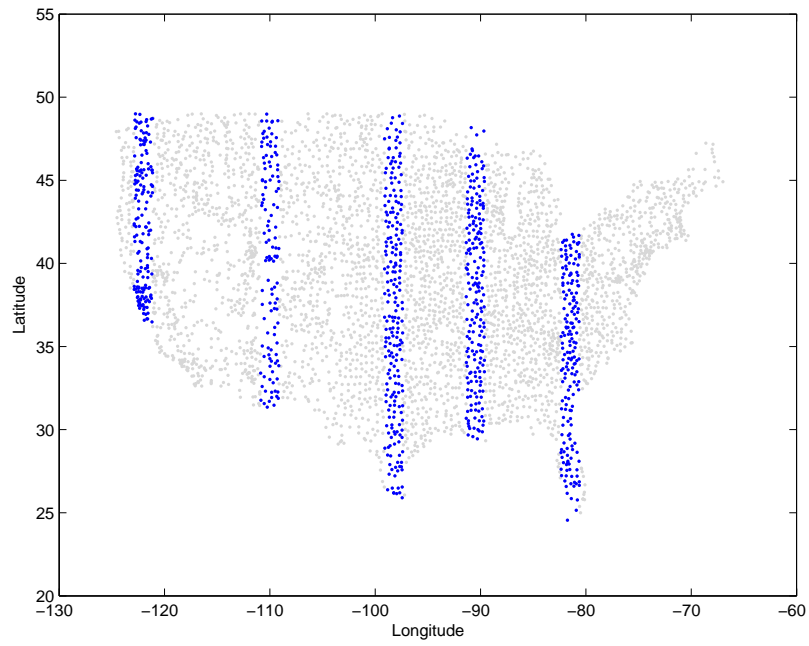


Figure 4.5: Zone map for the frost-free days data

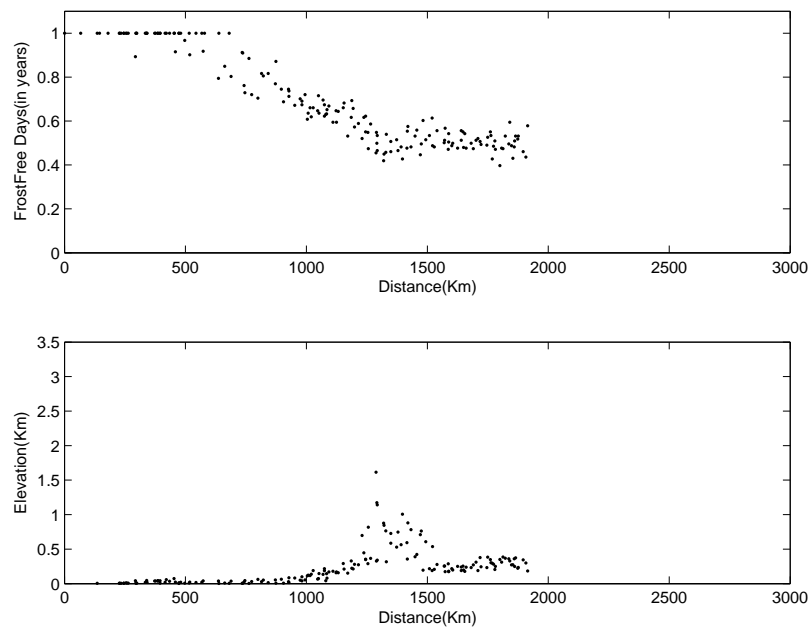


Figure 4.6: Frost-free days and elevation for zone 1

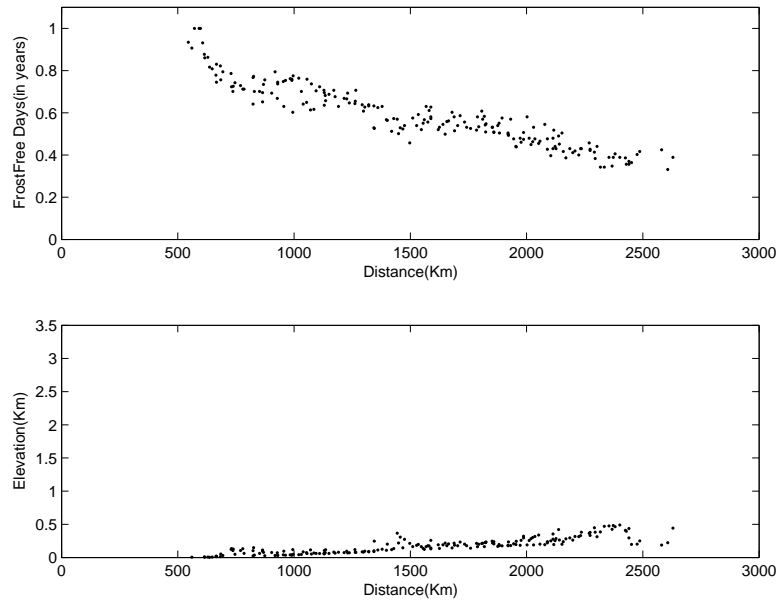


Figure 4.7: Frost-free days and elevation for zone 2

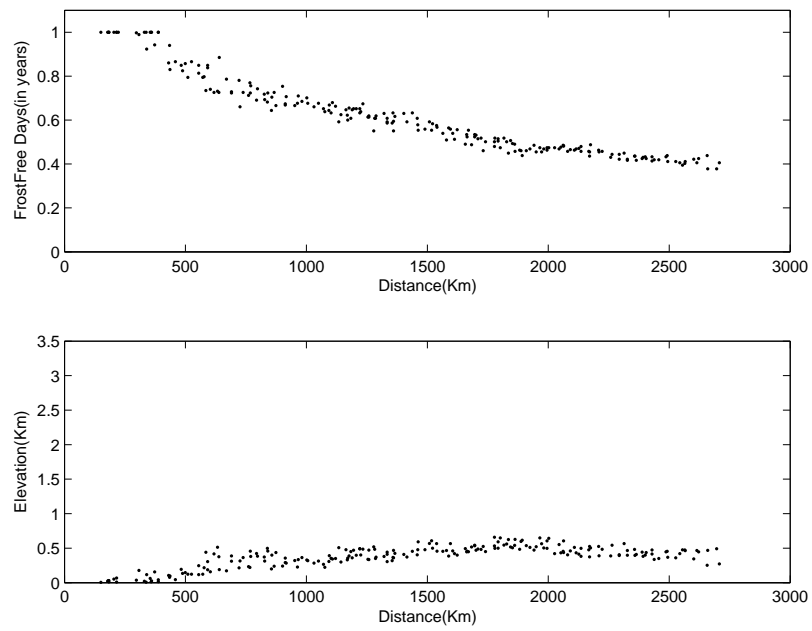


Figure 4.8: Frost-free days and elevation for zone 3

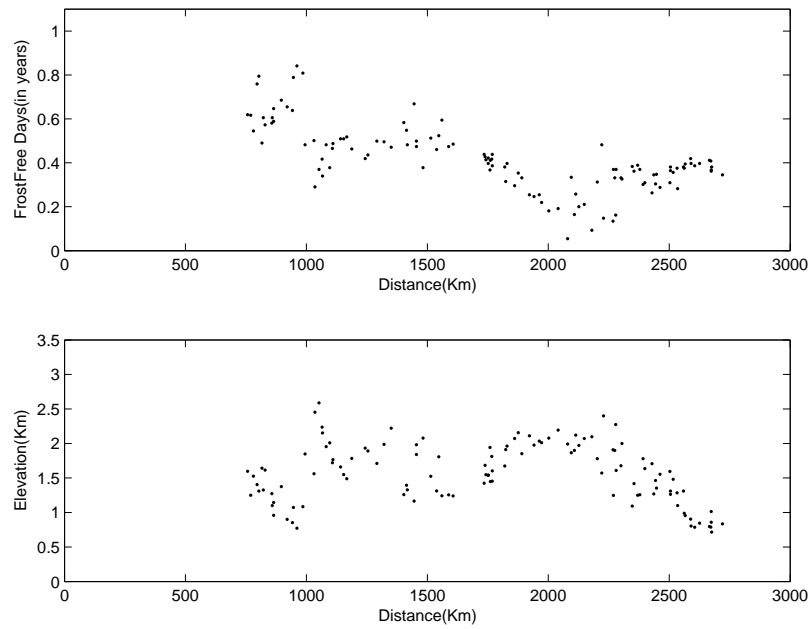


Figure 4.9: Frost-free days and elevation for zone 4

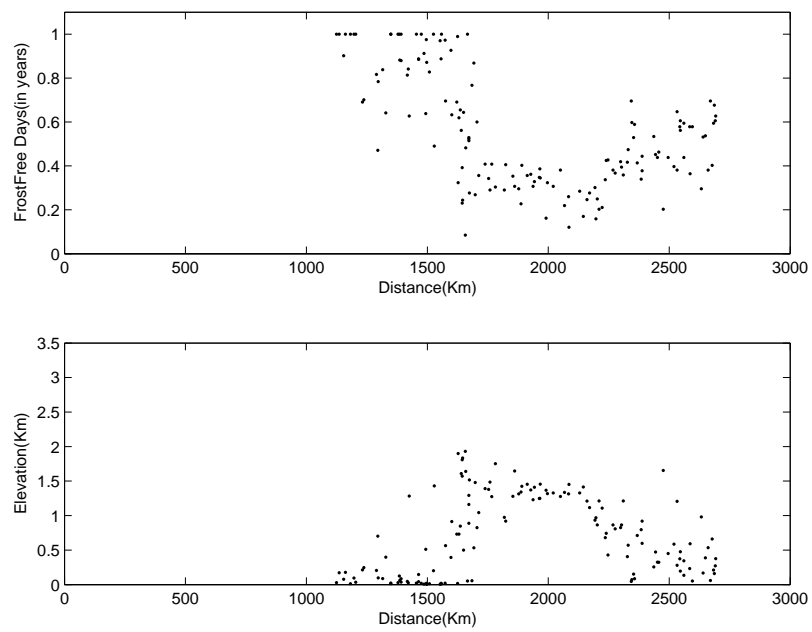


Figure 4.10: Frost-free days and elevation for zone 5

Table 4.5: Best fit results for $T(x)$ in zone 1

| Function | Formula | Parameters | Adjusted- R^2 |
|---------------|--------------------------------|--|-----------------|
| Rational 1 | $T(x) = \frac{p1}{x+q1}$ | $p1 = 14.61$ $q1 = 11.64$ | 0.8729 |
| Rational 2 | $T(x) = \frac{p1}{x^2+q1x+q2}$ | $p1 = 343.1$ $q1 = 7.664$ $q2 = 311.3$ | 0.8998 |
| Exponential 1 | $T(x) = ae^{bx}$ | $a = 1.17$ $b = -0.05222$ | 0.8929 |
| Exponential 2 | $T(x) = ae^{bx} + c$ | $a = 01.105$ $b = 0.05829$ $c = 0.07427$ | 0.8926 |

with least number of parameters (exponential 1 in Table 4.5) for our model. (Note the R^2 values of the two exponential functions are close.) However, for small x , the function value becomes larger than 1, which is the upper limit of breeding length function $T(x)$, so we truncated the function where the value exceeds 1. The growth function $T(x)$ we used in our simulation is:

$$T(x) = \min(1.17e^{-0.05222x}, 1) \quad \text{for } x \geq 0 \quad (4.36)$$

Figure 4.11 shows the curve given by formula (4.36) along with the data points (zone 1).

4.8 Model Parameters

To determine empirical values for the demographic parameters of the model we surveyed the literature on collared dove biology and natural history. Most of the information on collared dove reproduction is from Great Britain and central Europe (Poland, Germany, Hungary, and the Netherlands). Differences in climate and growing season length between Europe and the southeastern US are likely to influence the values of model parameters. These differences remain a source of error for our model. The survival rates are different for adult and juvenile doves. For juveniles, it ranges from 25 to 50% and for adults, it ranges from 45 to 77% [54]. Since we do not have age structure in our model, for survival rate, s , we used the average of average rates for adults (birds > 1 year old) and for juveniles (birds < 1 year old), 62.7%, and 34.2%, respectively [54]. Likewise a range of values is reported for

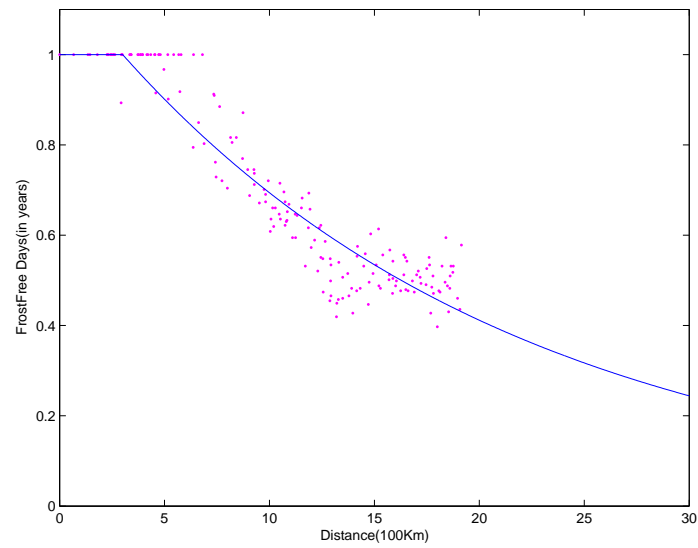


Figure 4.11: Best fit $T(x)$ in zone 1

Table 4.6: Parameters of the model

| Symbol | Used in simulation |
|----------|--|
| δ | 1.5 |
| σ | 18.6(estimated using the Christmas bird count (CBC) data |
| c | 0.558 (2 eggs/nest times 27.9 % survival rate) |
| s | 0.4845 |
| m | 6 |

clutch size and reproductive success. However, the number of birds fledged is less than the number of eggs. Nest success rate, defined as percentage of chicks fledged from eggs laid, ranges from 29% in Manchester, England, 15.6% in India in the dry period, to 39% in India in the monsoon period [54]. For our model, we used the average of these three numbers (approximately 27.9%). The number of eggs laid is approximately 1-2 per nest. We assumed that the number of eggs laid is two per nest per clutch and multiplied by the survival rate of 27.9% to get our parameter value of c , the average number of offspring surviving to fledging. The reported number of clutches per year is 3-6 for central European populations [12]. The number of broods may be greater in warmer climates and longer growing seasons. We defined the parameter m in our model to be the maximum number of clutches per year and used 6, the largest number reported. For US data, we used the number of breeding pairs observed as an estimate for the parameter, δ , the maximum density of nest sites available. However, the number from south eastern United States ranges from 0.08-5.70 pairs per square kilometer (median = 0.31). The corresponding value from Europe reported ranges from 0.003-0.17 pairs per square kilometer [12]. We used 1.5 for our δ , which was the value used by Veit and Lewis in their analysis [66]. The parameter values used in our simulation are listed in Table 4.6.

4.9 Bird Data

We used abundance data for the Eurasian collared dove collected by the National Audubon Society (NAS), the United States Geological Survey (USGS) and the Canadian Wildlife Service (CWS). Specifically, we used data from the NAS Christmas bird count (CBC) and the USGS/CWS North American breeding bird survey (BBS). The CBC and BBS generate

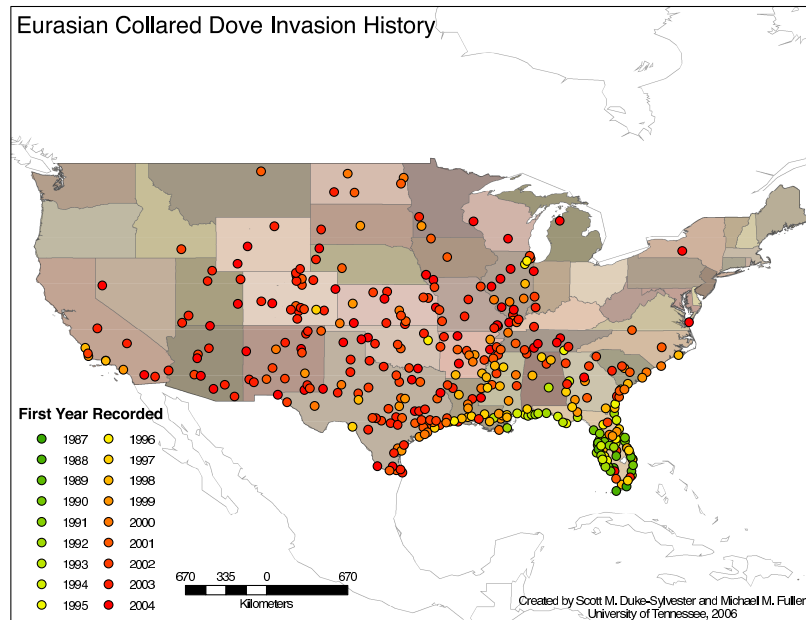


Figure 4.12: Map for CBC data

annual abundance records at numerous survey locations for all bird species occurring in North America. We used CBC records from 1971 – 2004, and BBS records from 1966 – 2004 which includes the period of introduction and invasion for the Eurasian collared dove. The Eurasian collared dove appears in BBS records beginning in 1986 and in CBC records beginning in 1987 (see Figure 4.12). The CBC and BBS data represent the number of birds observed in one or more circular survey sites. A CBC survey site represents a single circle of 12km radius and is censused by one or more observers over a single 24 hour period sometime within a two week window around Christmas [3]. The BBS survey is performed along a 39.2km linear route, with 50 separate survey circles located every 0.80km along each route [16]. Each BBS site is surveyed during the peak of the breeding season (May-July depending on location). The diameter of each BBS survey circle is approximately 0.80km, depending on topography and vegetation cover. Thus the BBS data represent a linear transect 40km long and 0.80km wide. During a BBS survey, each circle along the route is censused for a 3-minute period. The CBC and BBS data sets provide raw abundance data and the CBC data also includes density data (birds per hour and birds per mile). We converted the CBC birds per mile data to birds per km. To calculate the corresponding density (birds per km) in BBS data, we divided the total number of birds seen along the route by the length of the

sum of the diameters of the survey circles (40km).

4.10 Numerical Simulation - 1 Spatial Dimension Model

In our analysis, we used two different bird data sets (BBS and CBC) to estimate the bird density. Since we estimated our breeding season length function, $T(x)$ from the frost-free days data in zone 1 (see Table 4.4), we only used the CBC and BBS data collected from the sites located in zone 1. Table 4.7 shows the number of CBC and BBS sites in zone 1 and also the number of sites found within 10 miles of a weather station located in zone 1. If we restricted the CBC and BBS sites located near weather stations in zone 1, the error due to the variation in the breeding length might be small. However, there are only a small number of data points available and this is also a possible cause of error. Therefore, we included all CBC and BBS sites located in zone 1 without any restriction on the location with respect to weather stations in zone 1.

With these bird data, we are almost ready to run a simulation with our model. However, we needed to estimate the parameter σ , per capita rate of pair formation. The following is the outline of the steps we used to estimate the parameter and to compare our model with one of the bird data sets (BBS) and make a prediction of the spread of the doves.

Step 1 Estimate the wave front distance from the CBC data .

Step 2 Calculate the wave front distances from the simulation with different values of σ .

Step 3 Compare the sum of squared error between distances in Steps 1 and 2.

Step 4 Run the simulation with the best σ found in Step 3 and estimate the wave front distances.

Step 5 Estimate the wave front distance from the BBS data.

Step 6 Compare the results in Steps 4 and 5.

In Step 1, we used the CBC data to estimate the wave front distance. Figures 4.13, 4.14, 4.15 and 4.16 show the CBC bird density (birds per km) from 1989 to 2004. For each

Table 4.7: Number of CBC and BBS data points

| Year | CBC sites in Zone 1 | CBC sites near weather stations | BBS sites in Zone 1 | BBS sites near weather stations |
|--------------|---------------------|---------------------------------|---------------------|---------------------------------|
| 1988 | 1 | | 1 | |
| 1989 | 2 | 1 | 1 | |
| 1990 | 7 | 4 | 1 | |
| 1991 | 8 | 6 | 1 | |
| 1992 | 11 | 8 | 2 | |
| 1993 | 13 | 9 | 4 | 1 |
| 1994 | 16 | 11 | 7 | 2 |
| 1995 | 18 | 14 | 8 | 3 |
| 1996 | 20 | 15 | 14 | 4 |
| 1997 | 19 | 16 | 16 | 4 |
| 1998 | 25 | 18 | 17 | 3 |
| 1999 | 29 | 19 | 23 | 5 |
| 2000 | 31 | 20 | 23 | 5 |
| 2001 | 32 | 21 | 31 | 8 |
| 2002 | 36 | 22 | 28 | 9 |
| 2003 | 35 | 22 | 32 | 10 |
| 2004 | 37 | 21 | 40 | 14 |
| <i>Total</i> | 390 | 227 | 249 | 68 |

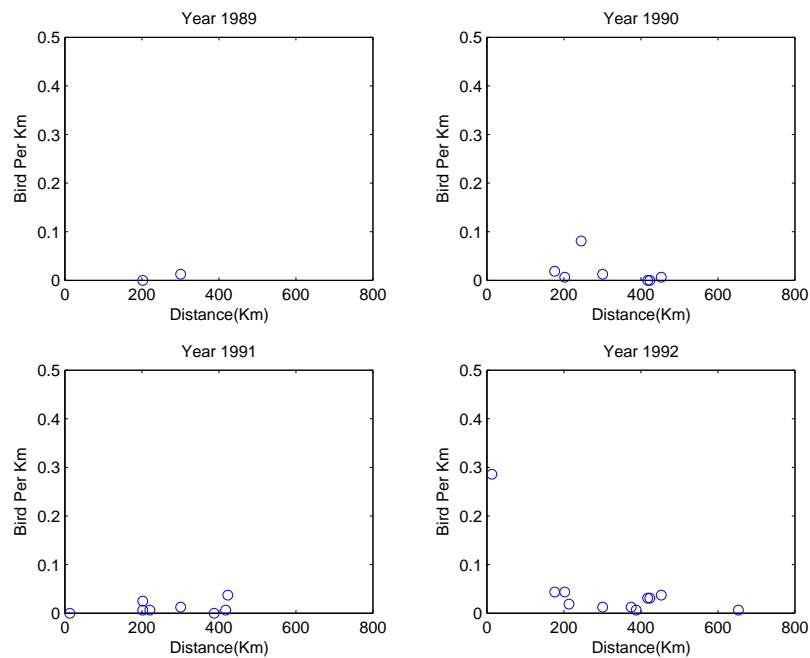


Figure 4.13: Bird density for year 1989-1992 (CBC)

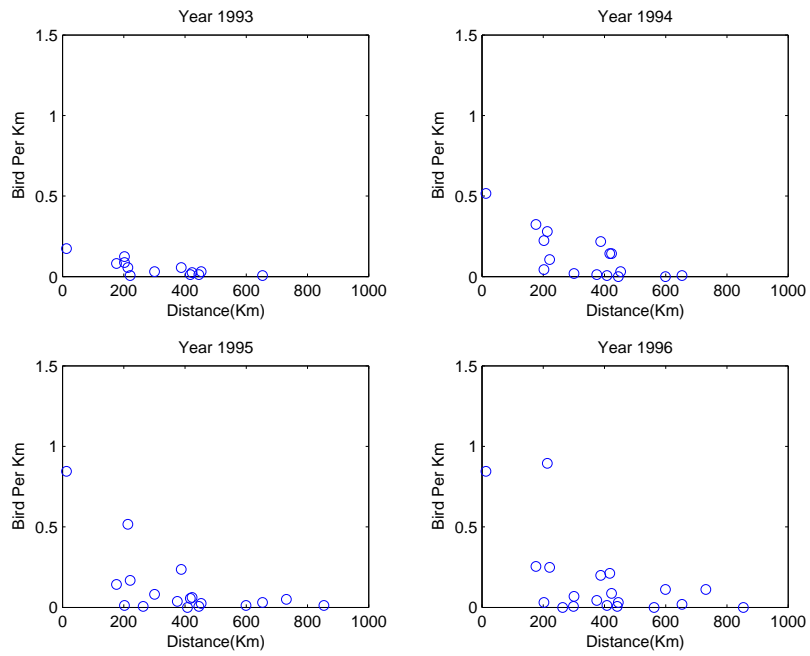


Figure 4.14: Bird density for year 1993-1996 (CBC)

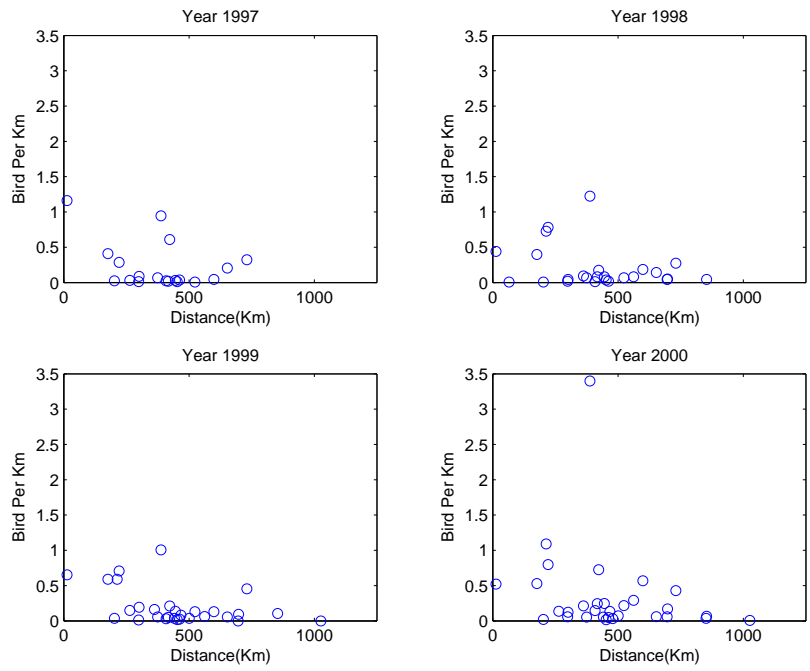


Figure 4.15: Bird density for year 1997-2000 (CBC)

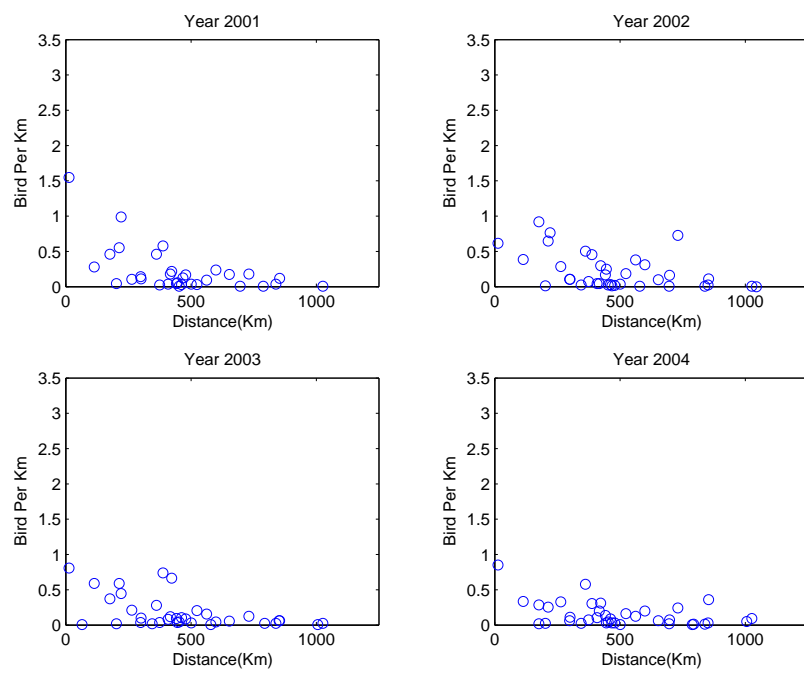


Figure 4.16: Bird density for year 2001-2004 (CBC)

year, we chose the CBC data point located furthest from the reference point. For example, the furthest data point is approximately at 650km for year 1992 in Figure 4.13. Then, we estimated the wave front distance for year 1992 is to be 650km. Note the distance is a south-north distance measured from our the reference latitudinal line at $24^{\circ}33'N$. In Figure 4.17 the CBC wave front distance is plotted each year from year 1989 ($t = 0$) to 2004 ($t = 15$). We can see that the collared dove reaches approximately 1000 km by the year 1999 ($t = 10$) from the Figure 4.17. Note we only used the data from year 1990 to 2004 (15 data points) for our estimate of σ described in the next step.

In Step 2, we ran the simulation with different values of σ starting with the initial population calculated by applying the kernel to the graph given in Figure 4.18. The other parameter values are given in Table 4.6. We calculated the bird density at each location for every year. We used the threshold density value of 0.03 to determine the wave front distance. This means the point where the density (birds per km) falls below 0.03 is the wave front distance for that year.

In Step 3, we compare the results obtained in Steps 1 and 2 and calculated the sum of the squared error. We determined the value of σ which minimized the error. We found the best value of σ is 18.6 and used this σ to run our simulation.

In Step 4, we ran the simulation with our growth function (4.15), dispersal kernel (4.35), and the breeding season length function estimated using the frost-free days data in zone 1 (4.36). In our program, we used 2^{15} grid points for our spatial domain of $[0, 35]$ (corresponds to the one dimensional domain from 0 to 3500km). To compute the integral in our model efficiently, we used the Fast Fourier Transform (FFT) [4]. Given initial population density, the density curve is plotted each year after the growth stage. In other words, if we start with the initial population N_0 , the first plot represents the bird density after the birds disperse and grow.

We calculated the bird density for 45 years starting with the same initial density given in Figure 4.18. The bird density curve is plotted each year (see Figure 4.19). Note that each bird density was plotted after the growth period, so each curve is not smooth. Because the number of clutches is discrete, i.e., it takes on a nonnegative integer, there is a jump in

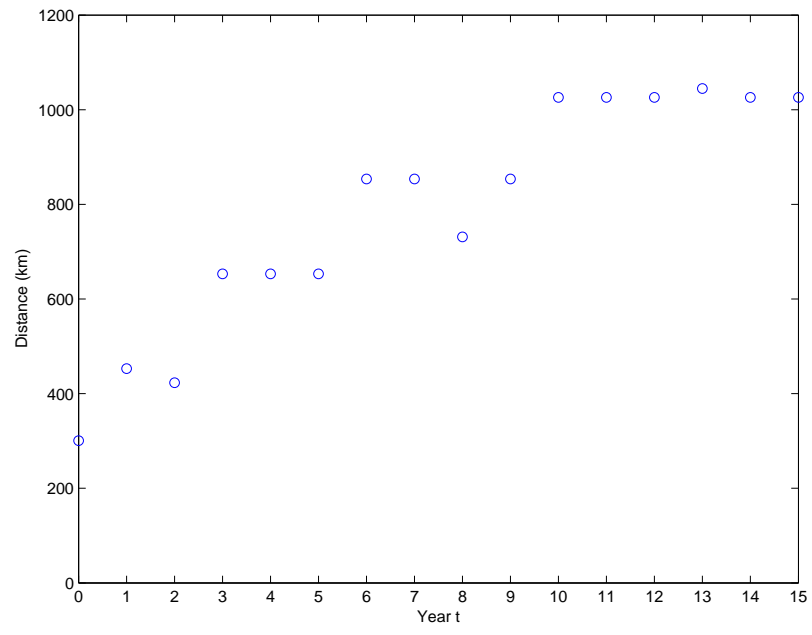


Figure 4.17: Wave front location (CBC)

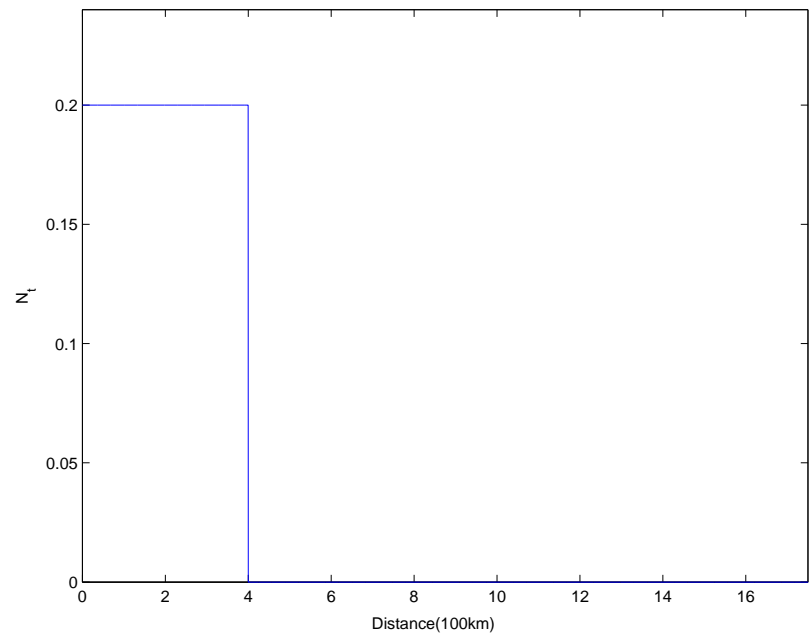


Figure 4.18: Graph used to calculate N_0

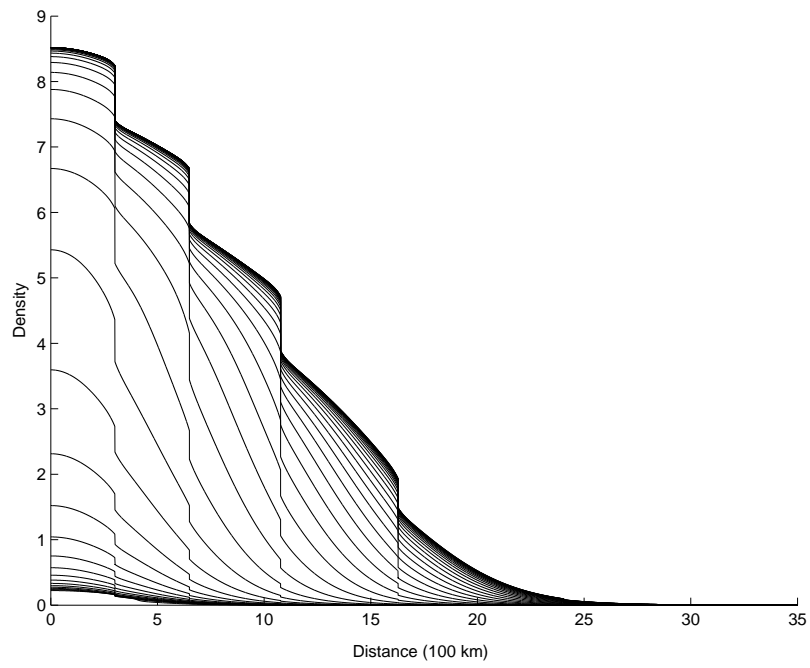


Figure 4.19: Simulation result for population density (zone 1)

the number of offspring at the border where the number of clutches changes. For example, there is a big step at the location approximately 300km from the origin. Up to this point, the breeding season length is long enough to produce 6 clutches. Just after this point, the breeding season length is a little short to produce 6 clutches but can produce at most 5 clutches.

The wave front distance generated in our simulation for 45 years with $\sigma = 18.6$ is given in Figure 4.20 with $t = 1$ corresponding to the year 1990, using the threshold value 0.03 again.

In Step 5, we estimated the wave front distance using the Breeding Bird Survey data (BBS). Figures 4.21, 4.22, 4.23 and 4.24 show the bird density (birds per km) from year 1989 to 2004. The BBS wave front distance was calculated in the same way as CBC data (see Step 1) and the wave front distance from year 1989 ($t = 0$) to 2004 ($t = 15$) is shown in Figure 4.25.

In the last step, we compared our simulated estimate of the Eurasian collared dove along a south to north corridor with the BBS data. Figure 4.26 shows the wave front location estimated from the BBS data and the corresponding wave front location generated using

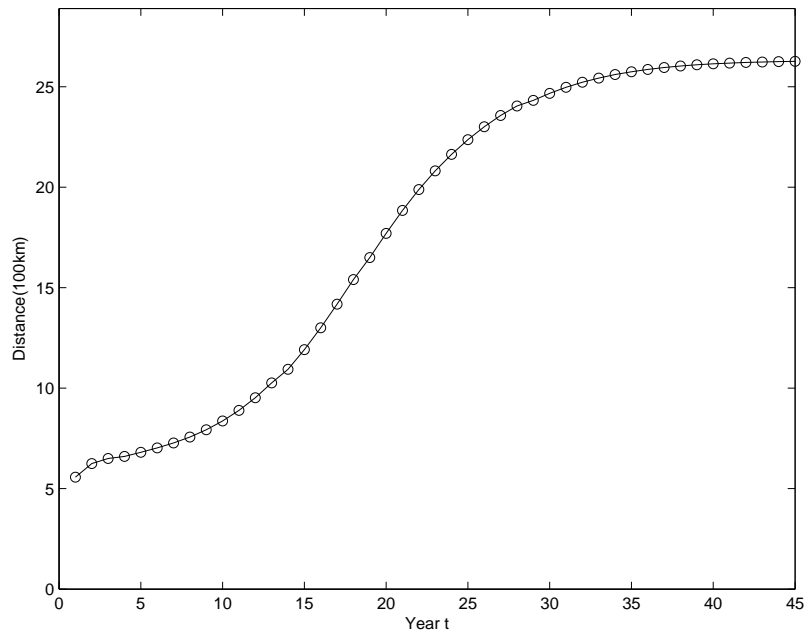


Figure 4.20: Wave front distance (zone 1)

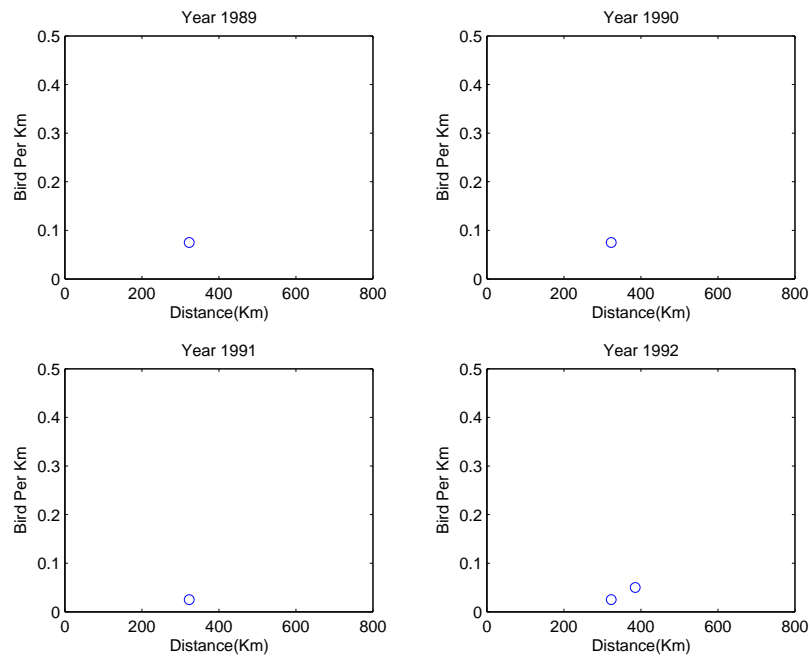


Figure 4.21: Bird density for year 1989-1992 (BBS)

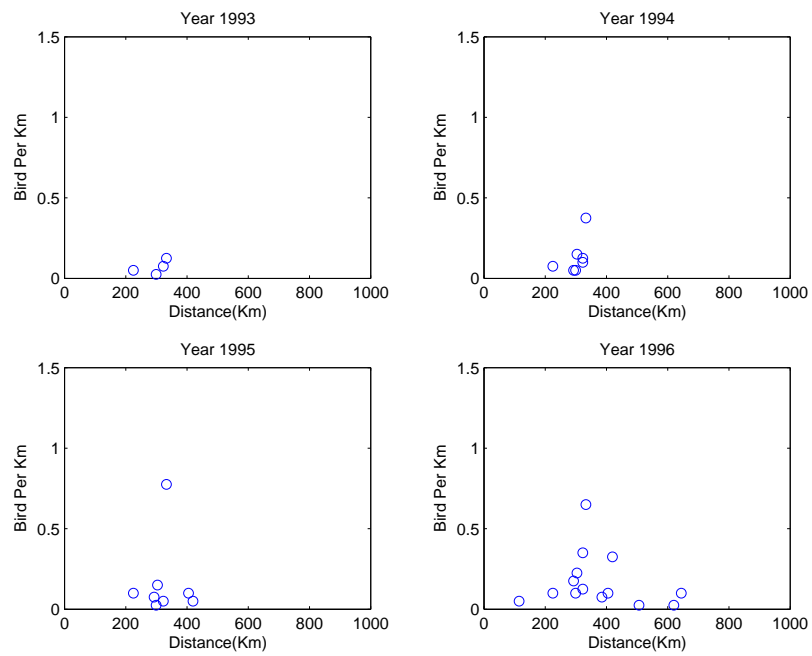


Figure 4.22: Bird density for year 1993-1996 (BBS)

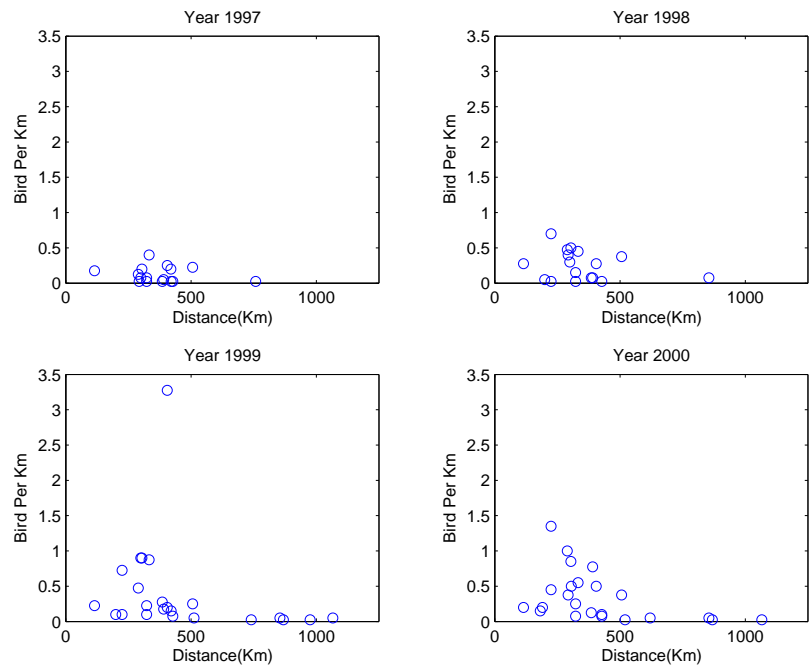


Figure 4.23: Bird density for year 1997-2000 (BBS)

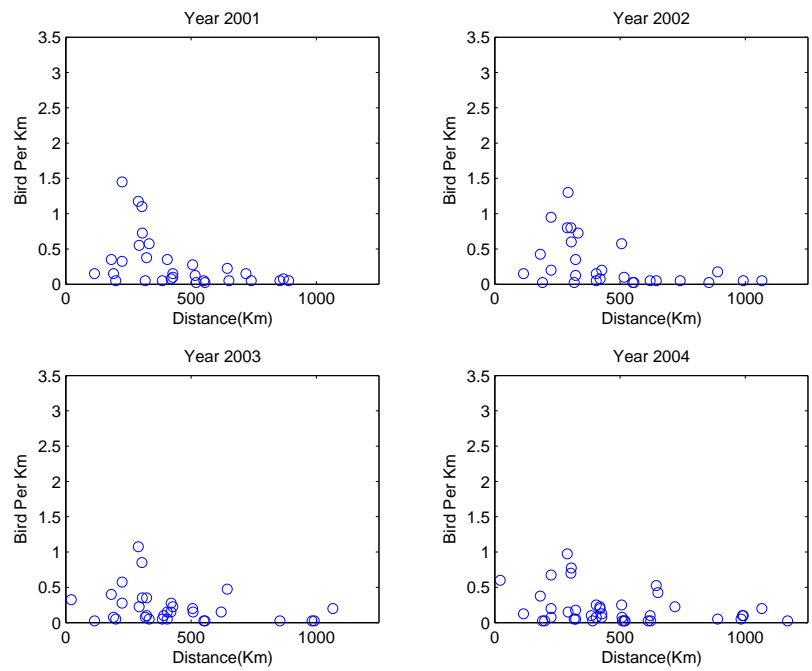


Figure 4.24: Bird density for year 2001-2004 (BBS)

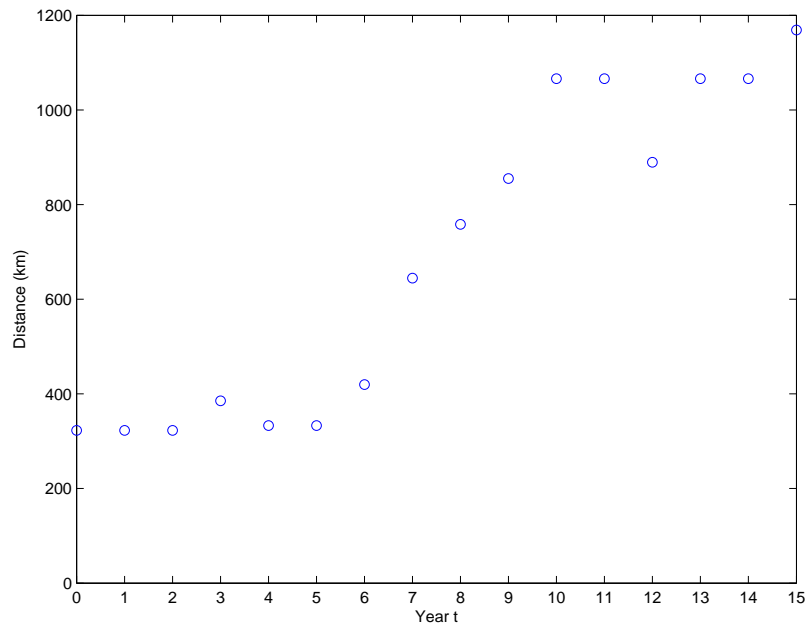


Figure 4.25: Wave front location (BBS)

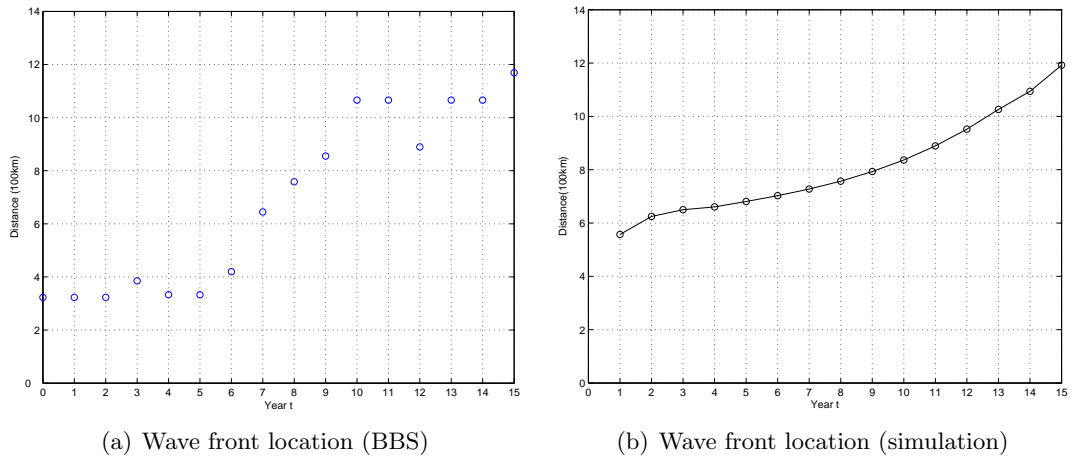


Figure 4.26: Wave front locations from BBS data and simulation result.

our model.

4.11 Conclusions

We constructed a model for the spread of Eurasian collared dove in the United States. Our novel contribution is the use of a growth function explicitly dependent on the habitat. Our model takes into account the fact that the breeding season length is not constant. We used the data on the number of frost free days to estimate the length of the breeding season. The number of frost free days is affected by not only the latitude but also the altitude, humidity and other factors. Generally, the number of frost free days gets smaller as you move north. The growth function in our model includes the difference in the maximum number of clutches depending on the length of breeding season.

When we compare our simulation result with the BBS data in terms of the wave front distance, there is a similarity in the pattern of the change in the distance. At the beginning, the rate of change is slow but it gradually increases. Since we have only 15 points (corresponds to the time interval of 15 years) of data from the BBS bird data, our prediction and the data did not match very well. Specifically, our simulation results provide the faster rate of spread at the beginning than the data indicate. According to the BBS data, the doves do not seem to spread much during the first five years. It is possible that some environmental differences, such as habitat quality affected the spread. Doves might stay near farms rather than disperses to a less suitable habitat. Since we don't know the exact initial population density, this error might have caused the difference between our result and the BBS data. Also, error in the estimation of the parameter σ might have caused a difference. When we determined the best value of σ , we used the threshold value 0.03 to determine the wave front distance. At a different threshold level, the error between our simulated wave front distance and the CBC data might be minimized at different value of σ . However, for the last 8 years, our result seems to be a good estimate.

From the simulation result shown in Figure 4.20, the spread of the collared dove gradually increases and then again starts slowing down. This is because the doves cannot produce enough offspring to sustain the population when the breeding season length is too short. In

Figure 4.20, the limit of the wave front distance is approximately 2630km from the origin. This distance corresponds to approximately $48^\circ N$ latitudinal line (the US-Canadian border in the North West America).

In this dissertation, we presented a model in one spatial dimension, which represents the spread of the doves to north. We plan to extend our model to two spatial dimensions. For the dispersal kernel, we may assume the dispersal of doves is radially symmetric. Also, we can estimate the breeding season length, $T(x, y)$, where x and y represent the north-south distance and east-west distance from the same reference point used in our one dimension model in a similar manner using all the data points of frost-free days which are well distributed across the states.

Also, we can add an age structure (juveniles and adults) to take into account the differences in the rate of survival, s , and the dispersal behavior.

Bibliography

- [1] L. J. S. Allen, D. A. Flores, R. K. Ratnayake, and J. R. Herbold. Discrete-time deterministic and stochastic models for the spread of rabies. *Applied Mathematics and Computation*, 132:271–292, 2002.
- [2] H. Behncke. Optimal control of deterministic dynamics. *Optim. Control Appl. Meth.*, 21:269–285, 2000.
- [3] C. E. Bock and T. L. Root. The Christmas Bird Count and avian ecology. *Stud. Avian Biol.*, 6:17–23, 1981.
- [4] W. L. Briggs and V. E. Henson. *The DFT: An Owner’s Manual for the Discrete Fourier Transform*. Soc. for Industrial and Applied Math.(SIAM), Philadelphia, 1995.
- [5] A. J. G. Cairns. Epidemics in heterogeneous populations: aspects of optimal vaccination policies. *IMA J. of Math. Applied to Med. and Biology*, 6:137–159, 1989.
- [6] J. E. Childs, A. T. Curns, M. E. Dey, L. A. Real, L. Feinstein, and O. N. Bjornstad. Predicting the local dynamics of epizootic rabies among raccoons in the United States. *PNAS*, 97(25):13666–13671, 2000.
- [7] D. Clancy. Optimal intervention for epidemic models with general intervention and removal rate functions. *J. Math. Biol.*, 39:309–331, 1999.
- [8] J. S. Clark, M. Lewis, and L. Horvath. Invasion by extremes: population spread with variation in dispersal and reproduction. *The American Naturalist*, 157:537–554, 2001.
- [9] C. F. B. Coombs, A. J. Isaacson, R. K. Murton, R. J. P Thearle, and N. N. Westwood. Collared doves(*Streptopelia decaocto*) in urban habitats. *The Journal of Applied Ecology*, 18:41–62, 1981.

- [10] C. Cosner, S. Lenhart, and V. Protopopescu. Parabolic systems with nonlinear competitive interactions. *IMA Journal of Applied Mathematics*, 44:285–298, 1990.
- [11] M. J. Coyne, G. Smith, and F. E. McAllister. Mathematic model for the population biology of rabies in raccoons in the mid-Atlantic states. *American Journal of veterinary research*, 50(12):2148–2154, 1989.
- [12] S. Cramp. *Terns to Woodpeckers*, volume IV of *Handbook of the Birds of the Middle East and North Africa. The Birds of the Western Palearctic*. Oxford University Press, Oxford, Great Britain, 1985.
- [13] J. del Hoyo, A. Elliott, and J. Sargatal, editors. *Sandgrouse to Cuckoos*, volume 4 of *Handbook of the Birds of the Worlds*. Birdlife International, Barcelona, Spain, 1997.
- [14] F. Van den Bosch, R. Hengeveld, and J. A. J. Metz. Analyzing the velocity of animal range expansion. *Journal of Biogeography*, 19:135–150, 1992.
- [15] O. Diekmann. Run for your life. a note on the asymptotic speed of propagation of an epidemic. *J. Diff. Equat.*, 33:58–73, 1979.
- [16] S. Droege. The North American Breeding bird survey. In J. R. Sauer and S. Droege, editors, *Survey Designs and Statistical Methods for the estimation of avian population trends*, volume 90 of *U.S. Fish Wildl. Serv. Biol. Rep.*, pages 1–4. 1990.
- [17] L. C. Evans. *Weak Convergence Methods for Nonlinear Partial Differential Equations*, volume 74. American Mathematical Society, Providence, 1990.
- [18] L. C. Evans. *Partial Differential Equations*. American Mathematical Society, Providence, 1998.
- [19] N. D. Evans and A. J. Pritchard. A control theoretic approach to containing the spread of rabies. *IMA Journal of Mathematics Applied in Medicine and Biology*, 18:1–23, 2001.
- [20] J. Fisher. The collared turtle dove in Europe. *British Birds*, 53:153–181, 1953.
- [21] R. Fister. Optimal control of harvesting in a predator-prey parabolic system. *Houston Journal of Mathematics*, 23(2):341–355, 1997.

- [22] R. Fister, S. Lenhart, and J. S. McNally. Optimizing chemotherapy in an HIV model. *Electronic Journal of Differential Equations*, 1998(32):1–12, 1998.
- [23] W. H. Fleming and R. W. Rishel. *Deterministic and Stochastic Optimal Control*. Springer-Verlag, New York, 2005.
- [24] P. J. Francis. Optimal tax/subsidy combinations for the flu season. *J. of Econ. Dynamics and Control*, 28:2037–2054, 2004.
- [25] D. Greenhalgh. Some results on optimal control applied to epidemics. *Math. Biosci.*, 88:125–158, 1988.
- [26] M. A. Guerra, A. T. Curns, C. E. Rupprecht, C. A. Halon, J. W. Krebs, and J. E. Childs. Skunk and raccoon rabies in the eastern United States: Temporal and spatial analysis. *Emerging Infectious Diseases*, 9(9):1143–1150, 2003.
- [27] F. He, A. Leung, and S. Stojanovic. Periodic optimal control for competing parabolic Volterra-Lotka-type systems. *J. Comput. Appl. Math.*, 52:99–217, 1994.
- [28] R. Hengeveld. Mechanism of biological invasions. *Journal of Biogeography*, 15:819–828, 1988.
- [29] R. Hengeveld. *Dynamics of Biological Invasions*, chapter 8: Birds invading Europe and North America. Chapman and Hall, London, 1989.
- [30] R. Hengeveld and F. van den Bosch. The expansion velocity of the collared dove *Streptopelia decaocta* population in Europe. *Ardea*, 79:67–72, 1991.
- [31] M. I. Kamien and N. L. Schwarz. *Dynamic Optimization: The Calculus of Variations and Optimal Control in Economics and Management*. North-Holland, Amsterdam, 1991.
- [32] M. Kot. Discrete-time traveling waves: ecological examples. *Journal of Mathematical Biology*, 30:413–436, 1992.
- [33] M. Kot. Do invading organisms do the wave? *Canadian Applied Mathematics Quarterly*, 10:139–170, 2002.

- [34] N. V. Krylov. *Lectures on Elliptic and Parabolic Equations in Hölder Spaces*. American Mathematical Society, Providence, 1996.
- [35] S. Lenhart and V. Protopopescu. Optimal control for parabolic systems with competitive interactions. *Math. meth. Appl. Sci*, 17:509–524, 1994.
- [36] S. Lenhart, V. Protopopescu, and S. Stojanovic. A two-sided game for nonlocal competitive systems with control on the source terms. *Appl. Math. Optim.*, 28:113–132, 1993.
- [37] S. Lenhart, V. Protopopescu, and A. Szpiro. Optimal control for competing coalitions. *Nonlinear Anal: Theory, Meth. Appl.*, 28:1411–1428, 1997.
- [38] A. W. Leung. *Systems of Nonlinear Partial Differential Equations, Applications to Biology and Engineering*. Kluwer Academic Publishers, DOrdrecht/Boston, 1989.
- [39] M. A. Lewis and R. W. Van Kirk. Integrodifference models for persistence in fragmented habitats. *Bulletin of Mathematical Biology*, 59:107–137, 1997.
- [40] X. Li and J. Young. *Optimal Control Theory for Infinite Dimensional Systems*. Birkhäuser, Boston, 1995.
- [41] J. L. Lions. *Optimal Control of Systems Governed by Partial Differential Equation*. Springer-Verlag, New York, 1971.
- [42] D. L. Lukes. *Differential Equations: Classical to Controlled, Mathematics in Science and Engineering*, volume 162. Academic press, New York, 1982.
- [43] C. Martin, L. Allen, M. Stamp, M. Jones, and R. Carpio. A model for the optimal control of a measles epidemic. In *Computation and Control II, Proceedings of the Third Bozeman Conference*, pages 265–283, Boston, 1992. Birkhauser.
- [44] R. Morton and K. H. Wickwire. On the optimal control of a deterministic epidemic. *Advances in Appl. Probability*, 6:622–635, 1974.
- [45] J. D. Murray, E. A. Stanley, and D. L. Brown. On the spatial spread of rabies among foxes. *Proc. R. Soc. London B*, 229:111–150, 1986.

- [46] R. J. O'Connor. Biological characteristics of invaders among bird species in Britain. *Phil Trans R. Soc. Lond.*, 314:583–598, 1986.
- [47] Division of Viral and Rickettsial Diseases (DVRD). Rabies. From National Center for Infectious Diseases (NCID) web site concerning rabies (<http://www.cdc.gov/ncidod/dvrd/rabies/>). Centers for Disease Control and Prevention.
- [48] P. Ögren and C. F. Martin. Vaccination strategies for epidemics in highly mobile populations. *Applied Mathematics and Computation*, 127:261–276, 2002.
- [49] C. V. Pao. *Nonlinear Parabolic and Elliptic Equations*. Plenum Press, New York, 1994.
- [50] E. Paradis, S. R. Baillie, W. J. Sutherland, and R. D. Gregory. Patterns of natal and breeding dispersal in birds. *Journal of Animal Ecology*, 67:518–536, 1998.
- [51] L. S. Pontryagin, V. G. Boltyanskii, R. V. Gamkrelize, and E. F. Mishchenko. *The Mathematical Theory of Optimal Processes*. Wiley, New York, 1962.
- [52] V. Protopopescu and R. T. Santoro. Combat modeling with partial differential equations. *European Journal of Operational Research*, 38:178–183, 1989.
- [53] L. A. Real, C. Russell, L. Waller, D. Smith, and J. Childs. Spatial dynamics and molecular ecology of north American rabies. *Journal of Heredity*, 96(3):1–8, 2005.
- [54] C. M. Romagosa. Eurasian collared-dove (*Streptopelia decaocto*). In A. Poole and F. Gill, editors, *The Birds of North America*, number 630. The Birds of North America, Inc., Philadelphia, PA, 2002.
- [55] C. M. Romagosa and R. F. Labisky. Establishment and dispersal of the Eurasian collared-dove in Florida. *Journal of Field Ornithology*, 71:159–166, 2000.
- [56] C. M. Romagosa and T. McEneaney. Eurasian collared-dove in North America and the Caribbean. *North American Birds*, 53:348–353, 1999.

- [57] C. A. Russell, D. L. Smith, L. A. Waller, J. E. Childs, and L. A. Real. *A priori* prediction of disease invasion dynamics in a novel environment. *Proc. R. Soc. Lond. B*, 271:21–25, 2004.
- [58] USDA Wildlife Services. National Rabies Management Program. From USDA Animal and Plant Health Inspection Service web site concerning the National Rabies Management Program (<http://www.aphis.usda.gov/ws/rabies/>). USDA Animal and Plant Health Inspection Service.
- [59] S. Sethi and G. L. Thompson. *Optimal Control Theory: Applications to Management Science and Economics*. Kluwer Academic, Boston, 2000.
- [60] S. P. Sethi. Quantitative guidelines for communicable disease control program: a complete synthesis. *Biometrics*, 30:681–691, 1974.
- [61] J. Simon. Compact sets in the space $L^p(0, T; B)$. *Ann. Mat. Pura Appl.*, CXLVI:65–96, 1987.
- [62] P. W. Smith. The Eurasian collared-dove arrives in the Americas. *American Birds*, 41:1370–1379, 1987.
- [63] National Audubon Society. The 104th Christmas Birds Count. *American Birds*, 58:122–124, 2004.
- [64] H. R. Thieme. A model for the spread of an epidemic. *J. Math. Biol.*, 4:337–351, 1977.
- [65] H. R. Thieme. Asymptotic estimates of the solutions of non-linear integral equations and asymptotic speed of spread of populations. *J. Reine u. Angew.*, 306:94–121, 1979.
- [66] R. R. Veit and M. A. Lewis. Dispersal, population growth, and the Allee effect: dynamics of the House Finch invasion of eastern North America. *American Naturalist*, 148:255–274, 1996.
- [67] K. Wickwire. Mathematical models for the control of pests and infectious diseases: a survey. *Theoretical Population Biology*, 11:182–238, 1977.

- [68] C. K. Wikle. Spatial modeling of count data: A case study in modeling breeding bird survey data on large spatial domains. In A. Lawson and D. Denison, editors, *Spatial Cluster Modeling*, pages 199–209. Chapman and Hall, 2002.
- [69] C. K. Wikle. Hierarchical models in environmental science. *International Statistical Review*, 71:181–199, 2003a.
- [70] C. K. Wikle. Hierarchical Bayesian models for predicting the spread of ecological processes. *Ecology*, 84:1382–1394, 2003b.
- [71] C. K. Wikle and M. B. Hooten. Hierarchical Bayesian spatio-temporal models for population spread. In J. S. Clark and A. Gelfand, editors, *Applications of Computational Statistics in the Environmental Sciences: Hierarchical Bayes and MCMC Methods*. Oxford University Press, 2005.

Vita

Erika Asano was born in Utsunomiya, Japan. After graduating from Utsunomiya-Girls High School, she attended Washington English Center in Seattle, WA. Then, she attended Eastern Washington University in Cheney, WA and received a B.A. in Physics in 1989. She returned to Japan and worked as a process engineer at Canon, Inc. in Tokyo, Japan. Then, she decided to go back to school to attend University of Washington in Seattle, WA in 1995. She earned a B.S with double major in applied and computational mathematical sciences and biology in 1998. She started graduate study in mathematics at University of Tennessee, Knoxville, graduating with the Ph.D degree in August in 2006. She has accepted a position as assistant professor in the Environmental Science, Policy and Geography Program at the University of South Florida, St.Petersburg, FL, beginning August, 2006.